INSTITUTO SUPERIOR DE ENGENHARIA DO PORTO
MESTRADO EM ENGENHARIA MECÂNICA




Analysis of wood plywood joints in large pallets using numerical finite element analysis

RAFAEL RODRIGUES ROCHA
outubro de 2025

POLITÉCNICO
DO PORTO

ISEP INSTITUTO SUPERIOR DE ENGENHARIA DO PORTO

Analysis of wood/plywood joints in large pallets using numerical finite element analysis

Rafael Rodrigues Rocha

Dissertation to fulfil the requirements to obtain the Master degree in Mechanical Engineering, with a specialization in Mechanical Constructions

Supervisor: Raul Duarte Salgueiral Gomes Campilho
Company supervisor: Nuno Ricardo Esteves Domingues
Jury:
President:
Armando José Vilaça de Campos
Vowels:
Raul Duarte Salgueiral Gomes Campilho
Ricardo Fernando Rodrigues Pinto

Porto, October 2025

Acknowledgments

I would like to express my sincere gratitude to all those who contributed, directly or indirectly, to the completion of this work.

First, I would like to express my gratitude to my supervisor, Dr. Raul Duarte Salgueiral Gomes Campilho, for the trust he placed in me to carry out this project. I am profoundly grateful for his availability, academic rigour, and continuous support, all of which were essential to the successful completion of this work.

I would like to express my sincere gratitude to all individuals at NEFAB Portugal who contributed to this project in any capacity. I would like to express my sincere gratitude to the engineering team at NEFAB, and in particular to engineers Nuno Domingues and Diogo Pereira, for their support and valuable knowledge sharing. Special thanks are due to Hugo Silva, the production process manager, for his role in organising the logistics and providing support for the manufacturing of the test specimens. In addition, gratitude is extended to the production staff who prepared the specimens, for their patience and for sharing their practical expertise.

I would like to express my profound gratitude to my family for their unconditional support and encouragement throughout my academic career, particularly during the most arduous periods.

I would like to express my gratitude to all my friends who enhanced the experience of my academic career and provided consistent support throughout the process.

Abstract

The global packaging industry has evolved toward more sustainable and efficient solutions, particularly in logistics and goods transportation. Wooden pallets remain dominant in freight handling due to their structural simplicity, low cost, and compatibility with various transport systems. However, industry trends demand optimization of these structures for sustainability, cost-effectiveness, and adaptability to custom sizes. This is particularly relevant for companies like NEFAB Portugal, which provide industrial packaging solutions for sectors such as automotive and telecommunications. As the demand for customized pallet sizes grows, there is an increasing need to analyse the mechanical performance of large dimensions pallets created by joining wooden beams. Actually, the use of adhesives and mechanical joints in pallet construction raises key questions regarding strength, cost, and durability under real-world loading conditions, which emphasis the need for structural verification.

The primary aim of this dissertation is to study and compare seven different joint geometries for wooden beams used in pallet structures. These configurations were tested experimentally and simulated using Finite Element Analysis (FEA) to identify the best performing design. The research involved material characterization, manufacturing of joint specimens, static mechanical testing, and validation through numerical models. The joints were also assessed based on fabrication complexity, environmental sustainability, and cost-effectiveness. This comprehensive study supports NEFAB Portugal in optimizing future pallet designs, contributing to a more sustainable and efficient packaging strategy.

The results show that specific joint geometries, particularly those combining adhesives with mechanical reinforcements, provide superior load-bearing capacity and cost efficiency compared to conventional methods.

KEYWORDS: Pallet, Wood joint, Sustainability, Finite Element Analysis, Packaging solutions, Adhesives.

Resumo

A indústria global de embalagens evoluiu para soluções mais sustentáveis e eficientes, particularmente na logística e no transporte de mercadorias. As paletes de madeira continuam a dominar o manuseamento de mercadorias devido à sua simplicidade estrutural, baixo custo e compatibilidade com vários sistemas de transporte. No entanto, as tendências da indústria exigem a otimização destas estruturas para que sejam sustentáveis, rentáveis e adaptáveis a tamanhos personalizados. Isto é particularmente relevante para empresas como a NEFAB Portugal, que fornecem soluções de embalagem industrial para sectores como o automóvel e as telecomunicações. À medida que a procura de paletes de tamanhos personalizados aumenta, há uma necessidade crescente de analisar o desempenho mecânico das paletes de grandes dimensões criadas através da união de vigas de madeira. De facto, a utilização de adesivos e juntas mecânicas na construção de paletes levanta questões fundamentais relativamente à resistência, custo e durabilidade em condições de carga reais, o que reforça a necessidade da sua verificação estrutural.

O principal objetivo desta dissertação é estudar e comparar sete geometrias diferentes de juntas para vigas de madeira utilizadas em estruturas de paletes. Estas configurações foram testadas experimentalmente e simuladas através do Método de Elementos Finitos (MEF) para identificar o design com melhor desempenho. A investigação envolveu a caraterização de materiais, o fabrico de amostras de juntas, ensaios mecânicos estáticos e validação através de modelos numéricos. As juntas foram também avaliadas com base na complexidade de fabrico, na sustentabilidade ambiental e na relação custo-eficácia. Este estudo abrangente apoia a NEFAB Portugal na otimização de futuros designs de paletes, contribuindo para uma estratégia de embalagem mais sustentável e eficiente.

Os resultados mostram que geometrias específicas da junta, particularmente as que combinam adesivos com reforços mecânicos, proporcionam uma capacidade de carga superior e uma eficiência de custos superior aos métodos convencionais.

PALAVRAS-CHAVE: Palete, Junta de madeira, Sustentabilidade, Método de elementos finitos, Soluções de embalagem, Adesivos.

Index

Figures Index

Tables Index

Acronyms and Symbols

Acronyms

AHP	Analytical Hierarchy Process
AR	Augmented Reality
ASTM	American Society for Testing and Materials
CAD	Computer Aided Design
CADD	Computer Aided Design and Drafting
CAE	Computer Aided Engineering
CAM	Computer Aided Manufacturing
CE	Circular Economy
CMC	Carboxymethyl Cellulose
CNC	Computer Numerical Control
COV	Coefficient Of Variation
CPL	Continuous Pressure Laminates
CZM	Cohesive Zone Model
DfA	Design for Assembly
DfC	Design for Cost
DfE	Design for Environment
DfM	Design for Manufacturing
DfMn	Design for Maintenance
DfR	Design for Reliability
DfX	Design for X
DL	Direct Labour
DM	Direct Material
EN	European Standard
FEA	Finite Element Analysis
GHGs	Greenhouse Gases
HPL	High Pressure Laminate
I4.0	Industry 4.0
IMUs	Inertial Measurement Units
ISEP	*Instituto Superior de Engenharia do Porto*
ISO	International Organization for Standardization
ISTA	Internacional Safe Transit Association
KPIs	Key Performance Indicators
LCA	Life Cycle Assessment

LVL	Laminated Veneer Lumber
MADM	Multi-Attribute Decision Making
MCDM	Multicriteria Decision Making
MEF	*Métodos de Elementos Finitos*
MODM	Multi-Objective Decision Making
MOF	Metallic Organic Framework
NPD	New Project Development
PLA	Polylactic Acid
PLP	Pallet Loading Problem
PVA	Polyvinyl Acetate
RP	Reference Point
SDGs	Sustainable Development Goals
TOPSIS	Technique for Order of Reference by Similarity to Ideal Solution
UTM	Universal Testing Machine
ZIF	Zeolitic Imidazole Framework

Symbols

R^2	Coefficient of correlation	-
ρ	Density	g/cm^3
L	Distance between supports	mm
y	Distance to neutral axis	mm
δ_{max}	Failure displacement	-
Tg	Glass temperature	°C
P_{max}	Load capacity	N
M_f^{max}	Maximum bending moment	Nmm
σ_{max}	Maximum stress	MPa
I	Moment of inertia	mm^4
ν	Poisson ratio	-
G_{IIC}	Shear fracture toughness	MPa $m^{1/2}$
G	Shear Modulus	MPa
τ	Shear strength	MPa
G_{IC}	Tensile fracture toughness	MPa $m^{1/2}$
σ_t	Tensile strength	MPa
b	Thickness	mm
h	Width	mm
E	Young's Modulus	MPa

1. Introduction

1.1. Contextualization

The packaging industry plays a crucial role in global trade, ensuring the protection, preservation, and efficient transportation of goods. As trade volumes continue to grow, the sector is constantly adopting innovative materials and technologies to enhance product safety, streamline supply chains, minimise environmental impact, and reduce costs. The evolution of packaging solutions has been marked by a transition from rudimentary cardboard boxes to advanced smart packaging, which has enhanced the ability to trace goods while aligning with sustainability objectives. Nevertheless, it is important to note that packaging alone is not sufficient to ensure efficient logistics functions. The transportation and storage of packaged goods rely heavily on pallets, which serve as standardised platforms for efficient handling across warehouses, shipping containers, and trucks. The construction of these pallets, which may be made from wood, plastic, or composites, optimises space, prevents product damage, and facilitates smooth logistics operations, making them essential component of the supply chain.

It is imperative for the packaging industry to ensure a balance between efficiency and environmental responsibility, aiming to ensure the safe transportation of goods while minimising ecological impact. Given that pallets represent the predominant averages of global freight transportation, it is imperative to address the issue of pallet wooden beams exceeding standard market dimensions. A potential solution to accommodate larger shipments is to join wooden beams to create extended pallet structures. However, due to the significant amount of possible joint geometries, a detailed analysis of the most used ones in the industry is conducted.

This study focuses on six specific joining geometries, analysing their cost-effectiveness and efficiency to determine the optimal solution. The internship was conducted at NEFAB Portugal, a member of the NEFAB Group, which manages projects in various industries, including automotive and telecommunications. The present study is part of a research project that aims to provide NEFAB Portugal with an optimal solution for the studied palette but also giving a valuable database for future applications in wooden pallet construction.

1.2. Objectives

The primary objective of the present study is to assess the optimal solution for a specific pallet provided by NEFAB Portugal, as well as to provide a database of the most common joint geometries. The following tasks were performed to conduct this study:

- Literature research;
- Problem definition;
- Definition of geometries with the NEFAB's engineers;
- Experimentally joint evaluation;
- Static FEA analysis of the joints;
- Comparison of the joints;
- Cost and sustainable analysis;
- Definition of the optimal solution.

1.3. Methodology

The study began with a comprehensive literature review, aiming to provide a better understanding of the development of the study. This task involved researching the packaging industry, environmental challenges, and potential solutions. The review was based on a range of sources, including scientific articles, company websites, and books, with the aim of ensuring a comprehensive and up-to-date analysis. Sources were selected based on their publication date, relevance, and citation frequency.

The core study was initiated with the definition of the encountered problem and then the definition of the geometries to be analysed. The most common joining configurations were selected, and additional innovative geometries were derived from them. Following the definition of the geometries, the study proceeded along two parallel paths: experimental testing and FEA.

For the experimental phase, specimens were produced at the NEFAB office to ensure that the joints closely resembled those used in real pallet production, rather than idealised laboratory-made joints with reduced imperfections. Next, a series of tests were conducted, and a comparative analysis was performed on the performance of all joints. Concurrently, FEA simulations were conducted to complement the experimental results. Since the materials used are essentially wood based, an inverse method was employed to determine their properties. This approach ensures greater consistency between the experimental and numerical results.

Finally, a cost and sustainable analysis was performed to assess the most cost-effective and sustainable joint configuration, integrating data from both the experimental and FEA analyses.

1.4. Thesis structure

The thesis is composed of four main sections, which are the following:

The **Introduction** section presents the contextualization of the work, the objectives of the work, the methodology used during the study, and the thesis structure.

The **Literature review** section introduces the theoretical foundations necessary for the development of this thesis. The study begins with an overview of the global packaging industry, followed by a detailed discussion on sustainable approaches in the sector, both globally and within Portugal. The review also explores a broad range of concepts related to product development, including design methodologies, material selection, computer-aided design (CAD), and joining methods. A more in-depth examination of sustainability in pallet design is finally presented, covering relevant methodologies, materials, and sustainability assessment tools.

The **Development** section begins with a detailed presentation of the company hosting the internship. This is followed by a comprehensive description of the materials and methodologies employed, including the design approach, product description, adhesive used, and joint geometries considered. The experimental phase is introduced in this framework, and it encompasses the materials utilised (e.g., wood and plywood), the fabrication process, the configuration of the test setup and the conditions under which it was conducted, and the resulting data. The section also includes a numerical analysis, beginning with an introduction to FEA, which outlines the software and constitutive models that are utilised. The material properties are then defined through an inverse method. After the establishment of these properties, the FEA is conducted, and the results are then directly compared to the experimental data. Finally, a cost and sustainability analysis are finally conducted, thus enabling the section to conclude with a final proposal.

The **Conclusion** section summarises the initial motivation for the work, the development process that was followed, and the main results obtained. After the analysis of the collected data, a final assessment is made to ascertain the most efficient joint solution. This section also discusses the limitations encountered during the execution of the work and, considering these constraints, it proposes future research.

2. Literature review

2.1. Packaging industry

The packaging industry is one of the most ancient industries on earth. Packaging always been here to assist man since Prehistory, an era in which materials like larges leaves, nutshells and seashells were used as packages [1, 2]. Theses naturals containers were crucial to protect food and valuables. After many years of evolution, it was during the first Industrial Revolution, due to mass production, that packaging begins to have more importance on the daily lives of humankind [2]. More recently, the packaging industry has undergone three major changes: beginning with a shift in substrate materials from 2000 to 2009. Due to the strong growth of new consumers, mainly in Asia, the focus was lowering the costs, by shifting from packaging based on metal and glass to flexible and rigids plastics, which are more affordable and reduce the materials used. Another important changes from 2010 to 2020 starts due to a health and wellness trend and acceleration of online shopping with COVID-19, for that the industry needed to increase their production by innovating high-functionality and sustainable packaging. Since the beginning, the packaging industry has always been evolving and, from 2020 to nowadays an important third change, this industry is moving towards a more sustainable approach and having a lower environmental impact with more optimized packages, due to consumers pushing for sustainability and real actions [3].

2.1.1. General concepts

The main objective of packaging is to protect the product against mishandling and impact during transportation or/and environmental conditions, simplify the transport and manipulation. The creation of a good package requires various stages, but the two main time consumers are the product design and materials selections. For the product design, it is necessary to know the product format and how it will be transported. What will provide the nominal dimensions and areas that need more protection and necessities for simplifying the transport and manipulation. Along with the design of packaging comes the material selection, usually leading to paper/carboard, flexible plastics, rigid plastics and metals, as shown in Figure 1. A crucial point nowadays in the materials selection is to know if it is possible to reuse the packaging. Sometimes, due to industry restrictions, the use of reusable organic materials such as paper and cardboard is not accepted, which compels the use of metals or plastics. In these situations, the focus is primarily on design to satisfy the requirements.

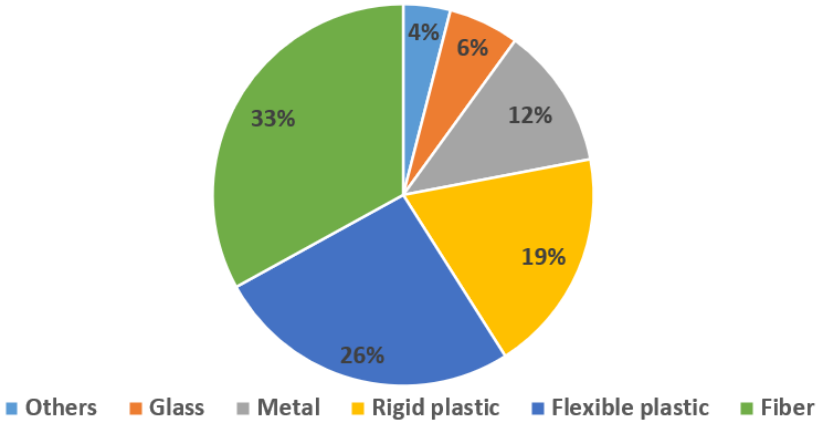

Figure 1 - Distribution of packaging material's market volume worldwide in 2020, by material type (adapted from [4]).

The packaging industry is a vital part of the economy nowadays. For example in 2023 the packaging market size was estimated to 1.20 trillion USD [3]. This industry is a major employer, directly or indirectly. It employs countless people, including design, manufacturing, transporters, sales, and marketing.

2.1.2. World and national industry

As shown in Figure 2, the Asian packaging market is leading with 32% of the global market value in 2022, due to the rapid expansion and wealthier middle-class population in developed regions, like China. Middle-class population in developed regions is spending more in non-essential purchases and engaging more online shopping, which help driving the growth of the packaging market. Europe follows (27%) whit a rapid evolution focused on a sustainable and environmental approach, where 74% of European population states say that the packaging waste have a major impact in their purchase [3]. In third, North America has 24% of the global value. Finally, less developed regions, such as the Middle East, Africa, and Latin America, face greater challenges in development due to lower average income levels or sparse populations. A poorer population induces difficulties on online shopping or order food as often as a richer population, which decreases the market size in those regions.

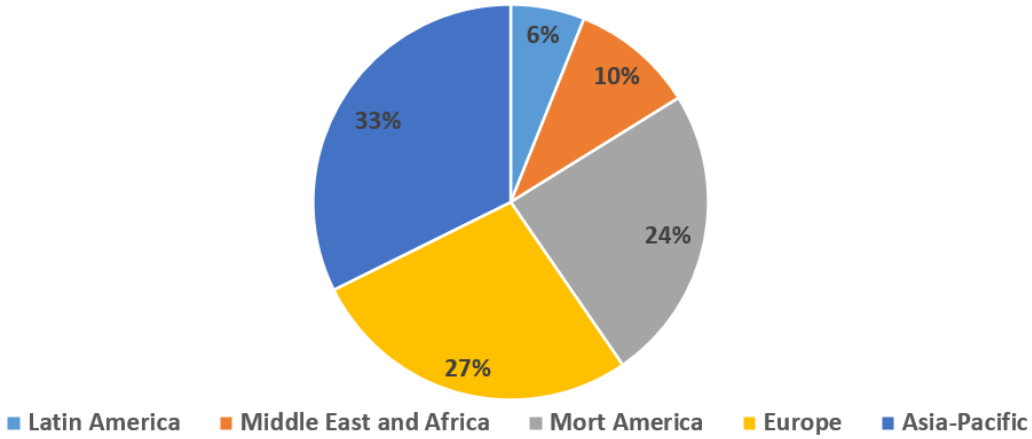

Figure 2 - Global packaging market size, in 2022, by region (adapted from [4]).

As shown in Figure 3, the packaging industry is the principal user of plastic in 2019. This material type goes against the sustainable and environmental approach, which promotes waste and a big environmental impact. Most waste is generated when a product is opened, as the protective material is no longer needed. For example, plastic bags used for online clothing purchases often contribute to this waste. However, waste in packaging can also be due to a bad design and manufacturing process, which can lead to over protecting the product [5].

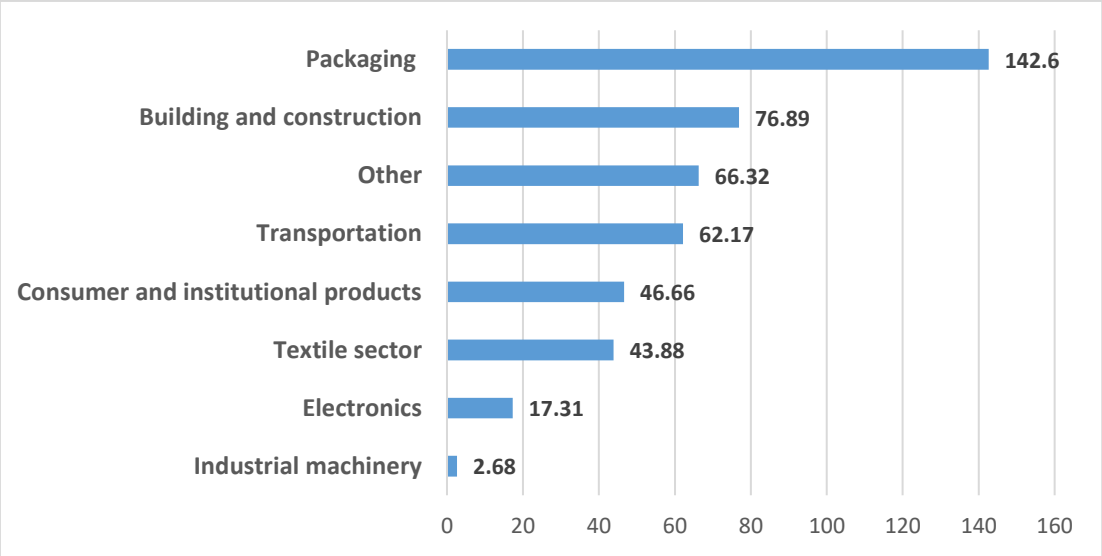

Figure 3 - Annual global plastic use in million tonnes, in 2019 (adapted from [6]).

To a smaller scale, in 2021 Portugal was 12th overall in the world with €834.46 million in sales, behind Greece, Italy, France and Spain. As shown in Figure 4, Portugal was 14th with the highest recycler rate in Europe with almost 65% of recycling rate, which is the target till 2025 (red line).

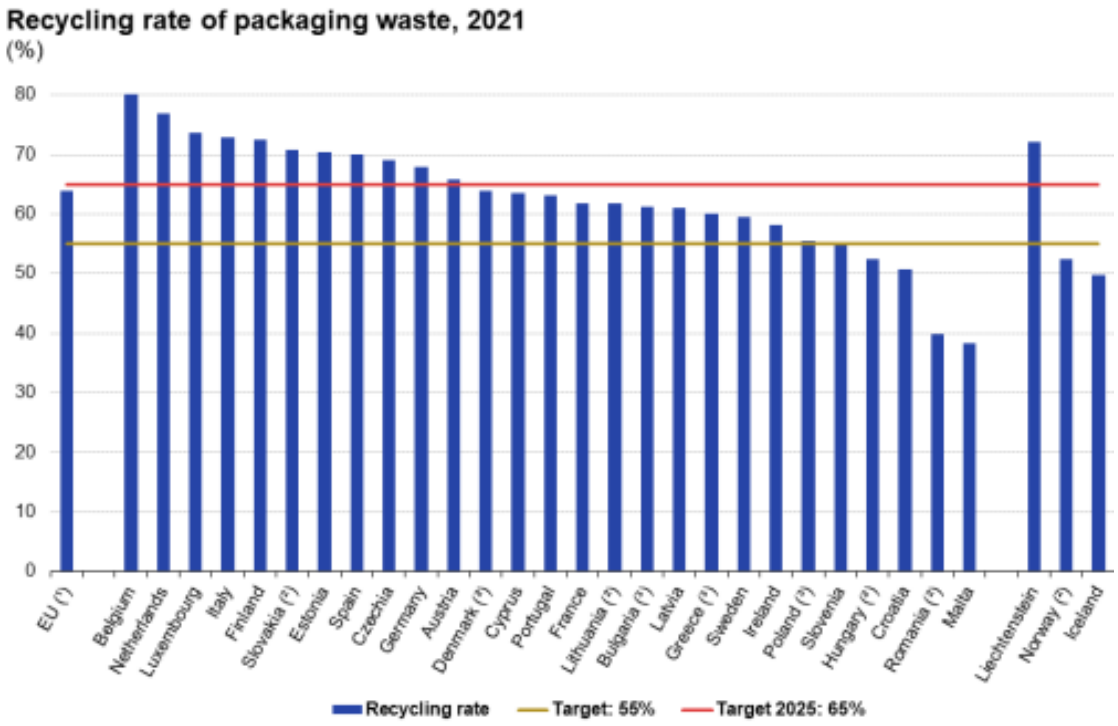

Figure 4 - Recycling rate of the packaging waste in Europe, 2021 [7].

None of those countries have a 100% recycling rate, which averages waste is present. Based on Figure 5, in Portugal 1.77 million tonnes (172 kg/cap) of packaging waste were generated in 2019. Paper/cardboard and plastic packaging were the principal waste, which can be generated, for example, from factories, supermarket, automative industry and others. Compared to 2010 (157 kg/cap), the packaging waste increased by 9.4% in 2019 [8], indicates room for improvement, by changing materials in some packages to more sustainable materials.

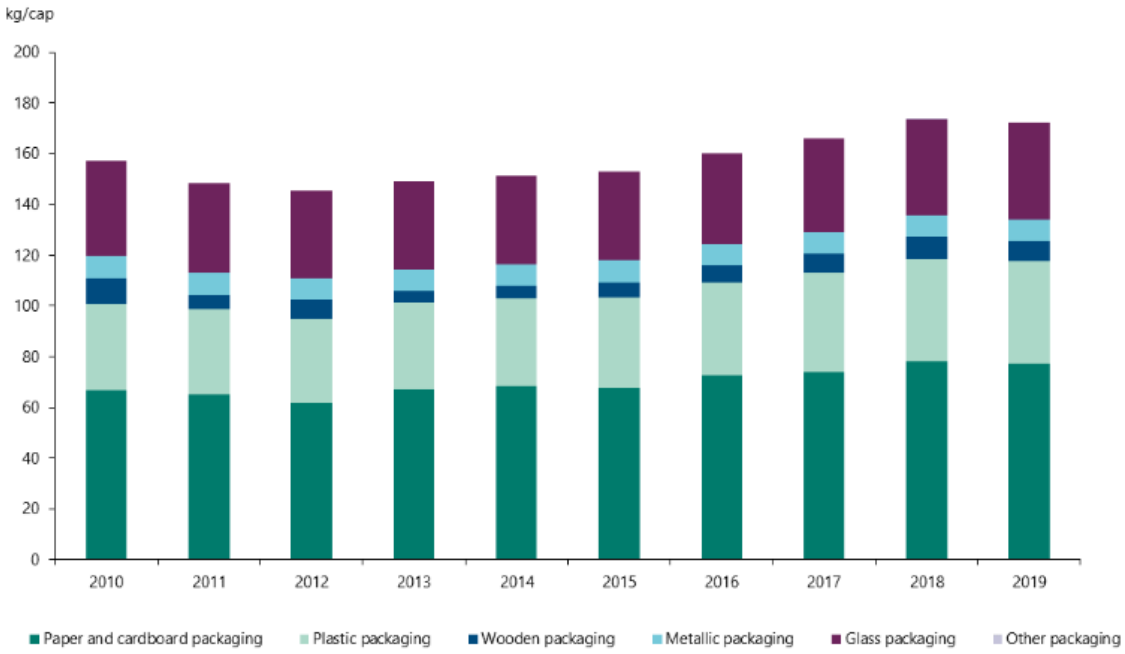

Figure 5 - Packaging waste generation in Portugal between 2010 and 2019, in kg per capita [8].

2.1.3. Project guidelines for packaging

The main objective of guidelines in a project is to have references that assure a coherence, efficacity and durability in the product development. In the packaging industry, standardisation aims to guaranty a homogeneous quality and simplify the collaboration between different teams in every product development step [9]. The standards used and the precision needed in the packaging industry is various in function of the sector working on. For example, pharmaceutical packaging requires high levels of quality and hygiene, compare to packaging used in construction. Globally the following standards are used:

- ISO 9001 (Quality management) - This standard ensure that organizations can consistently produce packaging solutions that meet customer expectations and comply with relevant regulatory standards;
- ISO 14001 (Environmental management) - This standard helps organizations to improve their environmental performance through more efficient use of resources and reduction of waste.

In Europe, the EN 13427 and EN 13428 standards define the minimum criteria for packaging. Standard EN 13427 promotes sustainability, by choosing more eco-friendly materials that can be easily recyclable and biodegradable. However, this regulation also emphasizes safety and

performance requirements, which involve preventing contamination and protection. To complement the EN 13427 standard, the EN 13428 standard establishes rules for the reuse and recycling process to minimize the possible environmental impact. Those two standards promote sustainability and reduce the environmental impact of packaging waste [10]. Along with those regulations, other standards are used, such as the ASTM D4169 and ISTA 3A standards, based on performance testing, permitting to ensure the package quality [11, 12].

In some cases, when the packaging has restriction, in the dimensions and weight, which turn impossible to perform physical tests, software such as Abaqus® can be used to predict and evaluate the performance. Using software also helps sustainability, by avoiding the use of materials in prototype creation, to be after destroyed to determine the package performance. Following the path to minimize waste, other software can assist and help companies to determine the environmental impact from the start of development to the implementation of the packaging in the market. The software GreenCalc® (Figure 6) measures the emissions, waste and returnability of the package [13]. This tool enables companies to possibly reduce environmental footprint, which can lead to a more sustainable industry.

Figure 6 - GreenCalc® representation [13].

2.1.4. Sustainability in the packaging industry

Over the last 50 years the main plastics used were fossil-based, due to their low cost and good properties, including durability, lightness, resistance to chemicals and corrosion. The use of plastics significantly increased in the last decades. In 1950, 1.5 million tons were produced, whereas 359 million tons were produced in 2018 [14]. This significant increase can be explained by the increase in society's consumption, which lead the industry to produce more plastics even at the expense of the environmental impact [15].

To contrast all these years, the concepts of sustainability and Circular Economy (CE) are becoming more important nowadays. In 2015, the United Nations created *"The 2030 agenda for sustainable development"*, which is composed by seventeen goals that will lead the World to a sustainable development. Amidst all these goals, the most relevant for the packaging industry is the 12th – *"Ensure sustainable consumption and production patterns".* This goal is

divided into different objectives, for example, achieving the sustainable management and efficient use of natural resources and substantially reduce waste generation through prevention, reduction, recycling and reuse, among others [16].

To achieve a sustainable approach, the materials used in the packaging have an important role. As seen before, the traditional plastics derived from fossil fuels are the main material used in the packaging industry, which are a major contributor to environmental pollution. To solve these environmental problems, companies are trying to change to more eco-friendly materials. For example, applied biodegradable and compostable materials, such as polylactic acid (PLA) derived from corn starch, are becoming more applied due to the fact those materials deteriorates naturally in the environment [17].

Along with the materials used, CE can be a new approach aiming to minimise the environmental impact by rethinking packaging design. In contrast to the traditional linear economy, based in the take-make-use-destroy concept [18], CE aims to create a loop where materials are always reusable in the production cycle (Figure 7). To accomplish these goals, companies design their product with their end-of-life in mind [9], which can result, for example, in packaging entirely conceived by the same material. Another example, when two different plastics are used in the same product could be easily separate one from the other for a more effective recycling.

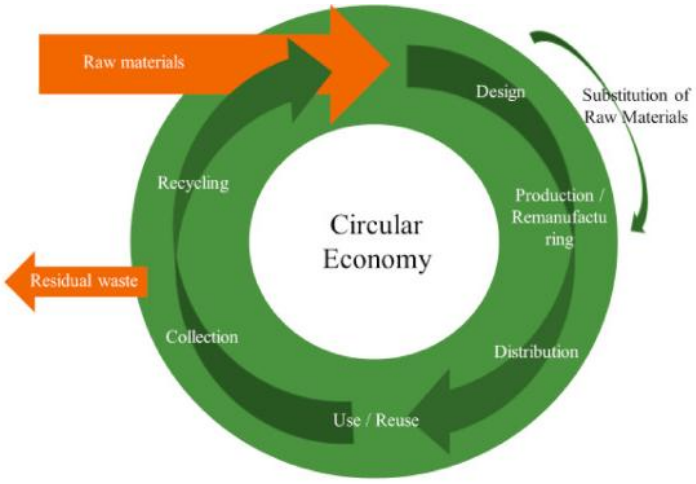

Figure 7 - Representation of the CE concept [18].

2.1.5. Advances in materials and processes

In phase with sustainability, the packaging industry grew rapidly, by including more technologies and modernize packaging. Due to the customers´ demand and sustainability requirements, modern packaging does not play a single role, which is to passively protect the product. Modern packaging aims to be smarter and active (Figure 8), and materials are engineered to perform specific functions behind the regular packaging. Materials like zeolitic imidazole framework (ZIF), a metallic organic framework (MOF), or carboxymethyl cellulose (CMC), an organic polymer, can provide real-time information about the condition, freshness and safety of a product. ZIFs are capable of selectively adsorbing and releasing molecules based

on the size, shape and surface properties of the molecules. This feature helps to increase the shell-life of goods, by selectively remove gases (oxygen, carbon dioxide and ethylene) [19].

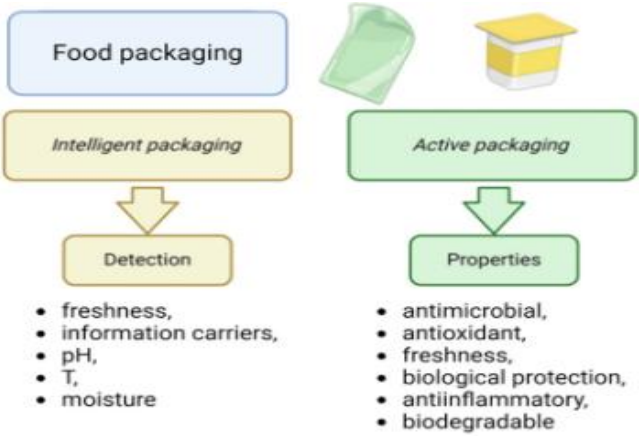

Figure 8 – The effects of different types of packaging (adapted from [20]).

All these materials have potential to create new and improved smart and active packaging. However, some challenges need to be addressed before these materials find a place in the market. ZIFs, for example, at a larger scale production are costly and they need to be studied to establish the possibility of migration of ZIFs from packaging to food, which can potentially impact the human health and environment [21].

A challenge in the modern packaging industry is the use of technological processes using intelligent packaging materials. The use of technology like 3D/4D printing is well established in companies, due to the decreasing costs of 3D/4D printer, possibility to produce forms of any geometry through one-step additive process and fast prototyping. To assure sustainability and overcome the challenges in 3D/4D printing, it is possible to use 5D/6D printing technologies [20]. 5D/6D printing represent revolutionary advancements in additive manufacturing, extending beyond traditional 3D printing. While 3D printing focuses on creating static objects with three dimensions, 5D printing incorporate additional functionalities, such as flexibility and dynamic behaviour. This allows a printed object to adapt and respond to environmental stimuli, such as temperature and pressure. Building on this, 6D printing introduces a temporal dimension, enabling objects to evolve over time. This innovative approach allows the use of smart materials that can sense and react to their surroundings. Together, 5D and 6D printing open new perspectives for a new era of smart manufacturing, where products are not only functional but also adaptive and interactive [22].

2.2. Product development

Product development can be defined as the process of creating, designing, and bringing new products to market or enhancing existing ones to meet the market demands. This process is comprised of multiple stages, including idealization, design, prototyping, testing, production and launch, often guided by guidelines. This multidisciplinary endeavour integrates insights from business strategy, engineering, design, and marketing to ensure that the product is both functional and appealing to consumers, thus ensuring competitiveness in the market. By driving

innovation and addressing evolving customer preferences, product development plays a crucial role in helping businesses adapt to market trends and maintain a competitive edge [23].

2.2.1. Contextualization of product development

Product development refers to all the necessary steps from the first idea of a product to market launch. For that, the usual strategy is the new product development (NPD), which can be applied to three types of products, the innovative products that have never been designed and developed before, the product that already exists in market but is new to the company, and new versions or variations of existing products [24]. The NPD strategy is based on the following steps (Figure 9) to build a successful product:

1) **Idea generation** is the starting point for any potential future product. For that, companies brainstorm for a new product idea or ways to improve an existing product. The main objective of this stage is to have as many ideas as possible but only keeping the most valuable ones. To evaluate the viability of the idea, a SWOT analysis permits to evaluate the Strengths, Weaknesses, Opportunities and Threats of the product;
2) **Concept development** refers to the creation of a product concept, which includes the target market, the features, and benefits of the idea. This step defines the product and proceeds with the development of the most viable solutions;
3) **Prototype construction** can be referred to a simple drawing or computer-aided prototype, which can identify the risks later the product creation. This stage enables companies to study the market risks and to establish a development strategy;
4) **Initial conception** permits the first creation of the product. During this step, companies need to exchange ideas with suppliers to manage material sourcing and define the possible product production;
5) **Testing and validation** verify of the product satisfies all the requirements for market;
6) **Product launch** it is the final step, where the product is ready to be added to the market and constitutes the final success measurement of the product.

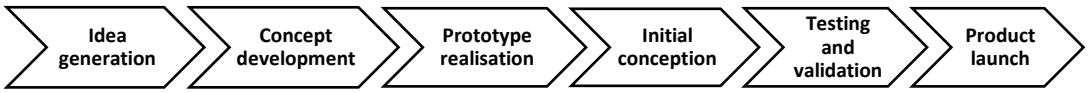

Figure 9 - NDP stages (adapted from [25]).

Having an efficient NPD process permits to have rigorous feasibility analysis, precise resource management, and clear task assignment. With this tools, companies can develop products that not only meet market needs but also drive sustainable growth [25].

2.2.2. Design for X methodology

The Design for X (DfX) methodology, also known as Design for Excellence, represents an approach whereby the letter "X" represents one of numerous quality criteria, including cost,

quality, reliability, manufacturability, or sustainability (Figure 10). This approach can have a considerable impact on the overall time development, given that ensuring the accuracy of product design at the outset is a far more cost-effective strategy than addressing issues that emerge later in the development process or after the product has been launched [26].

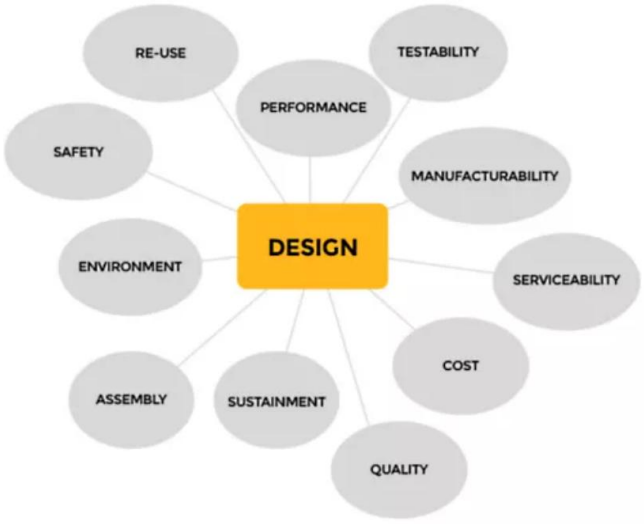

Figure 10 - DFX diagram [26].

As shown in the Figure 10, DfX comprises additional subsections that may be employed. In order to gain a more comprehensive understanding of the global concept of DfX, it would be beneficial to examine some of the sub-sections in closer detail [27].

- Design for Assembly (DfA) refers to a design that simplifies the assembly process. For that purpose, components should be easily assembled by simple operations, leading to fewer possibilities for errors;
- Design for Cost (DfC) is based on cost management techniques to control the cost of product development and manufacturing;
- Design for Reliability (DfR) permits to define the ability of a component or system to perform its required functions under stated conditions for a specific period;
- Design for Maintenance (DfMn) focuses on making the product easier to maintain.

Focusing on the most common DfX concept, Design for Manufacturing (DfM) has a big importance, since it directly addresses cost. The DfM method can be separated in seven steps. The first and most essential step, relies on establishing the approach to product sourcing. This may be conducted by the company itself, with the understanding that it will rely on suppliers for certain activities. The second step is to estimate the manufacturing cost, including the cost of standard components, custom components, costs of assembly, and the overhead costs. With all the costs known and a preliminary cost of the final product, it is possible to advance for the next steps. The third, fourth, fifth, and sixth steps are based on cost reduction focusing on every part of the product development, such as reducing the costs of components, assembly, supporting production, and logistics. Minimizing manufacturing costs is not the only objective of the product development process. The final step is to consider the impact of DfM decisions on other factors, including the development time and product quality. In certain sectors, the

time factor is of paramount importance. Consequently, decisions regarding DfM must be considered in conjunction with the associated manufacturing costs.

More recently, due to the concern with environmental impacts of products, Design for Environment (DfE) emerged. DfE focus on the environmental impact of the product, by reducing the carbon footprint of the product, reducing the energy consumption, liquid discharges, and gaseous emissions. The DfE is founded upon the CE, whereby a product is examined for the potential for remanufacturing and subsequent reintroduction into the production cycle. This approach has the objective of reducing the environmental impact of the product. An effective DfE implementation can create a more sustainable society [28].

2.2.3. Design selection methods

Early in the product development process, product design will be merged in accordance with the identified needs and other specified requirements of the customer. At the start, the company may have a single or several concepts or just one, but a selection method is always present. When having several concepts, a more structured selection method can be used. Those methods can be simple or more elaborated, but these always benefit product development. The most relevant forms of selection methods are as follows: [29]:

- External decision – All concepts are sent to the customer or external entity for selection;
- Product champion – The selection is based on the choice by an influential member of the company;
- Advantages and disadvantages – The selection is based on a list, defining the strengths and weaknesses of each concept;
- Prototype and test – Executing prototypes for testing and choosing the best concepts based on the test data.

More elaborated methods using multicriteria decision-making (MCDM) provide a structural framework to organize and analyse complex problems, by considering multiple criteria simultaneously [30]. MCDM can be based on a Multi-Attribute Decision Making (MADM) or Multi-Objective Decision Making (MODM). MADM is used for a finite number of alternatives solution to a problem, and the selection is based on evaluating multiple attributes of each alternative. The goal is to identify and choose the best option. MODM is applied to choose between an infinite or very large number of possible alternatives, and choose the one that satisfies the best requirements [31]. The most widely used methods that combine MCDM and MODM are the Analytical Hierarchy Process (AHP) and the Technique for Order of Preference by Similarity to Ideal Solution (TOPSIS). The AHP method evaluates the relative importance of customer requirements and design features to aid decision making [32]. To implement the AHP method, Saaty established a four-step procedure. The first step is to define the problem and identify customer requirements. Once the requirements and alternatives are identified, a pairwise comparison of criteria and requirements is made using a nine-point Likert scale (Table 1) [33]. In the second step, the importance of the customer requirements is calculated. The third step is to test the consistency of these importance levels to ensure that the pairwise comparison score is acceptable. Finally, the fourth step determines the relative overall importance of the customer requirements and selects the alternative with highest score [32].

Table 1 - 9-point Likert scale (adapted from [33])

Intensity of agreement	Definition of intensity of agreement
1	Strongly disagree
3	Disagree
5	Somewhat agree
7	Agree
9	Strongly agree
2, 4, 6 and 8	Intermediate values

More recently, the concept of competitive benchmarking merge, whereby an organisation evaluates its performance, products, services or processes by comparing them to the world's best, including direct and indirect competitive industry. [34]. The TOPSIS method, a leading MCDM technique, can be used to analyse competitive benchmarking. It ranks alternatives according to their proximity to the ideal solution, which maximises benefits (e.g. quality) and minimises negatives (e.g. costs or risks), and their distance from the anti-ideal solution, which minimises positives and maximises negatives [32]. Using these methods enable a deeper understanding of which design fits better in the society, by considering every possible aspect, such as environmental impact, competitivity, cost production, and quality.

2.2.4. Materials for design

The materials and manufacturing processes used in product design are evolving rapidly, creating new opportunities for innovation. As illustrated in Figure 11, many modern materials represent an evolution of the primary materials used in the past. This progression has significantly expanded the range of materials available to designers.

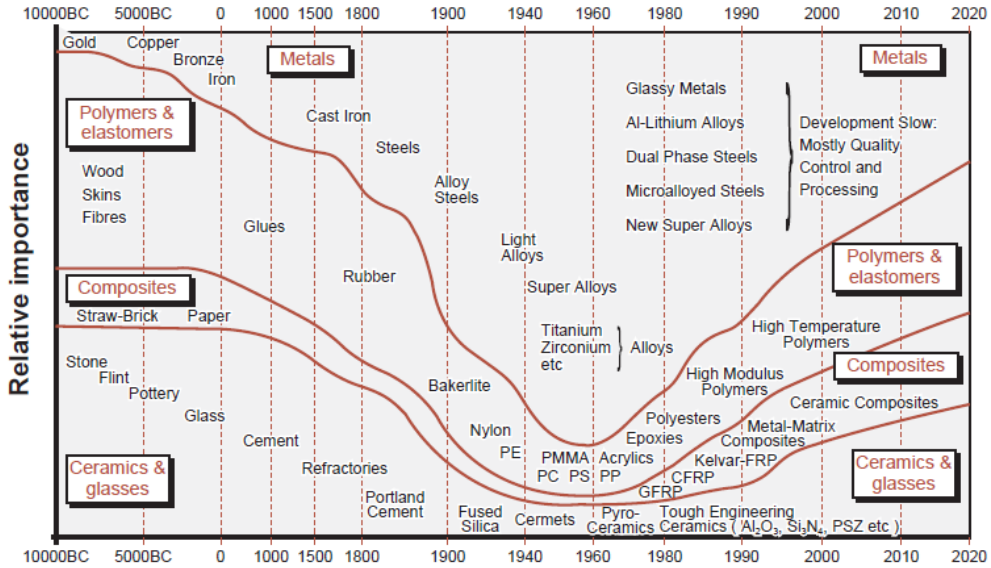

Figure 11 - Diagram of the different types of materials used in engineering over time [35].

In the selection of materials, designers have a multitude of options, each characterised by a distinctive combination of properties. However, certain attributes, including properties, processing methods and applications, are shared by some materials. These commonalities

permit the classification of engineering materials into six principal categories: metals, polymers, elastomers, ceramics, glasses and hybrids (Figure 12).

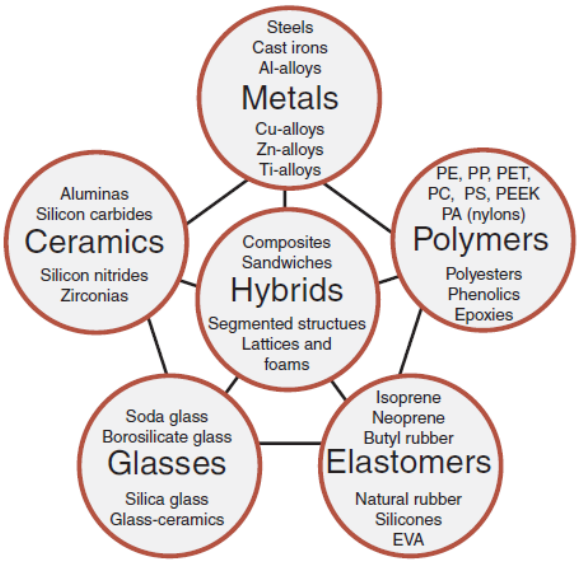

Figure 12 - Classification of engineering materials [35].

Metals are used because they have known properties. They are easily deformed when heated, making them ideal for forming processes. Metals can be strengthened through treatments. Even high-strength alloys retain sufficient plasticity to yield before fracturing. Despite their versatility, metals have the lowest resistance to corrosion and are prone to fatigue [35].

Polymers have a low Young's modulus (*E*), about 50 times less than those of metals, but can be almost as strong as metals. However, polymers offer unique design advantages due to their elasticity. These materials can be moulded into complex shapes in a single operation, eliminating the need for finishing operations when pre-coloured. Unlike metals, polymers resist corrosion but are highly temperature sensitive, becoming brittle under low temperature and few have useful strength above 200°C, limiting high temperature applications [35]. However, polymers play a crucial role in advancing sustainability by enabling lightweight, durable, and energy-efficient materials in various industries. Innovations in biodegradable and recyclable polymers reduce environmental impact, supporting a circular economy. Furthermore, bio-based polymers derived from renewable resources offer eco-friendly alternatives to traditional fossil fuel-based plastics [36].

Elastomers are long-chain polymers with unique properties above their glass transition temperature (Tg), since weak bonds melt while covalent bonds remain intact. This structure gives elastomers a low initial *E*, around 10^{-3} GPa Their varied properties make material selection complex and often require approximate values for comparison during design [35]. However, the flexibility and performance of elastomers make them indispensable in many applications.

Ceramics have a high *E* but are brittle, making them susceptible to stress concentrations. Despite these challenges, ceramics excel in specialised applications such as bearings and cutting tools due to their exceptional wear resistance. Their stiffness, hardness, corrosion resistance, and high temperature strength make them invaluable in demanding environments [35].

Glasses are non-crystalline (amorphous) solids that lack a regular crystalline structure. Equally to ceramics, these materials have no plasticity, making them hard, brittle, and susceptible to stress concentrations. Their irregular structure also results in low thermal and electrical conductivity, which distinguishes them from many other materials [35]. Despite their brittleness, glasses have several valuable properties. Their thermal properties allow them to be strengthened by tempering and to be fused into complex shapes. Glass also has excellent optical properties such as transparency, ultraviolet transmission, and versatility in optical applications such as eyepiece lenses, and objective lenses. These properties make glass a highly versatile material that is widely used in both scientific and industrial applications [37].

Hybrids are engineered materials that combine two or more families of materials in a specific configuration and scale, allowing designers to exploit the strengths of different materials while mitigating their limitations. A prime example is fibre-reinforced composites, which use fibres such as glass, carbon, or Kevlar embedded in a polymer matrix. These composites are light, stiff, and tough, but the polymer matrix limits their performance at high temperature, although excel at room temperature. Due to the complexity and cost of their manufacture, hybrid materials are typically used in applications where their superior performance justifies the higher cost [35].

As illustrated in Figure 13, material families are categorised into, classes, subclasses, and each defined by its unique properties or attributes. The combination of these attributes creates a property profile. Material selection involves matching the materials property profile to the specific design requirements. The material selection consists of four key steps: translation, screening, ranking, and review of supporting information. Initially, all materials are considered but, as the process progresses, materials with property profiles that are least suitable to the design requirements are gradually eliminated.

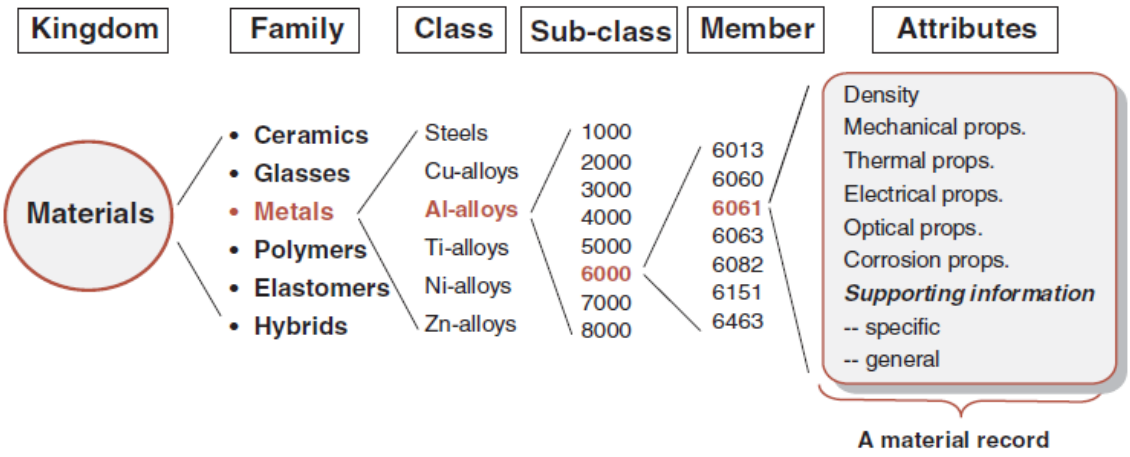

Figure 13 - Division of materials [35].

Translation involves defining the essential attributes of the material based on the product's functions, constraints, and objectives. These requirements are usually well-defined [35]:

- Functions refer to the primary roles of the material, such as supporting a load, resisting pressure, or transmitting heat;

- Constraints relate to fixed parameters, such as the dimensions required for the component to carry design loads or withstand pressure without failure;
- Objectives reflect the designer's goals, such as minimizing cost, achieving the lightest possible weight, or maximizing safety.

However, specific parameters can be modified to enhance the objective. The designer is free to alter dimensions that have not been constrained by design requirements and, most crucially, to select the material for the component. These are referred to as free variables [35].

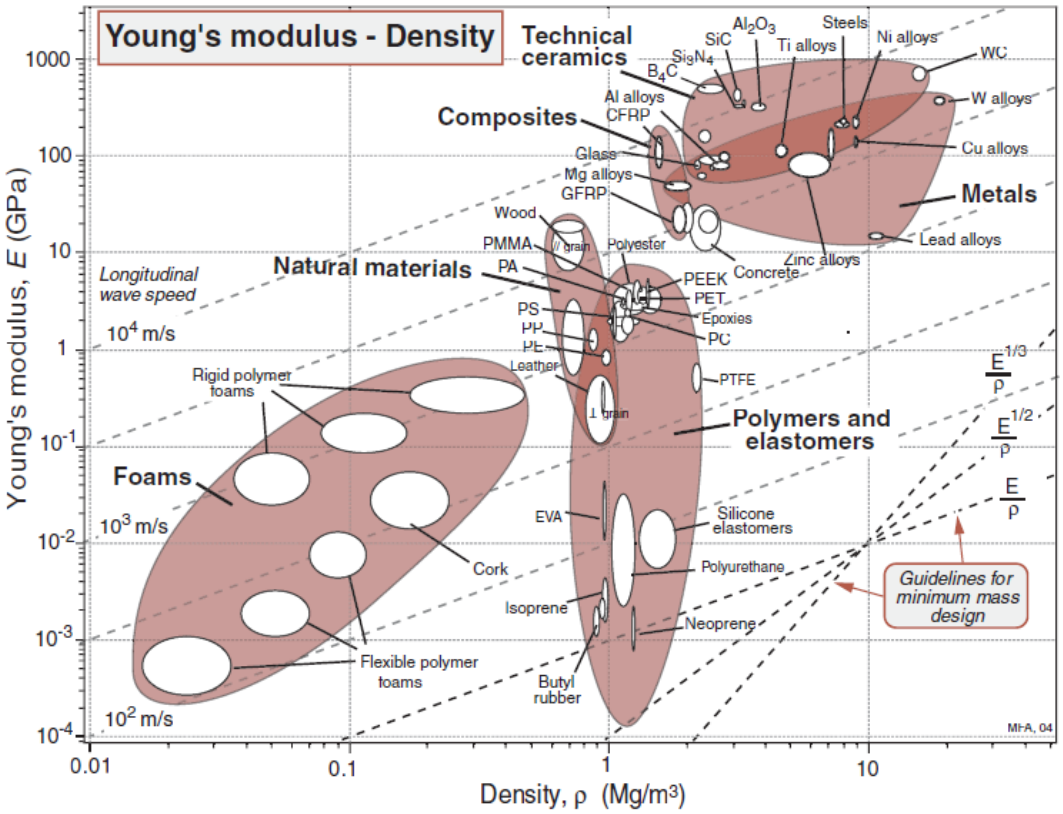

Figure 14 - Young's modulus – density [35].

The **screening** process serves to eliminate candidates whose attributes fall outside the limits set by the constraints, thus ensuring that only those who can fulfil the requisite duties are selected. In this step, engineers can use charts to facilitate the selection of materials. These charts condense a large amount of data by plotting one property against another, providing a concise and easily accessible averages of comparing materials. For example, Figure 14 plots E against density (ρ). The use of these charts is straightforward. Based on the known ranges or values of ρ and E from the translation step, lines are drawn to represent the specific values, creating a region of interest [35]. These charts effectively simplify complex data, allowing engineers to identify suitable materials efficiently and with greater clarity.

Ranking involves the creation of a list of materials that have passed the screening stage, ranked from most suitable to least suitable for the design. This is achieved using a material index that quantifies the suitability of a material based on its performance in relation to the intended

design. Material indices measure the performance of a material, which can be influenced by one or a combination of properties.

The **supporting information** stage is designed to identify potential issues and explore recent advances related to the material in question. This stage typically involves the presentation of descriptive, graphical, or visual data such as case studies, insights into corrosion behaviour, and information on material availability and pricing. Such data can be obtained from handbooks, datasheets, or online resources. The supporting information helps refining the material shortlist and guides the selection process. Local conditions, such as equipment compatibility and supplier availability, may also influence the final decision. By using systematic selection methods and a thorough understanding of material properties, engineers can design high-performance products. It is important to consider all materials in the early stages of design, without dismissing unfamiliar options, as they may ultimately prove to be the best choice [35].

2.2.5. Computer-aided design

The advent of digital technologies has profoundly impacted the way products are designed, analysed, and manufactured. In the present era, the creation of construction drawings or detailed designs without the assistance of computers is a challenging prospect, given the intricate nature of contemporary requirements and the necessity for dynamic resizing and customisation [38]. Among the most influential tools are CAD, Computer-Aided Engineering (CAE), and Computer-Aided Manufacturing (CAM), which play a central role in addressing the challenges of contemporary industries by streamlining the product lifecycle. From the initial conceptualisation stage to the final production phase, CAD, FEA, and CAM facilitate optimised workflows and ensure the delivery of products with enhanced precision and performance [39]. In addition to their contributions to efficiency and quality, these technologies also promote sustainability by minimising environmental impact. For instance, the replacement of physical prototypes with FEA simulations reduces the resource consumption and lowers the carbon footprint of the design process.

CAD, or Computer-Aided Design and Drafting (CADD), is a transformative technology that provides professionals with the ability to digitally design, draft, and generate technical documentation. By supplanting conventional manual and industrial drafting techniques, CAD facilitates the design process, enabling work in both two-dimensional and three-dimensional formats with enhanced precision and efficiency. This technology is founded upon a parametric methodology, which affords designers the ability to expeditiously develop and modify designs, adjust dimensions and parameters, and evaluate multiple concepts without the necessity of beginning again from the initial stages [40, 41]. Furthermore, the rendering capabilities of this technology facilitate the production of photorealistic visualisations, thereby facilitating effective communication of design concepts to stakeholders and ensuring transparency and clarity throughout the design process [40].

Once the 3D model has been completed, a FEA, which is the main subset of **CAE**, can be performed to evaluate the design's structural viability. This technique determines stresses and deflections in the structure by dividing it into smaller and simpler elements with known shapes

for which a mathematical solution can be found. The problem is then solved by using an assembly procedure [39]. There are three main stages to FEA: pre-processing, result generation, and post-processing, all of which critical to producing accurate and reliable results. The pre-processing stage is the most time consuming and involves dividing the structure into a mesh of finite elements. The choice of mesh type is critical as it affects both the accuracy and computational efficiency of the analysis. The mesh should be refined enough for accuracy but not overly detailed to avoid unnecessary computational time. At this stage it is important to define the analysis dimensions (1D, 2D, or 3D) and select the appropriate mesh element type (axisymmetric, plate, or shell). Material properties (such as elasticity and density) and boundary conditions (such as supports and forces) must also be defined to ensure that the model reflects real-world conditions. The next step involves the software generating a system of equations to describe the behaviour of the structure. The final post-processing phase focuses on analysing and evaluating the results provided by the software (Figure 15) [42].

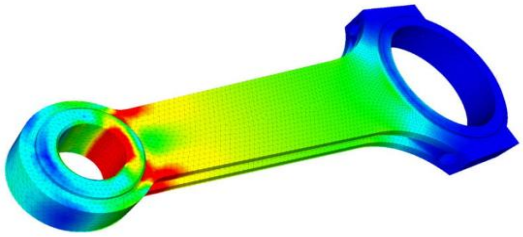

Figure 15 - FEA simulation of piston rod [43].

CAM refers to the utilisation of software for the creation of programs for computer numerical control (CNC) machines and finding optimal machining conditions. CAM facilitates the streamlining of a multitude of manufacturing processes, including milling, turning, turn-mill operations, cutting, probing, part inspection, and even additive manufacturing such as 3D printing. By converting digital models into machine instructions, CAM ensures precision and efficiency in the production of physical components. [40]. The integration of CAD, FEA and CAM enables the creation of a unified workflow from concept to production.

2.2.6. Joining methods

Industrial products frequently necessitate the utilisation of sophisticated manufacturing techniques, given the intricate shapes that are often inherent to such products. To address this challenge, the industry has traditionally employed two distinct technology groups: subtractive and neutral. However, industrial products are often constituted of multiple components, rather than a single, unified entity. To reduce costs and streamline the manufacturing process, these components are designed to be smaller and less complex prior to assembly, leading to the integration of additive technology [44].

Subtractive technology encompasses processes like machining and cutting. Machining involves successive passes of one or more tools to remove material until the desired shape is achieved, making it ideal for applications requiring high dimensional accuracy. Cutting, on the other hand, is a widely adopted method used extensively for sheets, tubes, and profiles. This process

employs various techniques, including press cutting, laser cutting, and water jet cutting, to achieve precise results [45].

Neutral technology focuses on reshaping material from its initial form into an intermediate or final shape with minimal material loss. Techniques such as rolling, forging, inlaying, stamping, and bending fall under this category, as these efficiently manipulate material flow without significant waste [45].

Additive technology encompasses a range of processes, including adhesive bonding, bolting, and welding, which possibly require the use of external materials to bond two components. In this context, it is essential to consider several factors, such as the type of material being bonded, the loading on the joint, and the area to be bonded. By taking these factors into account, it is possible to select the most appropriate additive technology for a given application.

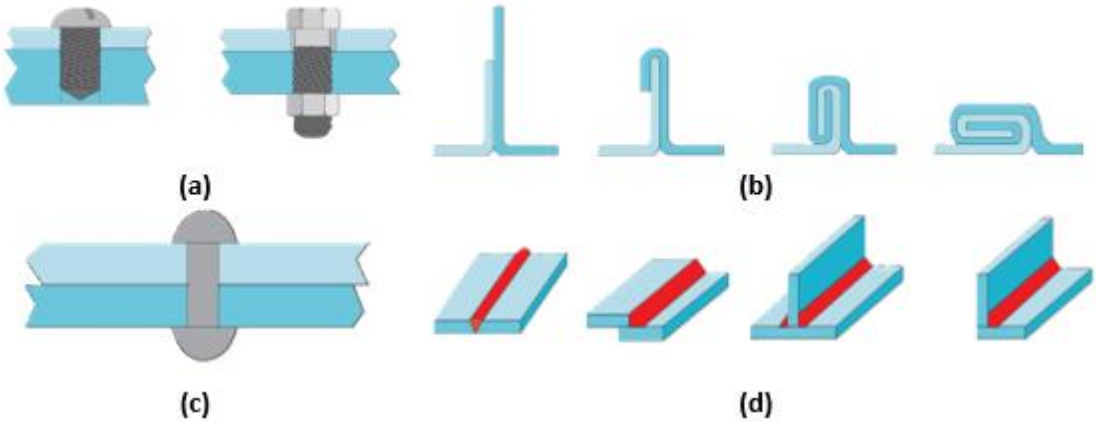

Figure 16 - Bolted joint (a), riveting (b), plastic forming (c) and welding (d) (adapted from [45]).

The utilisation of additive technology enables the creation of non-permanent joints, such as bolted joints (Figure 16a), which permit the separation of components when necessary. It is also possible to utilise permanent joints, such as riveted (Figure 16b), plastically formed (Figure 16c), welded (Figure 16d), and adhesive bonded, which facilitate the creation of a fixed and durable connection [45]. The processes of riveting and plastic forming are fundamental to the field of manufacturing, with applications across a range of industrial contexts. Riveting involves the mechanical fastening of components through the deforming of a metal pin, creating a secure joint. In contrast, plastic forming encompasses the reshaping of materials through deformation techniques, including bending, rolling, and forging, without the removal of material, thereby preserving the structural integrity of the material [46]. However, it should be noted that joints are inherently vulnerable, either due to mechanical or chemical factors. For instance, it has been observed that numerous failures in fatigue or corrosion tend to manifest at welded joints. Furthermore, from an efficiency standpoint, the process of joining can also present challenges. It frequently necessitates the use of additional components, such as fasteners, bolts, or welding filler metal, to secure the connection. This feature not only increases the complexity of the overall structure but also requires the application of higher safety factors. As a result, the introduction of extra weight is necessary to satisfy the structural requirements, ultimately reducing overall efficiency [44, 45].

Bolted joints are one of the most common ways to connect components in engineering [47], leading to high standardization [48]. This connection can work by using a bolt and nut (Figure 17b) to clamp parts together through a hole that passes through both components, or the bolt fastened directly in one of the two parts (Figure 17a) [47]. When using a nut, the threads on the bolt and nut ensure that the joint stays tight holding parts securely under compression. This initial compression creates a preload before any external load is applied [39].

Figure 17 - bolted connection using a nut (a) Bolted connection fasteners in a part (b) (adapted from [45]).

Nevertheless, the design of reliable bolted joints necessitates meticulous consideration of the stresses to which they will be subjected. These include mechanical loads, temperature variations, and exposure to corrosive environments, which have the potential to significantly impact joint performance [48]. Bolted joints can be categorized based on the mechanical loads, such as tension and shear (Figure 18).

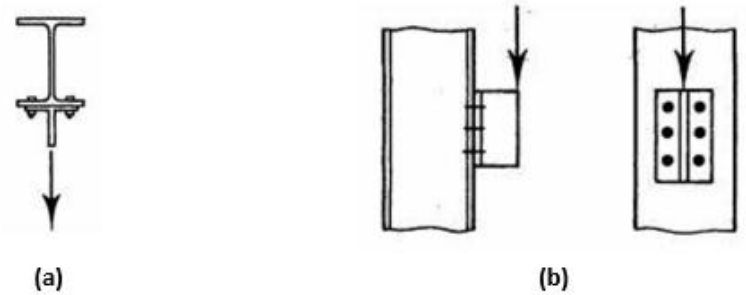

Figure 18 - Bolts subjected to tension load (a) and shear load (b) [49].

Tension connections can be classified as non-preloaded and preloaded. It is inadvisable to utilise non-preloaded connections in instances where the connections are subjected to frequent variations in tensile loading. However, these may be employed in connections designed to resist typical wind loads. Preloaded connections offer a significant advantage in demanding applications, as they enhance stiffness and reduce the risk of fatigue failure [50, 51].

Welding process is one of the metallic components joining with the best cost-benefit relation. This joining method is permanent, but still versatile being to be used in various range of materials, shapes, and dimensions. Usually, the strength of the joint is higher than the base material and welding permits secure a metallic continuity. Basically, welding can be done by two simple processes [45]:

- Fusion, the energy is given by electricity or by burning a gas or mixture of gases, providing the union by the mixture of the materials (base material and additive material);

- Mechanical energy, caused by the melting of the material. In this case, friction or impact are usually used to achieve the desired objectives.

Under the proper conditions, all steels can be welded. While designing welded components, it is preferable to select a steel that will result in a fast, and economical weld, although sacrificing other qualities such as machinability.

In recent years, adhesives have become increasingly popular for joining components in structural, semi-structural, and non-structural applications [50]. The process of adhesive bonding entails the application of an adhesive between the surfaces of two adherents, which then undergoes a solidification process to form a strong and durable bond. By joining two materials, adhesive bonding relies on physical or chemical interactions at the interface to ensure effective adhesion. The adhesive bond offers unique properties, such as the ability to distribute stress more evenly throughout the joint to ensure structural integrity. As illustrated in Figure 19, the adhesive bonding process can be divided into four principal bonding mechanisms: mechanical interlocking, physical bonding, diffusion, and chemical bonding. Each mechanism fulfils a specific function, and its efficacy may vary depending on the materials and preparation methods employed [52, 53]:

- **Mechanical interlocking** relies on the voids and irregularities in the adherent surface to increase the contact area, resulting in greater mechanical interlock and the formation of an effective bond. Surface preparation techniques are essential to improve surface roughness, which plays a critical role in promoting mechanical interlock [54];
- **Diffusion bonding**, which is predominantly used with thermoplastics, involves the application of a solvent to facilitate the diffusion of adherent materials near the interface;
- **Chemical** bonding is dependent upon the interplay of intermolecular forces and chemical reactions, permitting the creation of robust connections between surfaces. These bonds may involve covalent or ionic interactions, hydrogen bonding, and Van derWaals forces. Covalent bonds form through the sharing of electrons between atoms, while ionic bonds result from electrostatic attraction between oppositely charged ions. Additionally, hydrogen bonds and van der Waals forces provide supplementary adhesive strength, particularly in polar and non-polar materials [53].

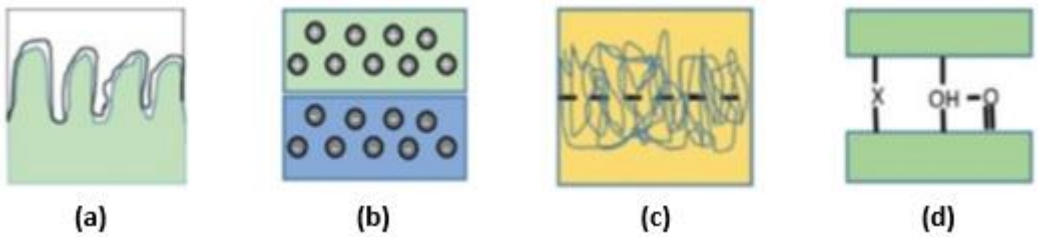

Figure 19 - Mechanical interlocking (a), physical bonding (b), diffusion bonding (c), and chemical bonding (d) [52].

To achieve effective adhesion, it is essential to ensure proper wetting of the adherent surfaces. Wetting refers to the ability of a liquid to spread across a solid surface and is fundamentally

influenced by the contact angle, surface energy, and surface tension. The contact angle (θ) is a critical parameter in this context and is defined as the angle formed between the solid surface and the tangent to the liquid surface at the point of contact. This angle can vary from 0° (complete wetting) to 180° (no wetting), corresponding to the form of an almost perfectly spherical droplet (Figure 20).

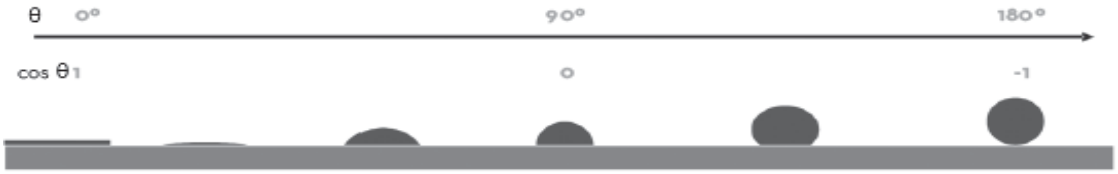

Figure 20 - Different angles of a drop [55].

Surface tension, a macroscopic expression of the cohesive forces between molecules or atoms at the interface of a liquid and its surrounding medium, plays a key role in the behaviour of liquid surfaces. In particular, a higher surface tension corresponds to a lower wetting capacity, as the cohesion of the liquid resists spreading over the solid surface [55, 56]. A wide range of joint configurations can be used to join structures; each tailored to specific applications and each offering distinct advantages. The overall topology of joints can be divided into two categories (Figure 21): perturbed and undisturbed shapes. Disturbed is defined as a joint topology with one or more offsets between the bonds, whereas undisturbed is defined as a joint topology where the bonds are aligned [57].

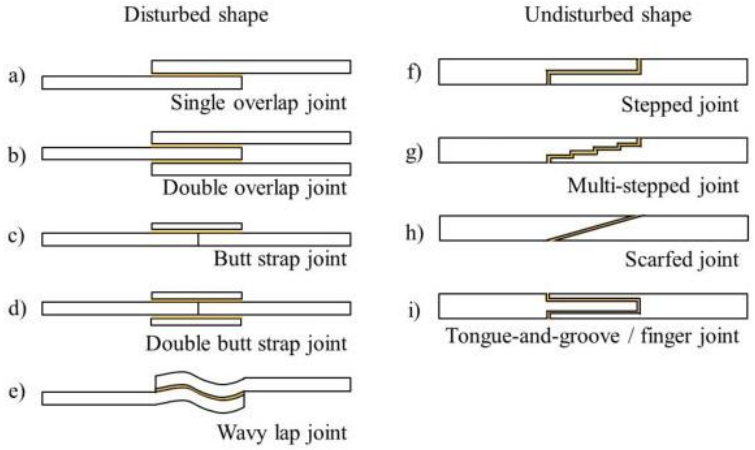

Figure 21 - Possible geometry of adhesive joints [57].

After exploring a variety of joining methods, it becomes clear that combining some of them can deliver superior performance. This innovative approach, known as hybrid joining, merges the most advantageous features of each individual method. For that, adhesives are most often integrated with other processes due to their many advantages. The adhesives commonly used in hybrid joining are structural adhesives, such as epoxy, polyurethane, acrylic, cyanoacrylate, anaerobic, and high-temperature adhesives. These adhesives are selected to ensure bonding of elements, offering high modulus and strength, as well as durable and permanent connections [58]. The combination of welding and bonding (Figure 22) has been practised since the mid-1950s. However, as it has evolved, a more advanced and efficient method is to apply adhesive to the components prior to resistance spot welding and then cure the adhesive. While adhesive

bonding alone lacks initial strength, this limitation is effectively overcome by combining it with a thermic or mechanical joining technique. The hybrid approach exploits the more uniform stress distribution of adhesives and the instant mechanical strength of spot welding, resulting in a highly effective solution for modern manufacturing processes [59].

Figure 22 - Weld-bonded joint [58].

Another effective combination is the use of fasteners and adhesives (Figure 23), which overcomes the individual limitations of each method when joining dissimilar materials, such as composites or composites with metals. In this hybrid approach, the fastener provides support for axial loads, while the adhesive relieves some of the stress on the fasteners and provides a more uniform redistribution of the remaining loads across the joint [58].

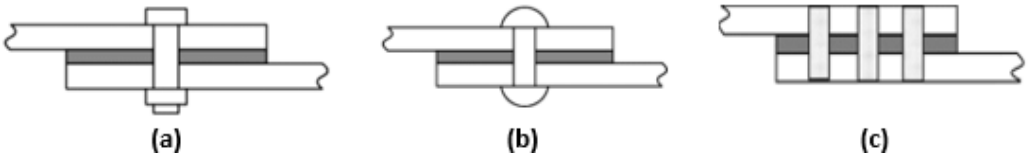

Figure 23 - Bolted-bonded joint (a), rivet-bonded joint (b), and pin-bonded joint (c) [58].

2.2.7. Adhesive selection and testing

Adhesives have become an indispensable component of the engineering industry, particularly due to their capacity to securely fasten and join disparate materials. A multitude of adhesive families exist, encompassing a vast array of standard formulations while also offering the flexibility to develop bespoke solutions tailored to specific design and performance requirements [60]. The process of selecting the most suitable adhesive can be very complex due to the wide variety of available adhesive types and the lack of a universal adhesive suitable for all applications [50, 58]. Figure 24 provides a comprehensive overview of the most common requirements and expected performance characteristics of a given adhesive family, offering a valuable starting point for the selection process [60].

	Viscosity (thick-ness)	Void filling	Heat resis-tance	Cold resis-tance	Flexibility	Chemical resis-tance	Humidity resis-tance	Work time	Cure time	Metal bonding (steel, alum.)	Plastic bonding (abs, styrene)	Polyolefin bonding	Wood	Paper card-board
Acrylic	M	G	G	G	G	G	G	FT–M	M–FT	G	VG	F	NS	NS
Anaerobic	L	P–F	G	G	G	G	G	M	M	F	P	NS	NS	NS
Cyanoacrylate	L	P–F	F	F	P–F	G	F	FT	FT	G	VG	G	NS	NS
Epoxy	M–T	VG	G	F	F	G	G	M–S	S	G	F	P	G	NS
Hot melt	T	VG	P–F	F	F–G	F	G	FT	FT	F	F	P	VG	VG
Polyurethane	M	G	F	G	G	G	F	M–S	M	G	VG	G	NS	NS
Polysulfide	T	VG	G	G	G	VG	G	M	M	G	F	NS	NS	NS
Silicone	T	VG	VG	VG	VG	VG	VG	S–M	M	F	F	F	NS	NS
Solvent-base	L–M	F	G	G	G	G	G	S–M	M	G	F	F	G	G
Water-base	L–M	P	F	F	P	P	P	M	M	P	P	P	VG	VG
UV	L–M	L–M	F	G	G	F	G	S	FT	G	G	F	F	F

F Fair; FT Fast; G Good; L Low; M Medium; P Poor; S Slow; T Thick; VG Very Good; NS Not Suggested

Figure 24 - Selection chart for determining appropriate adhesive family [60].

The adhesive selection is further compounded when it comes to bonding dissimilar materials, as it becomes critical to select an adhesive whose properties properly adhere to both substrates. In addition, certain substrate materials can adversely affect the bond strength of adhesives, either through chemical or physical interactions. Chemically, the presence of certain ionic or molecular species can weaken the bond. Physically, factors such as low energy surfaces and roughness can also reduce adhesive performance. In contrast, the selection and sizing of a bolted joint is often simpler, with established strength data and standardized grades and dimensions [61]. To simplify the selection of the most suitable adhesive for a given application, several key factors should be assessed [58]:

- The type and nature of the substrates to be bonded;
- The curing process and adhesive application method;
- The environmental conditions the bond will encounter during service;
- The stresses that the joint will experience under service conditions.

However, an incorrect joint selection can lead to joint failure. Understanding the cause of failure is critical to improving joint selection in future applications. When failure occurs, it is important to analyse and identify the type of failure [52]:

- **Adhesive or interface failure** (Figure 25a) is the most common type and occurs when the bond strength between the adhesive and the adherend is insufficient to withstand the applied forces. This failure is often attributed to factors such as poor surface preparation, material incompatibility, or improper curing conditions;
- **Cohesive failure** (Figure 25b) occurs in the adhesive material itself, indicating that the adhesive has been unable to withstand the stresses applied. This type of failure can result from overloading or exposure to conditions that exceed the inherent strength of the adhesive;
- **Substrate or adherent failure** (Figure 25c) occurs in the bonded material, averaging that the bond strength was inadequate for the application;
- **Mixed failure** can occur when the joint is subjected to a complex combination of loading conditions or flaws in the surface preparation, resulting in a combination of failure modes.

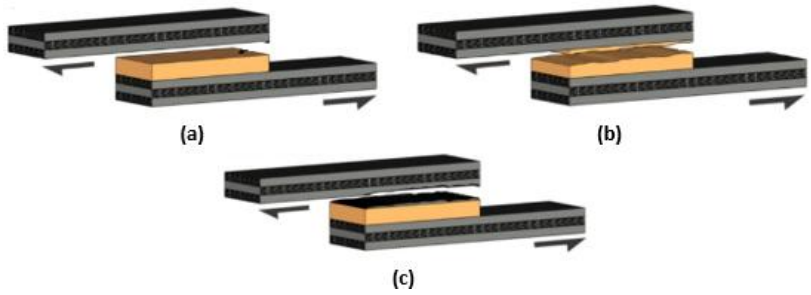

Figure 25 - Different types of failure on adhesives joints [52].

To avoid unwanted failures, testing is essential to ensure the short- and long-term performance of bonded structures. To obtain reliable results, it is common practice to adhere to established

norms and standards [61]. Testing methods generally fall into two main categories: destructive and non-destructive. As the name suggests, destructive testing damages the structure, while non-destructive testing leaves it intact.

Several types of destructive tests are commonly applied to adhesive bonds, including shear, tensile, peel, and impact tests. Since adhesives are most often subjected to shear loads, the lap shear test remains the most widely used experimental method to evaluate joint behaviour and strength. This test is particularly useful to identify failure mechanisms such as adhesive or interface failure, cohesive failure, and substrate failure. Two main shear test are used [50, 62]:

- **Single shear test** (Figure 26a): This is the simplest configuration in the category. Its main advantage is its conceptual simplicity. However, the substrates are not collinear, and a bending moment is created leading to significant peel stresses at the overlap ends;
- **The peel test** (Figure 26b) is used to specifically assess the bond quality of the in scenarios involving peel between rigid and a flexible assembly part. This test is particularly useful for comparative evaluation of adhesives and surface treatment methods. It provides valuable information about the adhesion and cohesion properties of the adhesive layer [63];
- **Double shear test** (Figure 26c): This configuration solves the problem of load offset by applying the load symmetrically, ensuring that the adhesive layer receives a centred load application. This configuration provides a more accurate representation of the shear behaviour.

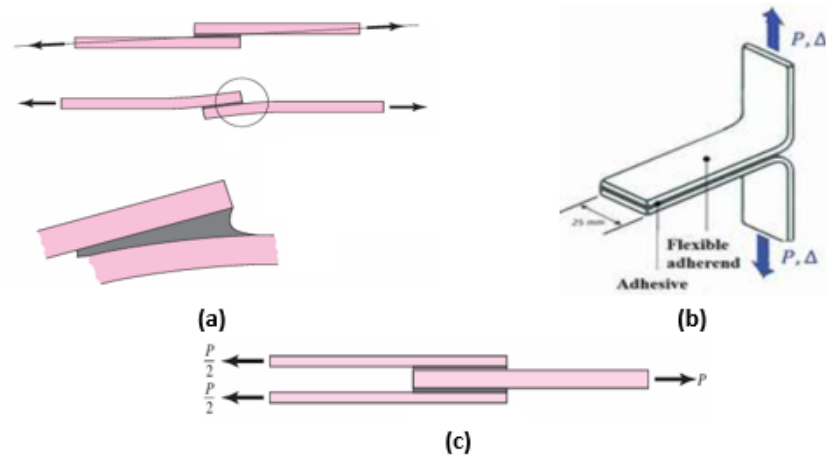

Figure 26 - Single shear test (a), peel test (b), and double shear test (c) (adapted from [50, 63]).

Further tests can be carried out to better characterise the adhesive properties. Dynamic loading such as shock, impact, and vibration can lead to fatigue and eventual failure of the system. Vibration outputs such as natural frequencies, damping ratios, and mode shapes provide knowledge for interpreting the dynamic behaviour of the bonded joint [59]. However, to fully understand the long-term performance of the bond, accelerated ageing tests can be performed to reduce the time required to evaluate material response. It is important to correlate test conditions with actual service exposure and identify failure modes that reflect realistic end-of-life scenarios. Accelerated ageing can be achieved by methods such as increasing temperature, loading, or exposing materials to higher concentrations of degrading chemicals. Care must be

taken to avoid introducing degradation mechanisms that do not occur under normal service conditions to ensure that the results are relevant to real-world applications [64].

Non-destructive testing methods can also be applied to bonded joints, offering the advantage of assessing the integrity of the joint without causing damage. The primary objective of any non-destructive test is to establish a correlation between the strength of the bond and measurable physical, chemical or other parameters without inducing damage. These tests can be performed either before or after the bonding process [65]:

- **Pre-bonding** testing ensures proper surface preparation and suitability of the bond. Key methods include assessing surface wettability (measuring how water spreads on a surface to confirm cleanliness) and advanced techniques such as the Fokker contamination test, which detects surface contamination by measuring electron emission energy;
- **Post-bonding** inspections verify the quality of the bond. These range from simple visual inspections to detect visible defects such as holes, to advanced methods such as ultrasonic testing, thermal imaging, and radiography to detect internal defects.

In summary, testing adhesive joints is essential for ensuring their reliability and durability in various applications. Pre-bonding tests confirm the proper preparation of surfaces, while post-bonding tests validate the quality of the final bond. By combining these methods, manufacturers can achieve stronger, more consistent joints, and mitigate potential failures.

2.3. Sustainable pallet design

The concept of sustainability can be divided into three important factors, namely economic, social, and environmental sustainability. Authors name those factors differently, which include components [66, 67], aspects [68-70], perspectives [71, 72], or pillars [73-76]. This tripartite description is often, but not always, presented with the three different factors as being of equal importance, as shown in Figure 27a) and b). This representation is intended to expose the idea that society can only achieve sustainable if all three parts of sustainability are equally supported. However, this representation reflects a model of weak sustainability as it inaccurately suggests a balance between the three dimensions. For that, the economy should function as a subsystem within society, which in turn exists as a subsystem of the environmental domain, as shown in Figure 27c) [77].

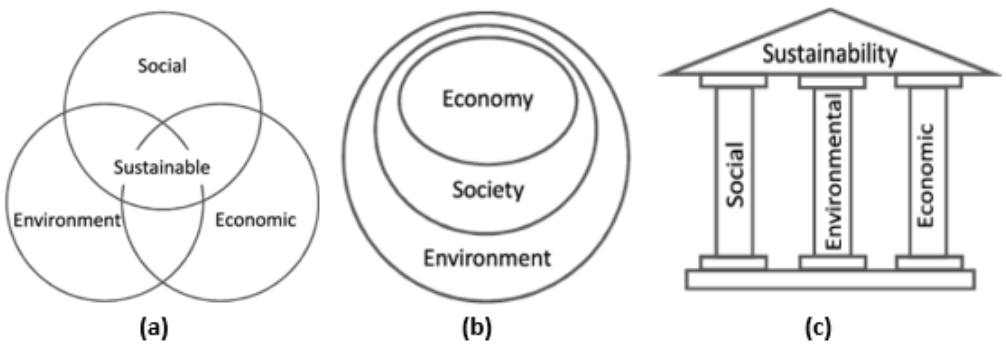

Figure 27 - The various forms as a descriptor of sustainability [77].

2.3.1. Contextualization to sustainable pallets

As companies work to enhance the efficiency and sustainability of their supply chains, it is essential to critically assess every aspect of their shipping and distribution processes to fully understand and mitigate their environmental impact. Pallets serve as a cornerstone of product handling and transportation, playing a vital role at all levels of the supply chain and significantly influencing logistical efficiency, and ecological outcomes [78, 79]. As shown in Figure 28, the global pallets market size was valued at USD 59.91 billion in 2018 and it is projected to reach USD 128.68 billion by the end of 2032 [80].

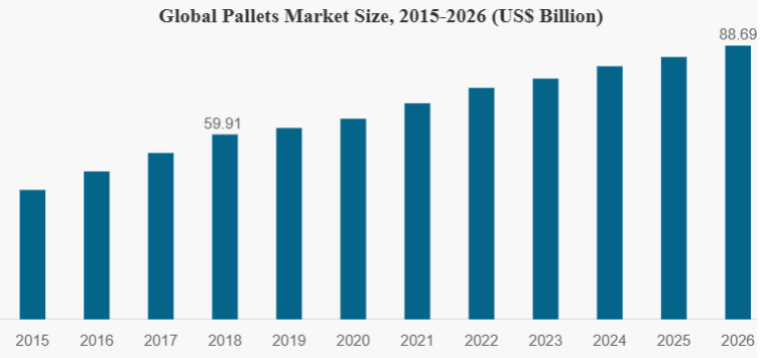

Figure 28 - Global pallets market size, 2015-2026 (US$ Billion) [80].

However, the vast scale of pallet usage brings environmental concerns to the forefront. As illustrated in Figure 29, 86.5% of produced pallets in 2018 were made of wood [80]. This intensive use of wood for pallets can be explained due to their strength and their easy manufacturing. On the other hand, plastic pallets, while offering enhanced durability and reusability, have intrinsic environmental implications. These pallets are predominantly manufactured from plastic derived from fossil fuels, resulting in elevated carbon emissions throughout the production process. Furthermore, the disposal of these materials at the end of their useful life presents a significant challenge, as plastic pallets are inherently difficult to recycle and frequently contribute to long-term environmental contamination [78, 81]. Overall, the traditional reliance on wooden and plastic pallets raises pressing questions about resource consumption, waste management, and overall sustainability. As companies and governments strive to address climate change and environmental degradation, the need to reconsider pallet design and materials has become more urgent than ever [81].

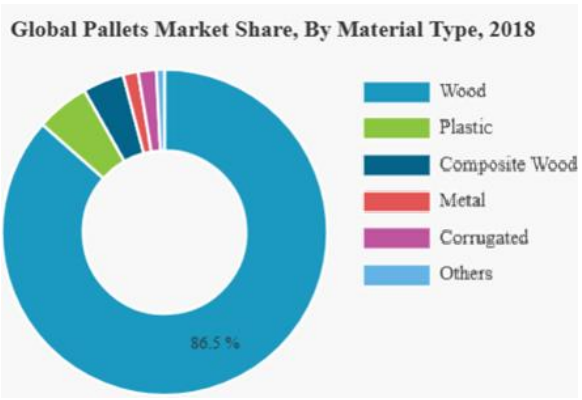

Figure 29 - Global pallets market share in 2018 by material type (adapted from [80]).

2.3.2. Sustainable design

Nowadays, sustainability has assumed a central role in society. The prevailing challenges confronting the industry pertain to maintaining competitiveness through the optimisation of system while maintaining good cost and service levels, whilst concomitantly mitigating adverse environmental impacts [82]. The proliferation of products traversing extensive and dispersed supply networks has given rise to significant concerns regarding the sustainability of the packaging utilised for these goods [83]. To respond to the growing demand for sustainability, the packaging industry must incorporate the potential environmental impacts into the fundamental design process. As demonstrated in Figure 30, companies should aspire to the optimal packaging system, which lead to a balanced equilibrium of cost and packaging material, while still taking into account carbon dioxide (CO_2) emissions [13].

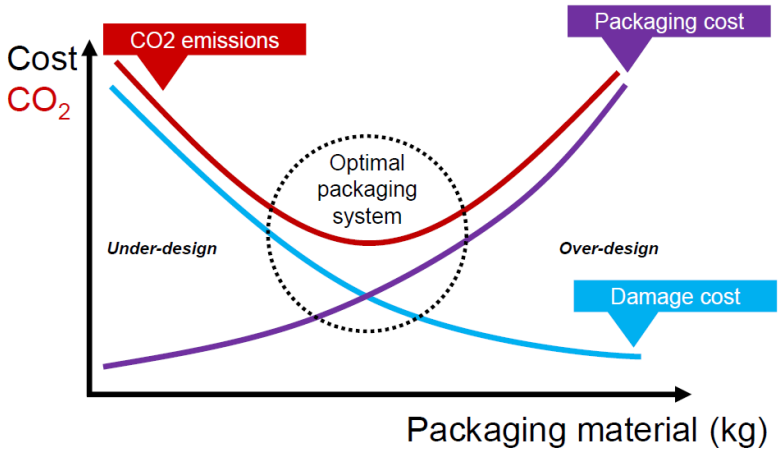

Figure 30 - Sustainable design approach [13].

The increase in the quantity of waste and emissions have a significant impact on the environment. To mitigate this effect, the four Rs provide a framework to control and ultimately reduce the growing waste and emissions. The four R´s stand for [13, 84]:

- **Recycling:** This process entails the transformation of aged and utilised materials, and components, or components into new entities, whether for the same function or a distinct one. This concept can also be integrated into the initial product design by creating easily recyclable solutions, by incorporating high recycled content, and aiming for products with strong circularity potential;
- **Reusing:** This practice encourages a non-linear approach to product utilisation, whereby items are utilised multiple times before being disposed of. This approach serves to extend the lifecycle of the items in question;
- **Recovering:** This concept is centred upon the design of products with a view to facilitating their repairability by simplifying the assembly and disassembly. This approach enables the restoration and reuse of the products at the conclusion of their useful life;
- **Reducing**: This practice aims to prevent waste from being generated, which is intrinsically linked to recycling, reusing, and recovering. The adoption of these practices

results in a decrease in the need of raw materials, thereby minimising environmental strain.

The implementation of the four R´s has the potential to significantly minimise waste production and contribute to the development of a circular economy [84]. In this context, pallets, which are widely used in logistics and transportation, offer a prime example of these principles in action. These can be recycled into new materials, reused across supply chains, repaired to extend their lifespan, and ultimately reduce the need for virgin resources. The optimisation of pallet management through the four R's not only enhances sustainability but also demonstrates how thoughtful design and usage can drive positive environmental change [83, 85].

2.3.3. Materials for sustainability

The role of materials in achieving sustainability is crucial. These form the foundation of all products and structures, impacting the environment at every stage of their lifecycle. Sustainable materials aim to reduce resource consumption, lower emissions, and create value throughout their use and reuse. Sustainable materials can be defined as materials derived from renewable resources. These materials must have a zero/minimal impact on the environment and society for their extraction and production. Examples are recycled metals, bio-based polymers, and materials for renewable energy [86].

In Europe, packaging represents 39.6% of the total use of plastics, which are often composite materials. Since packaging is the most important sector for the plastic demands, this sector has an urgent need to implement new sustainable packaging materials [87]. The research activity concerning alternative packaging obtainable from sustainable resources (for example starch, poly (lactic acid), chitosan), is currently very active, aiming to find suitable alternatives to polymers derived from fossil fuels. Cellulose is another material that can be used to produce new sustainable composites, able to produce biodegradable films with several applications, such as single-use goods [86].

However, any transportation of goods, by plane, rail or road while, most of the time, is carried out using pallets. Pallets can be made from various materials, depending on load and protection requirements. Wood is regarded as the most sustainable and durable material that can be chosen. Wooden pallets are recyclable, which averages that they can be used for several purposes once their usefulness as pallets has come to an end. Parts of old pallets can also be incorporated into new pallets, and pallet parts that have been damaged or became worn can be replaced. A pallet that can be used and refurbished and used again is an eco-friendly choice [88].

2.3.4. Product life cycle

The product life cycle is defined as the period spanning from a product’s introduction to the market to its eventual withdrawal from circulation [89]. As illustrated in Figure 31, the product life cycle is typically comprised of four distinct stages. However, prior to entering these stages, a product must undergo a preliminary phase involving design, research, and development. Once

a product has been determined to be both feasible and commercially viable, it transitions to the subsequent stages of production, marketing, and distribution, thereby signifying the commencement of its life cycle. As illustrated in Figure 31, upon its introduction to the market, the product may experience an augmentation in demand from customers. After this, demand will reach a state of stability, which is characterised by maturity in Figure 31. Ultimately, demand will undergo a decline as new products emerge [90].

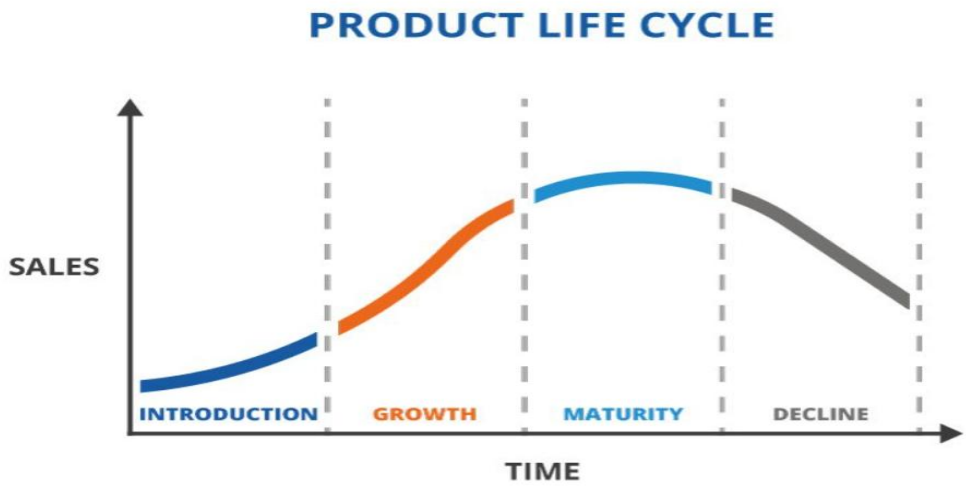

Figure 31 - Product life cycle [90].

The **introduction stage** constitutes the initial presentation of a novel product to customers, during which businesses typically incur considerable expenditures on advertising and promotional endeavours to generate awareness. From a financial perspective, this phase frequently yields unfavourable outcomes, as sales volumes tend to be modest. Promotional pricing strategies may be employed to stimulate customer engagement, while marketing expenses remain elevated, and the sales strategy undergoes refinement. If the product proves successful, it transitions to the **growth stage**, during which it attains popularity and market recognition. This phase is characterised by increased sales and revenue growth, reflecting the product's strengthening foothold in the market. The **maturity stage** represents the most profitable phase of the product life cycle, during which production and marketing costs typically decline as economies of scale are realised. Companies may explore opportunities for innovation or consider strategies to enhance their market share, such as product differentiation or diversification. As rival companies replicate the successful product, market share may be lost, and the onset of the **decline stage** may be indicated. During this phase, product sales may decrease due to market saturation or the emergence of alternative products. In response, companies may choose to rejuvenate the product through significant upgrades or by launching a next-generation model. If the improvements are substantial, the revamped product may re-enter the product life cycle as a newly introduced offering [89, 90].

However, the product life cycle can be more elaborate depending on the product. Pallets can have different life cycles, which can be divided into two configurations (Figure 32):

- Open-loop;
- Closed-loop.

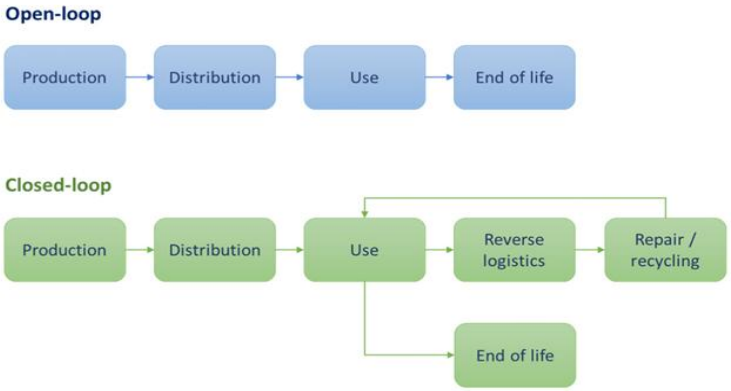

Figure 32 - Supply chain configurations (adapted from [91]).

An **open-loop configuration**, pallets are regarded as disposable assets, which are discarded after their final use. Within this supply chain, pallets are manufactured and distributed to users, who utilise them for transportation and storage purposes throughout their operations. Upon reaching the final user, various end-of-life options can be implemented. Pallets may either be shredded and separated for recycling or disposed of directly in a landfill. In the case of wooden pallets, the steel from nails can be recovered for recycling, while the wood material can be repurposed through incineration (with or without energy recovery) or transformed into mulch, animal bedding, or wood pellets [78, 91].

A **closed-loop configuration**, as shown in Figure 33, is more complex than the open-loop. The objective is to recover used pallets with the intention of repairing them (when feasible) and reusing them in subsequent transportation cycles. Following the utilisation phase, which typically encompasses multiple duty cycles, the pallets are transported to a recovery centre where they are inspected, repaired, and returned to service. Where a pallet is determined to be irreparable, it is either disposed of in a landfill or sent to recycling manufactures [78, 91].

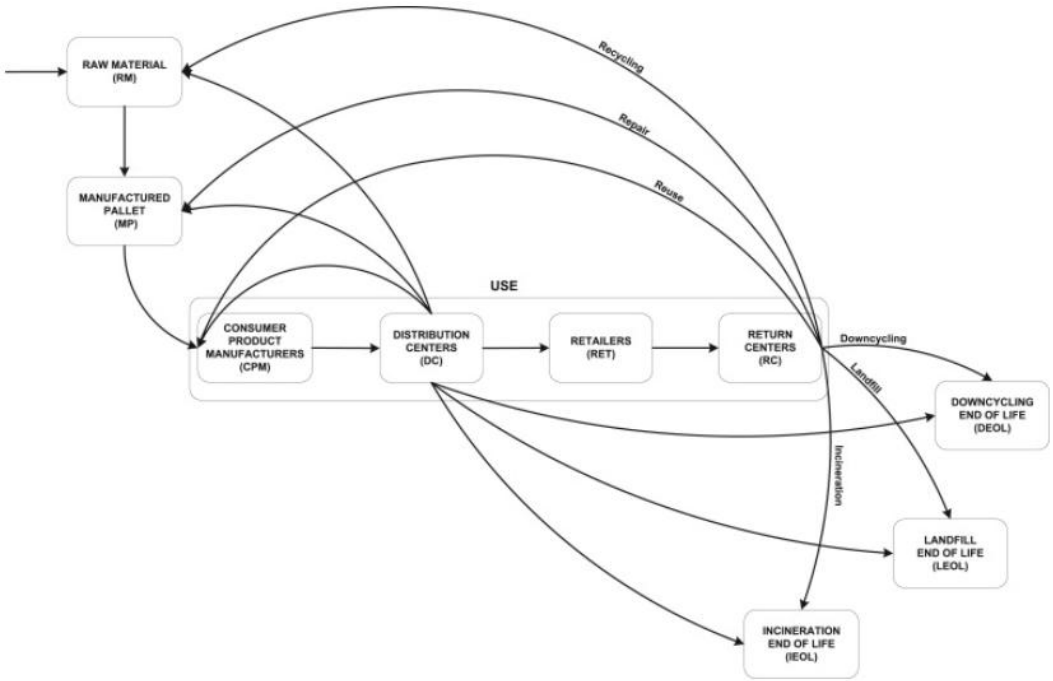

Figure 33 - Product life cycle of pallets (closed-loop) [78].

2.3.5. Measurement of sustainability

To advance towards a more sustainable industrial sector, it is essential to establish mechanisms to measure sustainability. In this context, a wide range of Key Performance Indicators (KPIs) are available to facilitate this assessment. These indicators can be defined as tools to quantify the efficiency and effectiveness of specific activities. Consequently, a performance indicator functions as a metric that can be utilised to evaluate and measure the efficiency and effectiveness of an action or process [92]. These indicators can be applied across various domains, including financial, customer, environmental, and social perspectives. However, the environmental KPIs emerge as one of the most frequently utilised metrics within industrial contexts [93, 94]. The utilisation of environmental impact KPIs facilitates the measurement and evaluation of the environmental effects across the entire supply chain. This process ensures that organisations remain aligned with their ecological objectives and comply with regulatory requirements. The most environmental KPIs are the following:

Energy consumption is related to both economic and financial aspects, as well as environmental considerations [95]. It quantifies the energy consumption involved in supply chain operations [96]. By doing so, it helps identify areas of inefficient energy use in the production and delivery of goods and services. Subsequently, the identification of areas of inefficient energy consumptions lead to the need of the implementation of renewable energy sources, which have a lower environmental impact [93, 95].

Material consumption main objective is to quantify the materials utilised in supply chain operations. Analogous to energy consumption KPIs, these indicators facilitate the identification of inefficiencies within the supply chain. Such inefficiencies may be attributed to the use of non-renewable materials or excessive consumption of certain materials, thereby highlighting areas where improvements can be made to enhance sustainability [93, 97].

Carbon footprint is the total amount of greenhouse gases (GHGs), primarily CO_2, emitted either directly or indirectly by an individual, organization, event or product. It is measured in carbon dioxide equivalents (CO_2e), a standardized measure that considers the different global warming potentials of different greenhouse gases, such as methane and nitrous oxide [98]. To calculate the GHGs, it is necessary to have data about all possible emissions during the product life cycle. The data will be then multiplied by the respective emissions factors [99].

Waste in industrial processes refers to activities that consume resources without adding value to the final product [100]. Waste KPIs involve monitoring the quantity, type and management of waste generated by an organisation or system. These indicators are critical to optimize the resource use and aligning practices with sustainability goals such as waste reduction, recycling and moving towards a CE. However, waste management is a broad concept that can be broken down into different KPIs, each addressing specific aspects of waste generation, treatment, and minimisation [93, 101].

As previously mentioned, a variety of KPIs can be utilised in an industrial context. These indicators enable companies to measure corporate sustainability performance, providing data that can inform the development of strategic plans. In this regard, the modern digital transition

and Industry 4.0 (I4.0) technologies play a crucial role. Industry 4.0 refers to the fourth industrial revolution, characterised by the integration of digital technologies into manufacturing and industrial processes. This transition assists companies in defining and implementing sustainability by correlating production with key metrics, thereby enhancing efficiency, reducing environmental impact, and fostering sustainable growth [94].

2.3.6. Evaluation for sustainability

In the contemporary era, characterised by mounting environmental challenges and the pressing necessity for sustainable development, software and digital tools have emerged as potent instruments in catalysing substantial change. These instruments empower organisations, governments and individuals to meticulously monitor, measure and mitigate their environmental impact. A salient example of such instruments are carbon footprint calculators, which furnish users with insights into their emissions, and energy management systems, which optimise resource utilisation. Software thus empowers users with actionable data and strategies to measure sustainability [102]. Beyond environmental monitoring, sustainability tools are instrumental in fostering circular economies, enhancing supply chain transparency, and aligning operations with the United Nations' Sustainable Development Goals (SDGs). As technology continues to evolve, the integration of artificial intelligence into sustainability efforts promises innovative solutions to global challenges, making software an indispensable component of the quest for a greener future [103].

In the context of mounting pressure from multiple stakeholders, businesses are compelled to formulate budgetary provisions for sustainability. In doing so, it is imperative that they are cognizant of the array of instruments and digital platforms at their disposal, which can facilitate the achievement of their sustainability objectives with optimal efficiency and efficacy. The following instruments are of paramount importance for businesses seeking to enhance their sustainability practices and mitigate their environmental impact [104]:

- Carbon management software is utilised for the measurement, management and reporting of carbon emissions, functioning as a tool for the quantification of greenhouse gas emissions and supporting the strategic decision-making process for carbon reduction initiatives. Software platforms such as Sphera® and Plan A® can be employed for this purpose;
- Life Cycle Assessment (LCA) and Product Carbon Footprint software are tools designed to assess the environmental impacts associated with all stages of a product's life cycle. These software solutions enable companies to identify areas for improvement and make informed decisions to mitigate the environmental impacts of their products. Software, such as GreenCalc®, as mentioned in the section 2.1.4, and Plan A® can be employed for this analysis;
- Decarbonisation software refers to tools specifically designed to aid in the planning and implementation of strategies aimed at reducing carbon emissions, transitioning to low-carbon or carbon-neutral operations, and facilitating sustainable transformation.

Typically, such software incorporates features such as emissions data collection, measurement, management, target-setting, reduction planning, and scenario modelling. For these purposes, software solutions such as Footprint Expert® and Plan A® can be utilised.

The utilisation of software and tools for sustainability enables companies to unlock a wide range of benefits. A notable benefit is the enhancement of operational efficiency, as organisations can achieve cost and time savings by automating the collection and calculation of emissions data. Furthermore, these tools facilitate the efficient storage and tracking of historical data, providing companies with valuable insights for informed decision-making and long-term sustainability planning [104].

2.3.7. State of the art

The aim of this section is to present a comprehensive review of the existing literature, theories, and advancements related to the packaging industry. Table 2 highlights examples of scientific studies specifically focused on pallet development.

Table 2 - State of the art in pallets development

Bibliographic reference	Description
Zhang et al. [105]	The article presents a comprehensive framework to enhance sustainability in China's pallet sector through the implementation of sharing systems and CE strategies. Using LCA, it demonstrates a potential reduction in environmental impacts by 95.2% to 97.3%, with greenhouse gas emissions dropping by up to 98.1% under CE practices. However, the utilisation of low-impact materials such as steel and fly ash pallets remains limited, necessitating market adjustments. The challenges identified include limited awareness of CE, and lack of tracking systems. Recommendations have been made to address these challenges, with a focus on enhancing logistics efficiency, optimising pallet reuse infrastructure, and promoting green logistics. These recommendations are intended to provide guidance to stakeholders in China and other global regions.
Dakić et al. [106]	This study investigates the application of augmented reality (AR) in optimising the pallet loading process within industrial and logistics contexts. The development of an algorithm for the Pallet Loading Problem (PLP) has been integrated with an AR system, enabling warehouse personnel to utilise visual guidance provided by scanning QR codes during the loading of boxes onto pallets. The experimental findings demonstrate that the implementation of AR system enhances efficiency and accuracy, leading to a reduction in both time and errors. The study emphasises the potential of AR in material handling and its adaptability to different scenarios, including robotics.

Table 2 - State of the art in pallets development (Continued)

Franke et al. [107]	The objective of this study is to develop a toolchain to detect pallet-related to loads events using Inertial Measurement Units (IMUs) and the SPARL dataset. Two sensors were benchmarked in logistics scenarios, and a random forest classification model was used for activity recognition. The dataset includes videos and sensor data, with preliminary results showing that logistic activities can be detected effectively. The study found that even an untuned random forest model performed well, and that small sampling rates were sufficient, though short-duration activities remained challenging to identify.
Bairapudi et al. [108]	This study sets out to compare 3D-printed bio pallets created using SLA and DLP techniques with traditional methods, with the aim of assessing mechanical properties, load capacity, and surface characteristics in accordance with the ISO MH1-2016 standard. The study found minimal differences (7–12%) in stress and displacement between the two techniques. SLA pallets exhibited higher surface roughness, while both methods provided adequate stability for product placement. The findings of this study suggest that 3D-printed pallets are a sustainable, customisable alternative to traditional materials.

3. Development

3.1. Company presentation

Originally from Sweden, NEFAB is a global company specialising in logistics, digital services, and the design of packaging solutions, with a particular focus on the industrial and transport sectors. The company's growth trajectory aligns with general industry trends towards sustainability and reducing environmental impact. The company's strategic emphasis on formulating packaging solutions that offer protection while being ecologically sustainable, through the conservation of resources, is an important factor in its continued growth and success.

During the 1980s, NEFAB initiated an international expansion strategy, establishing a global presence and enabling the company to more effectively serve a diverse range of customers across multiple regions. Presently, NEFAB has a global footprint, with a presence in 38 countries worldwide, as illustrated in Figure 34. The company employs a total of 4900 individuals across various departments, including engineering and production. Furthermore, NEFAB owns six testing laboratories across Europe, America and Asia, which are certified by ISTA, permitting the research and development of new materials or types of packaging.

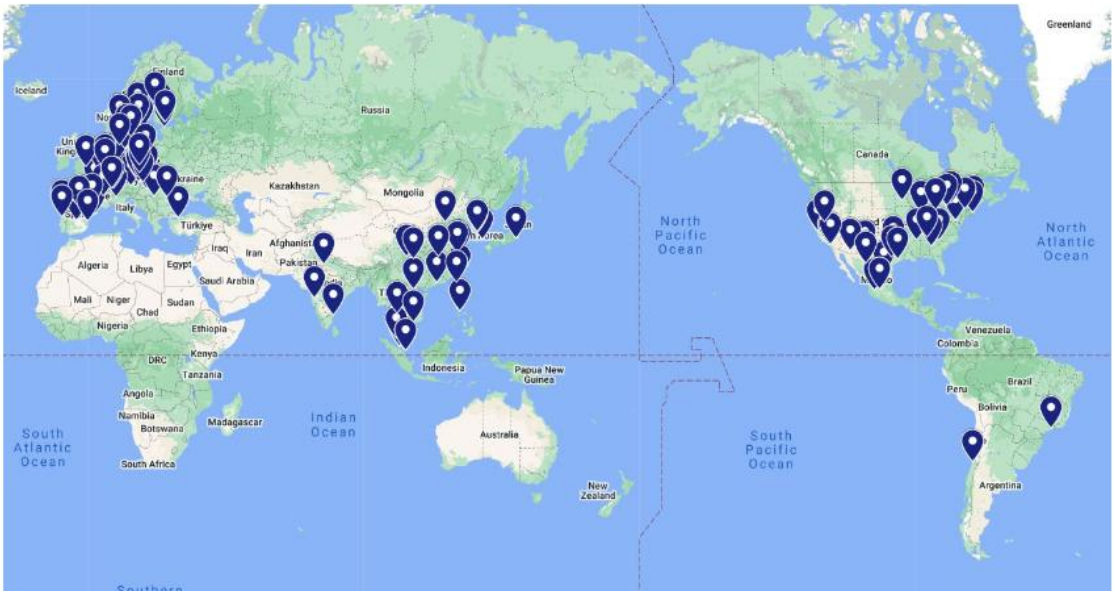

Figure 34 - NEFAB's worldwide presence [13].

NEFAB has a long history of innovation that began with the simple and innovative idea of a heat-resistant bread box. Over time, NEFAB has built a reputation as a supplier of innovative and

sustainable packaging solutions, and the company has begun to offer complete engineered packaging solutions to customers around the world.

During the 1920s, in the Swedish village of Ovanåker, a small village in the Swedish countryside, Sigurd Nordgren, a talented carpenter, but a poor entrepreneur, achieved the fulfilment of his professional aspirations by establishing a modest carpenter office. In 1946, the responsibility of the carpentry business was assumed by his older sons, Sven-Erik and Hans-Elov, while his younger sons, Carl-Åke, Knut-Allan and Nils-Arne, were engaged in the same business. The Nordgren brothers were engaged in the manufacture of toys, kitchen furniture, and functional items, including ironing boards. However, the company's true entry into the packaging industry was undoubtedly the creation of an innovative bread box. This innovative design, comprising a wooden structure with a masonite bottom, replaced the traditional cardboard box that crumpled in the heat when bakers took fresh bread out of the oven.

In 1949, Hans-Elov and Sven-Erik founded Nordgrens Emballagefabrik AB in Runemo, Sweden, at a time when the transport of goods and the demand for different types of packaging solutions were increasing, as many consumer goods companies began to centralise their warehouses. However, it was the innovative bread box, which was developed by the Nordgren brothers, that gained increasing popularity. In 1949, the Nordgren brothers received their first large order for 1000 boxes from the Kooperative Förbundet (KF) in Stockholm, Sweden. It is evident that, after this significant order, a series of more followed, creating the need for larger installations. Consequently, in 1951, Nordgren & Co. relocated a proportion of its production to a warehouse in Runemo, situated fifteen kilometres from Ovanåker. Figure 35 illustrates the various logos employed by NEFAB.

Figure 35 - Evolution of NEFAB logos [13].

In 1960, NEFAB started supplying stackable plywood boxes for the internal production of LM Ericsson, a Swedish-controlled technology company that manufactures fixed and mobile telephony equipment. In 1968, LM Ericsson expressed satisfaction with the stackable plywood boxes and requested that NEFAB would develop improved packaging solutions for the transportation of their telecommunication products, which were both sensitive and highly technological. This is the origin of NEFAB's Vikex box, now better known as ExPak. Vikex boxes were notable for their thickness, measuring 6 mm, in contrast to the 18-36 mm thickness of traditional wooden boxes. The comparison of a Vikex box and a traditional wooden box is demonstrated in Figure 36.

Figure 36 - Comparison of a Vikex box and traditional wooden box [13].

However, the Vikex box was not only lighter and smaller, but also foldable. This development led to a considerable growth in NEFAB's target market, as it became economically viable to transport packaging material over longer distances. This feature proved to be a crucial factor when NEFAB began to explore European markets on a larger scale during the 1970s.

In the early 1970s, NEFAB continued to research and produce better solutions for LM Ericsson's new and large activities. However, in the mid-1970s, LM Ericsson announced a potential decrease in its packaging requirements, indicating that NEFAB should not expect the same volumes in the future. In response to this situation, NEFAB decided to intensify its search for new customers among its export companies in Sweden to compensate for the reduction in volume from its main customer. In 1974, NEFAB introduced a new packaging solution (pallet) made of reusable plywood, and the solution quickly grew in the market due to its flexibility in terms of size and lightness, allowing easy handling.

During the 1970s, NEFAB initiated a trip to serve Swedish customers in foreign countries more efficiently and to reach new international companies. This expansion started in major European markets such as France and Spain. In 1983, NEFAB established its first presence in the US, in Peterborough, Canada, operating under the name of Vikex Industrial Packaging. Until this point in time, NEFAB's machinery had been manufactured in-house since the early 1950s. However, as the company expanded on an international level, it was decided that a central organisation should be created that would focus on producing the machinery for all the units around the world. Consequently, in 1989, NEFAB Teknik was founded with 25 employees. The organisational structure of NEFAB Teknik comprised three primary divisions: machine construction, maintenance, and control systems. The general aim of NEFAB Teknik was to simplify and reduce the set-up time of production units, while helping to harmonise production and product development.

The 1990s began with an international financial crisis that affected NEFAB. However, in 1992, the Canadian market experienced rapid growth, which led to the establishment of the Heavy-Duty division. This development was driven by the need to address the requirement for larger packaging in specific industries. Simultaneously, the automotive industry was undergoing major changes, such as the increasing number of companies in different markets to meet the demand for shorter delivery times. Consequently, a series of attractive business opportunities have emerged for NEFAB in the new flow of goods between the central production units of different car manufacturers, their suppliers, local assembly plants, and distributors giving birth to the

RePak concept (Figure 37). Like the Vikex, the Repak box is designed to be disassembled to save space during transport and storage. The primary distinction between RePak and Vikex is that RePak is intended for reuse and incorporation into the distribution network.

Figure 37 - RePak packaging solution [13].

In 2005, a manufacturing plant was built in Slovakia, enabling a major expansion in Asia. After this implementation, a plant was established in Beijing, China, in 2007, followed by two more in Xiamen and Wuhan, respectively, two years later. A significant development was marked by NEFAB's decision to enter the Indian market, a move that was accompanied by the establishment of the first plant in Manesar in 2007, followed by a second plant in Chennai in 2009. Alongside the geographical expansion and new material capabilities, a global engineering network was established to ensure that expertise, solutions, and learning could be shared more effectively across regions and markets.

To support their vision of becoming a total packaging solutions provider, NEFAB needed to enhance its capabilities in packaging materials and complementary service areas. To this end, NEFAB began a series of acquisitions in Europe, including Belgium, the Netherlands, Austria, Finland, Norway, Spain, Germany, and France. The rationale behind this strategic decision was to establish a global competitive advantage, enabling NEFAB to offer multi-material solutions to its global client base, as illustrated in Figure 38.

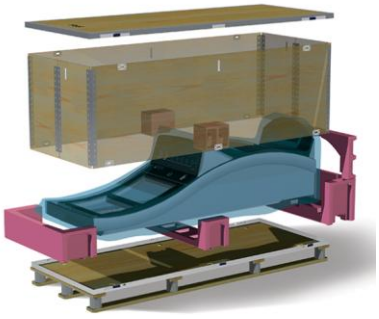

Figure 38 - Multi-material solution [13].

In 2010s, NEFAB intensified its focus on providing services to global customers in several key market sectors: Telecommunications, Energy, Vehicles, Healthcare and Aerospace. In 2010, NEFAB increased its presence in North America through the acquisition of Chick Packaging, expanding its ability to successfully serve specific industries and global customers in the US.

In the context of mounting pressures to reduce environmental impact and make packaging more sustainable, NEFAB's new strategy is to make a commitment to greater sustainability. In 2021, NEFAB reinforced its commitment to reducing CO_2 emissions and minimising total costs

in the supply chains of its customers. An integral component of this initiative was the introduction of GreenCalc®, NEFAB's established LCA software. GreenCalc® enables NEFAB to assist its client base in quantifying, evaluating and implementing financial and environmental savings through the provision of intelligent packaging and logistics solutions.

In 2020, NEFAB acquired Szkaliczki, a move that solidified its position as the European leader in sustainable thermoformed trays. Two years later, the Reflex Packaging Group, the global leader in sustainable thermoformed cushions, and Cargopack, the foremost Swiss enterprise in industrial packaging and logistics services, were acquired. In 2023 and 2024, the company acquired PolyFlex, a US industry leader specialising in environmentally friendly returnable solutions, and Plastiform, a US-based company offering high-quality thermoformed cushioning solutions. These strategic acquisitions enabled NEFAB to enhance its capabilities and respond more effectively to the demands of high-growth industries.

3.2. Materials and methods

To ensure a well-structured project, it is essential to clearly define the methods used and to identify the main problem. In this case, the issue lies in the limitations of available sizes for wood-based materials, which directly affect the design of large dimension pallets. Therefore, this section presents the adopted methodology, a description of the problem, along with a practical example. The proposed solutions for the construction of large dimension pallets are then presented.

3.2.1. Methodology

To achieve optimal outcomes in experimental tests and numerical analysis, two methodologies of five steps are employed. As shown in the Figure 39, the two procedures are initiated identically, by defining the geometries of the joints, the materials to be used, and the type of bonding. In this step, the viability of the different joint proposed is discussed.

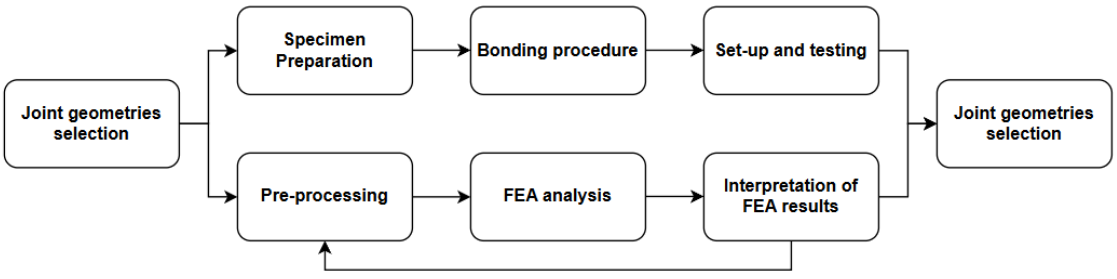

Figure 39 - Methodology used for the experimental part (top) and numerical analysis (bottom).

The subsequent experimental step is the preparation of the specimens, which refers to the process of cutting the raw materials that will be used to make the joints. After the preparation of all specimens, the next step is the bonding process. It is imperative to note that, depending on the selected bonding method, it may be necessary to meticulously clean and prepare the adherends that will be utilised for the adhesive bond. In such cases, the quality of the surface

preparation can have a significant impact on the results. Conversely, joints that are bonded using bolts or fasteners do not necessitate such meticulous preparation. After the bonding process, the testing procedure can begin. Following the completion of the testing process, a comparative analysis of the results can be conducted to identify which joint best performs in each application.

In parallel, it is possible to tackle on the numerical analysis, as soon as the joints are defined. For this purpose, following the definition of the joints, the preliminary procedure must be conducted. In this procedure, the dimensions, material properties, restrictions, and loads are defined. After this procedure, the FEA can be conducted. If the results are close to the experimental ones, the model is considered validated, and it is possible to compare the different joints. If the results are not close to the experimental ones, it is necessary to go back to the pre-processing phase to verify that all the inputs are correct. The objective of the numerical analysis is to complement the experimental results, by providing the stress along the joint and the damage evolution, which is not possible to obtain in the experimental tests.

3.2.2. Product description

Before the methodology demonstrated in Figure 39 can be applied to the study of different joint geometries, it is necessary to contextualise and frame the study of different geometries. The study begins with a pallet provided by NEFAB, designed for the transport of long products on pallets. In contrast to the standard Europallet, this pallet (Figure 40) has no standard dimensions, as it is custom-built to meet the customer's requirement for a length of 10 m and will only be used one time making this project an open-loop.

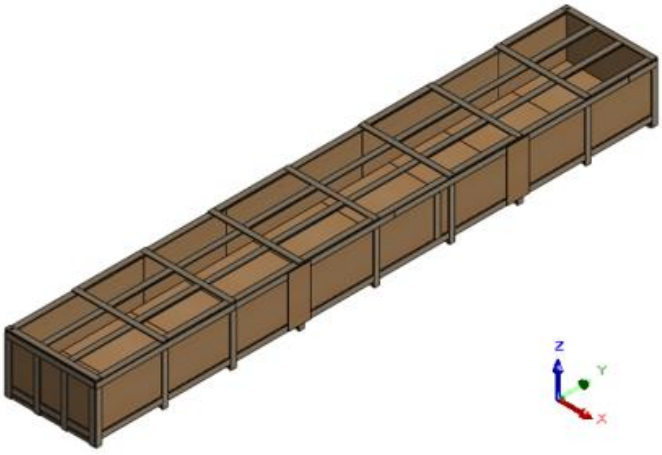

Figure 40 - 3D model of the pallet.

The key point of the project is the length limitations of the wood, making necessary the joining of various wooden beams. For this purpose, the study focuses on the determination of the best joint geometry to use in these cases. The results of the study will not only inform the design for the studied pallet but will also inform the design of future large pallets. The provided pallet from Figure 40 features a laminated structure to support the pallet floor that is commonly used to connect two wooden beams (Figure 41). This laminate consists of alternating wooden beams and then reinforcing the joint using plywood.

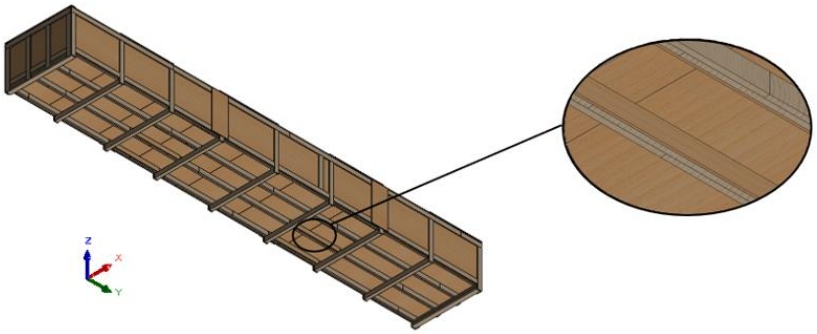

Figure 41 - Laminate structure that support the pallet floor (3D model).

To gain a more profound comprehension of the configuration of the provided pallet, it is possible to divide it into two primary components: the base, and the lateral and top protection. Figure 42 provides a representation of the components that constitute the pallet.

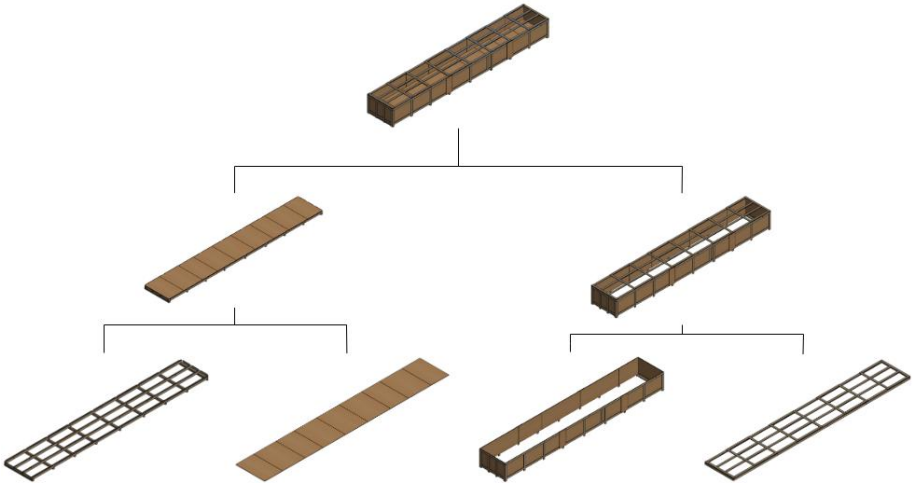

Figure 42 - Diagram of the pallet component (3D model).

As illustrated in Figure 43, the sides (represented in yellow) and the top (represented in red) are engineered to safeguard the product from external forces. The sides sections are composed of a wooden framework, and the laminate structure is employed to join the beams along their entire length, with plywood reinforcing the structure to enhance pallet overall stiffness. The uppermost section predominantly composed of interconnected wooden beams, facilitates the attachment of a tarpaulin, thereby ensuring the product's protection from the weather.

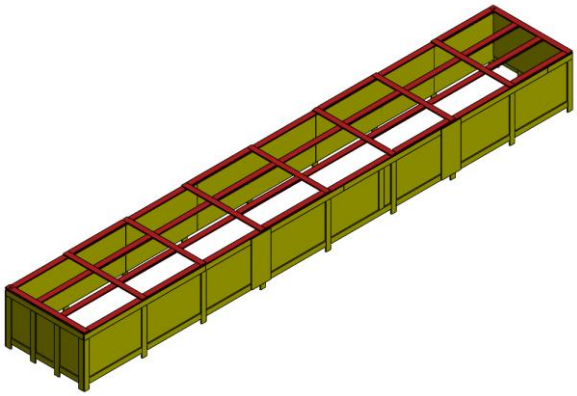

Figure 43 - 3D model of the side (yellow) and top (red) parts.

As demonstrated in Figure 44, the base is predominantly composed of wooden beams, which are joined by the previously mentioned laminate structure. Plywood sheets are then placed on top of the base, thus creating a protective barrier between the ground and the client's product.

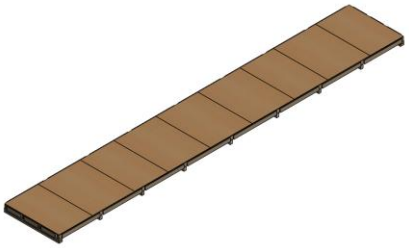

Figure 44 - 3D model of the base part.

The base is a critical component of the pallet as it must support the full weight of the customer's product and allow for lifting from below, as shown in Figure 45. It is therefore vital to emphasise that the joints in the base are critical structural points, making it the focus of the present study.

Figure 45 - Example of handling the pallet.

3.2.3. Product materials

The pallet under study present large dimensions, but it is not always possible to obtain wood beams in all the required lengths. In numerous countries, including Portugal, limitations on the length of available wood materials. As demonstrated in Table 3, the maximum lengths available for wood and plywood in the Portuguese market are 2500 mm and 2440 mm, respectively.

Table 3 - Wood and plywood standard in Portugal [109]

Wood		
Category	**Section [mm^2]**	**Length [mm]**
A	80x20	2500
B	100x30	2500
C	100x50	2500
D	80x80	2500
E	75x16/17	2400
F	100x70	2500
G	100x100	2500
H	100x25	2500

Table 3 - Wood and plywood standard in Portugal [109] (Continued)

I	100x20	2500
J	150x20	2500
Plywood		
Category	**Section [mm^2]**	**Thickness [mm]**
A	2440x1220	6
B	2440x1220	8
C	2440x1220	12

The pallet under study is composed of category B wood and category A plywood sheets. Table 4 present the properties of the wood and plywood used for the pallet. However, due to the length limitations inherent in the available materials, the pallet requires the integration of various beams to attain the desired length. It is therefore essential to explore a range of bonding techniques and joint geometries. As previously mentioned, depending on the part of the pallet, the joints may be subjected to significant stresses. Therefore, the choice of an inadequate joining method could result in the weakening of the pallet. The base of the pallet must be able to support the product without collapsing, and this is the key focus for the joints. It is for this reason crucial to test different joint geometries to select the most optimal solution.

Table 4 - Wood and plywood properties used on the pallet [109]

Wood	
Mechanical properties	**Values**
Moisture content [%]	12
Hardness, wood indentation [N]	2100
Modulus of rupture [GPa]	0.0421-0.0807
Flexure modulus [GPa]	8.10-10.2
Compressive Strength [MPa]	19.2-41.9
Shear strength [MPa]	5.20-11.0
Plywood	
Technical features	**Values**
Density [kg/m3]	422-514
Modulus of elasticity [N/mm2]	3800-5000
Face fastener holding [kgf]	135
Moisture content [%]	6-14

3.2.4. Adhesives

As referred before, the solution to this problem is creation of joints, which led to a larger dimension component. As a result, it is necessary to define the joining methods and joint geometries. With this goal, a variety of joining methods, such as nailing, bolting, adhesive joining, or even the combination of adhesive with bolts or nails, can be used. Using the combination of various methods is commonly used in the industry. For this reason, the study

compares the use of different techniques and geometries. Focusing on the adhesive, the adhesive employed as a reference at NEFAB is AQUENCE's WL 041/1, also known as DORUS MD 041/1. This is a white PVA (polyvinyl acetate) adhesive that becomes transparent after drying. It is specifically designed for surface and assembly applications in woodworking. It is considered suitable for a range of applications, including the bonding of solid wood, blockboard cores, and composed solid wood panels, as well as for assembly and carcass bonding. It is also effective for dowel insertion, mortise and tenon joints, and bonding continuous and high-pressure laminates (CPL/HPL). Additionally, it finds application in the edge banding process involving veneer, solid wood, and HPL edges, utilised in both cold and heated stationary presses.

AQUENCE WL 041/1 is distinguished by its medium viscosity and very short setting time, resulting in tough-elastic, workable glue joints with high bonding strength. It is notable for meeting the requirements of durability class D2 (Table 5) according to EN 204, offering excellent moisture resistance. In conjunction with AQUENCE CATALYST R 397, a 1% cross-linker, it attains the D3 water resistance classification, thereby significantly improving its performance in humid environments. The adhesive features a viscosity range of 9,500 to 14,500 mPa·s, a pH value between 4.5 and 6 at 20 °C, and a minimum film formation temperature of approximately +3 °C. The open time of the adhesive is contingent upon the quantity applied; it is approximately 7 minutes with 100 g/m² and up to 12 minutes with 200 g/m². When utilising the cross-linker, it is imperative to ensure that, due to the limited pot life of the cross-linker, the mixture is mixed and applied within approximately 7 hours. The addition of the cross-linker has been observed to extend pressing and setting times by 2 to 3 minutes. The application of the adhesive should be conducted on surfaces that are clean, close-fitting, and with a minimum temperature of +10 °C for both the workpiece and the adhesive [110].

Table 5 - Description of durability classes [111]

Durability class	Examples of climatic conditions and fields of application
D1	Interior, in which the moisture content of the wood does not exceed 15%.
D2	Interior with occasional short-term exposure to running or condensed water and/or to occasional high humidity provided the moisture content of the wood does not exceed 18%.
D3	Interior with frequent short-term exposure to running or condensed water and/or to heavy exposure to high humidity. Exterior not exposed to weather.
D4	Interior with frequent long-term exposure to running or condensed water. Exterior exposed to weather but with protection by an adequate surface coating.

3.2.5. Joints specification and requirements

The pallet supplied by NEFAB incorporates a variety of joint types. The location of each joint dictates the specific requirements it must meet, such as the load it is required to carry. The present study focuses on the most critical joints; those located under the pallet base (Figure 41). These joints are critical as they must support not only the weight of the product, but also

that of the pallet itself. The performance of these joints is evaluated by considering the most demanding scenario: a forklift fork pressing directly on the joint. To this end, a three-point bending test will be conducted, both experimentally and numerically. The current absence of a dedicated standard for wood-based joints is the motivation for NEFAB to investigate different joint geometries and bonding methods. The findings of this study have the potential to serve as a reference database for the design of future large-scale pallets.

However, for wood-based materials in general, a wide range of standards exist with the aim of ensuring quality, safety, mechanical performance, and durability. These standards may differ depending on the geographical location (e.g., Europe, North America, Asia), but several are recognised on an international scale. The ISO 12465 standard stipulates the requirements for plywood used in both general and structural applications under various environmental conditions (dry, tropical dry/humid, and exterior use). The scope of ISO 12465 encompasses a wide range of parameters, including veneer quality, glue bond performance, construction (lay-up), dimensional accuracy and tolerances, verification of conformity, and product marking.

In Europe, a variety of standards are applied to wood-based materials for global use. Among these, EN 338 is relevant to all softwoods and hardwoods intended for structural use. This standard establishes a system of strength classes that is utilised in design codes. On the other hand, EN 636 focuses on specifications for plywood. The utilisation of wood as an organic material gives rise to challenges such as moisture sensitivity and susceptibility to biological degradation. To address this problem, EN 350 provides guidance on methods to estimate and classify the natural durability of wood and wood-based products against biological wood-destroying agents such as fungi and insects. Another key concern is that of environmental exposure. EN 335, applicable to both solid wood and wood-based products, defines five use classes that represent different service conditions (summarised in Table 6) to which wood may be exposed. It also identifies the biological agents relevant to each condition, thus helping in selecting the appropriate type of wood or treatment. As previously mentioned, EN 204 is applicable to non-structural adhesives and classifies thermoplastic resin-based wood adhesives into four durability classes (D1 to D4, presented in Table 5), based on the dry and wet strength of bond-lines after conditioning under defined testing procedures.

Table 6 - Use classes for wood and wood-based products [112]

Use class	Service conditions	Moisture exposure	Main biological risks	Typical applications
Class 1	Indoors, always dry	Very low or none	None	Indoor furniture
Class 2	Indoors, occasionally humid	Occasional humidity	Mould, insects	Framing, roof structure
Class 3.1	Outdoors, sheltered, rarely wet	Moderate	Fungi, insects	Exterior joinery
Class 3.2	Outdoors, frequently wet	Frequent	Fungi, insects	Fences, balconies

Table 6 - Use classes for wood and wood-based products [112] (Continued)

Class 4	In contact with ground or water	Permanent or prolonged	fungal and insect attack	Playground structure
Class 5	Immersed in salt water	Very high	Marine organisms	Marine structure

3.2.6. Joint geometries

Knowing the materials and the requirements of the joints, it is possible to determine the joint geometries that will be studied. However, to establish a basis for comparison with the joints and to calibrate the properties of the wood in the numerical model, simple wooden beams of 80x70 mm^2 and 100x80 mm^2 are tested, as illustrated in Figure 46. This comparison allows assessing whether the joints can outperform solid wooden beams in terms of strength. Since joints inherently create discontinuities that may compromise the structural integrity, reinforcing them becomes essential.

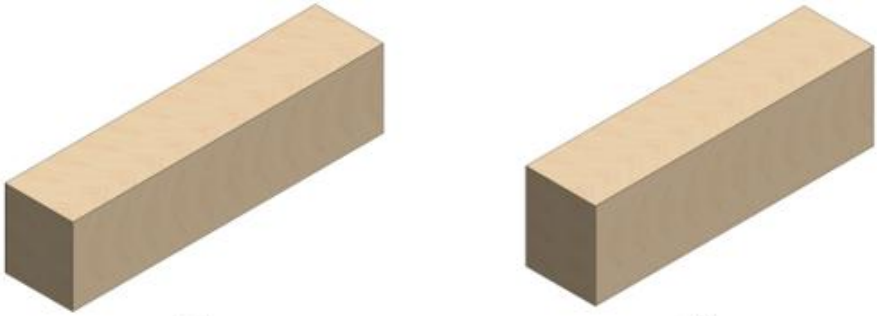

Figure 46 - (a) 80x70 mm^2 wooden beam and (b) 100x80 mm^2 wooden beam.

As a result of these considerations, seven distinct geometries have been developed. Figure 47a) presents the 3D model of a simple laminated joint. It consists of two beams that are adhesively bonded, and nails are used to increase the joint's strength. The utilisation of both plywood and wooden beams permits the reinforcement of discontinuities. Building on this design, the Figure 47b) shows a variant of the previous laminated joint, which follows the same principle but aligns the junction of the two beams on both sides within the same plane. In both cases, all elements are bonded and nailed, but the nails are not represented on the 3D model and will later be added to the numerical analysis.

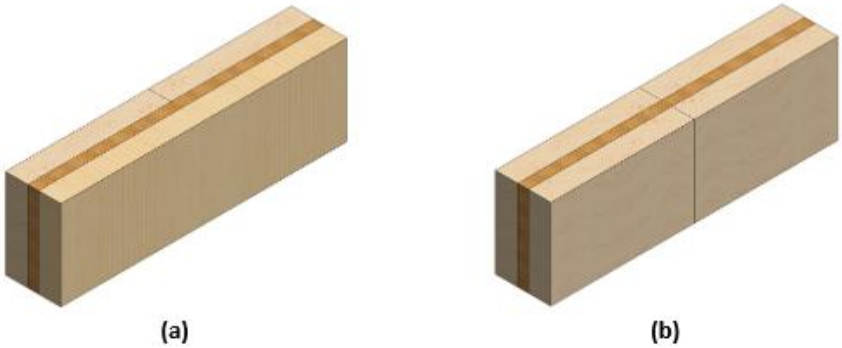

Figure 47 - (a) Simple laminated joint and (b) laminated joint with alignment of the junction.

Figure 48a) presents a double strap joint, which features the main beams joined by plots at both sides. The assembly of all components is achieved through the utilisation of nails and adhesive. Derived from the simple strap joint, the Figure 48b) presents a double strap joint with the same structure, but with the nails being replaced by wood fasteners, and not using adhesive. As referred before the nails are not represented on the 3D model and will later be added to the numerical analysis.

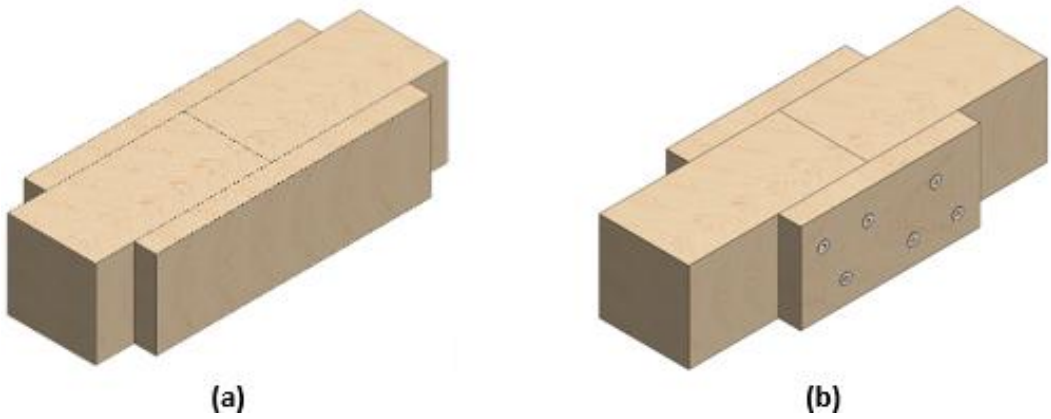

Figure 48 - (a) Double strap joint and (b) fastened double strap joint.

Figure 49a) shows a double strap joint that follows same geometrical principle of the previous two but using adhesive and bolts instead of nails/wood fasteners for the purpose of assembly. Figure 49b) presents a double strap joint that features a distinct design for the primary beams, since these are cut with a 45° chamfer. The beams are joined using wooden straps on both sides, which are bonded using wooden fasteners. However, adhesive is not used to compare with other geometries the chamfer impact on the joint.

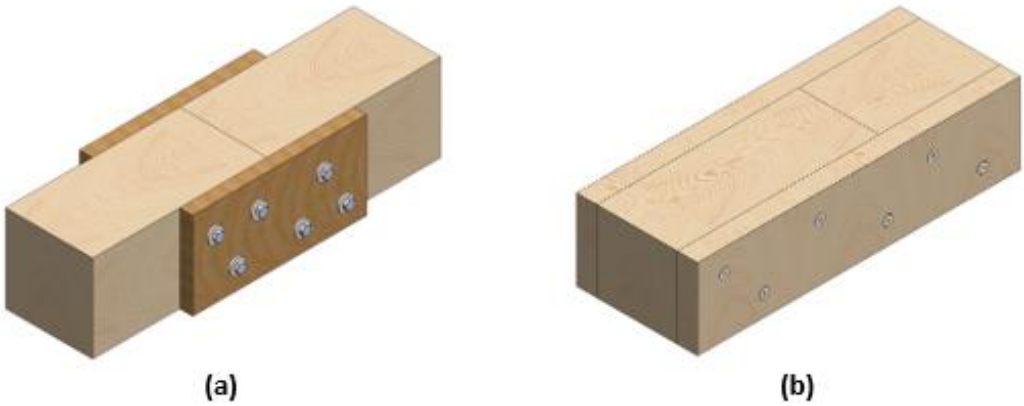

Figure 49 - (a) Bolted double strap joint and (b) double strap joint with chamfer.

Moreover, it should be noted that the fastened double strap joint and double strap joint with chamfer each have two versions, ether with M4 and M6 wooden fasteners. The same way, the bolted double strap joint present two version with M6 and M10 bolts This distinction enables the assessment of how the difference in bolt size has a significant effect on the strength of the joint. Table 7 provides a comprehensive overview of all geometries, including their respective materials, quantities, and dimensions required for assembling a single joint.

Table 7 - Geometries information

Case	Geometry	Material	Dimension	Quantity
Wooden beam	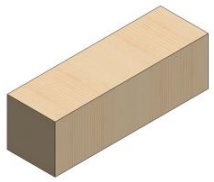	Wood	80x70x320 mm^3	1
			100x80x320 mm^3	1
Simple laminate joint		Wood	100x25x320 mm^3	1
			100x25x160 mm^3	2
		Plywood	100x12x320 mm^3	1
Laminate joint with junction alignment		Wood	100x25x160 mm^3	2
		Plywood	100x12x320 mm^3	1
Double strap joint	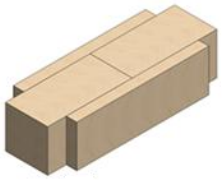	Wood	80x80x160 mm^3	2
			80x20x250 mm^3	2
Fastened double strap joint	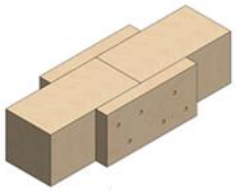	Wood	80x80x160 mm^3	2
			80x20x160 mm^3	2
		Wooden fasteners	M4	12
			M6	12
Bolted double strap joint	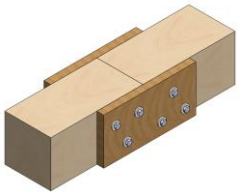	Wood	80x80x160 mm^3	2
			80x20x160 mm^3	2
		Bolt sets	M6	6
			M10	6
		Washers	M6	12
			M10	-
Double strap joint with a chamfer on the main beams		Wood	80x80x200 (chamfer) mm^3	2
			80x20x180 mm^3	2
		Wooden fasteners	M4	12
			M6	12

3.3. Experimental part

To carry out the experimental tests, it is necessary to manufacture the test specimens, which will then undergo a three-point bending test. Once tested, it will be possible to determine the mechanical properties of the joints, thus allowing for a direct comparison between the different geometries. This section introduces wood and plywood, as they are the main materials used in this study. The manufacturing process and the parameters applied during testing are then described. Finally, the mechanical properties and observed failure modes are analysed and compared.

3.3.1. Material characterization

Material characterization is fundamental to assess the joint behaviour and perform strength prediction. Thus, the next subsections present a general introduction of the materials used in the joints, followed by the detailed description and respective properties used for the experimental part.

3.3.1.1. Wood

Variability, or variation in properties, is common to all materials. Because wood is a natural material, and the tree is subject to many constantly changing influences, such as moisture, soil conditions, and growing space, wood properties vary considerably. Wood can be described as an orthotropic material, which is a subcategory of the anisotropic materials. As shown in Figure 50, orthotropic materials have unique and independent mechanical properties in the direction of three mutually perpendicular axes, which are longitudinal, radial, and tangential. The longitudinal axis is parallel to the fibre, the radial axis is normal to the growth rings, and the tangential axis is perpendicular to the fibre but tangent to the growth rings [113].

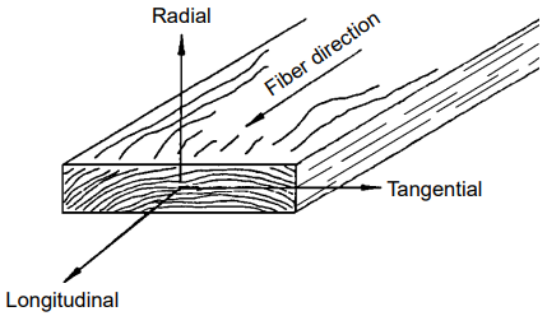

Figure 50 - The three principal axis of wood (orthotropic material) [113].

Because of natural growth characteristics of trees, wood properties can vary, due to the fact it may contain cross grain or may have knots. These wood characteristics must be considered when estimating the actual performance of wood. A knot is a portion of a branch that has become incorporated in the bole of the tree. These knots influence the mechanical properties of wood members by interrupting continuity and changing the direction of wood fibres. Because of that, most mechanical properties are lower in sections containing knots than in clear straight-grained wood. Because the clear wood is displaced by the knot, the fibres around the knot are

distorted, and the discontinuity of wood fibre leads to stress concentrations. Nonetheless, knots have a much greater effect on strength in axial tension than in axial short-column compression, and the effects on bending are less significant than those in axial tension [113].

The most used woods in industry can be categorized into softwoods and hardwoods, each serving different purpose based on their properties. Softwood is derived from trees with needle-like or scale-like leaves, such as coniferous, for example pine, cedar, and spruce. One of the main characteristics of softwood is its lower ρ, which makes it easier to work with and be more affordable than hardwood. Another notable characteristic of softwood is its grain pattern, which tends to have a straighter and more uniform grain patterns than hardwood trees. This straight grain makes softwood ideal for various applications, such as framing in construction or producing lumber for furniture making. On the other hand, hardwood is a type of wood that is derived from deciduous trees. These trees typically have broad leaves, which they shed seasonally, such as oak, maple, cherry, and walnut. In contrast with softwood, hardwood is a dense and heavy wood that is known for its strength and durability. Hardwoods also present a more complex structure and are generally more difficult to work with [114, 115].

In the thesis context, the selected wood is that used in NEFAB wooden pallets: radiata pine. This softwood is widely used in the industry due to its lightness, strength, ease of processing and lower cost compared to oak, making it an attractive choice for furniture manufacturing. Table 8 presents the wood properties provided by the supplier.

Table 8 - Radiata pine wood supplier properties [113]

Property	Value
Density	0.318-0.515 g/cm^3
Hardness, Wood Indentation	2100-3300 N
Tensile strength	42.1-80.7 MPa
Flexure modulus	8.10-10.2 GPa
Compressive strength	19.2-41.9 MPa
Shear strength	5.20-11.0 MPa
Tensile modulus	8-13 MPa

As referred before, wood can be considered an orthotropic material, leading to the need of *E*, shear modulus (*G*), and Poisson ratio (ν) in the three-directions depicted in Figure 50. Due to the insufficient information provided from the supplier, research was conducted focusing specifically on radiata pine wood, to ensure consistency between the experimental and numerical results. Table 9 presents the E, G, and ν for green core and outer wood, optimised for the orthotropic assumption, taken from reference [116].

Table 9 - Orthotropic properties for green core and outer wood *Pinus Radiata* [116]

Property	Stiff outer wood	Non-stiff outer wood	Stiff core wood	Non-stiff core wood
E_r [GPa]	0.49	0.30	0.26	0.31
E_t [GPa]	0.25	0.19	0.24	0.17

Table 9 - Orthotropic properties for green core and outer wood *Pinus Radiata* [116] (Continued)

E_l [GPa]	4.36	2.81	3.50	2.38
G_{tl} [GPa]	0.11	0.21	0.11	0.13
G_{lr} [GPa]	0.06	0.03	0.04	0.03
G_{rt} [GPa]	0.05	0.02	0.02	0.04
ν_{tl}	0.03	0.01	0.03	0.04
ν_{lr}	0.29	0.47	0.36	0.44
ν_{rt}	0.64	0.54	0.60	0.77

3.3.1.2. Plywood

Derived from wood, plywood is widely used in construction, furniture making, and various specialized applications. Plywood is an engineered wood product made from multiple layers of thin sheets (Figure 51), called veneers, crossband, and core, which are bonded together with adhesive. To add strength, the layers are arranged with the grain direction alternating, as shown in Figure 51. However, understanding the properties of plywood is essential to make informed decisions about its usage in different contexts [117].

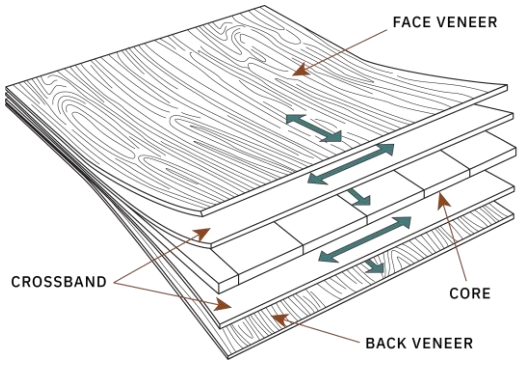

Figure 51 - Example of the layers of a plywood product [117].

One of the most significant features of plywood is its strength-to-weight ratio, permitting to support heavy loads without breaking or deforming. The alternating grain structure of the veneer layers gives it added tensile strength, making it stronger than solid wood of the same thickness. Along with the strength, plywood also offer high flexibility, compared to solid wood. Its ability to bend and conform to curves makes it a versatile material for applications requiring flexible shapes, such as furniture, cabinetry, and architectural designs. Flexible plywood is often used in boat building and for creating non-linear surfaces in interior designs [115, 118].

Plywood properties can differ depending on the wood used, adhesive quality, and the layers orientation. Due to these mentions, plywood can be divided into four different types, namely softwood plywood, hardwood plywood, marine plywood, and fire-retardant plywood. Softwood plywood is made from coniferous trees and is the most used type of plywood in construction. It is lightweight, cost-effective, and relatively easy to work with. Hardwood

plywood is stronger and more durable than softwood plywood, making it ideal for furniture, cabinetry, and decorative applications. It is made from hardwood species, such as oak, maple, and birch. Marine plywood is manufactured with waterproof adhesives and has superior moisture resistance. It is specifically designed for use in environments where it will be exposed to water for extended periods of time. Finally, fire-resistant plywood is treated with fire-resistant chemicals to slow the spread of fire. This type of plywood helps to meet building codes that require enhanced fire resistance [115]. In the thesis context, as for the wood, the plywood used is the most used in NEFAB's pallet, which is a beech plywood, and Table 10 presents the properties provided by the plywood supplier.

Table 10 - Plywood supplier properties

Property	Value
Density	422-514 kg/m^3
Modulus of elasticity	3800-5000 MPa
Face fastener Holding	135 kgf
Moisture content	6-14%

The same way of the wood, plywood can be considered an orthotropic material. For this reason, the same research realized for wood to find the nine elastic properties is conducted, focusing on the plywood. Resulting of the research, Table 11 presents the nine elastic properties for the orthotropic assumption, which are taken from reference [118].

Table 11 - Orthotropic properties for plywood [118]

Property	Value
E_l [GPa]	9.660
E_r [GPa]	5.410
E_t [GPa]	2.700
G_{tl} [GPa]	0.878
G_{lr} [GPa]	1.060
G_{rt} [GPa]	0.604
ν_{tl}	0.142
ν_{lr}	0.109
ν_{rt}	0.440

3.3.2. Fabrication procedure

After introducing the materials of the joints, the bonding procedure can be conducted. The bonding procedure is a fundamental process used to join two or more surfaces or materials securely, ensuring long-lasting performance and reliability. The success of bonding depends on several key steps, starting with surface preparation. All surfaces involved must be thoroughly cleaned to remove dust, oil, grease, or any contaminants that could interfere with adhesion. Joint fabrication was carried out at NEFAB using the company's equipment in this process.

Figure 52 presents the pressure glue applicator, pneumatic coil nailer, and drill, used in the fabrication process.

Figure 52 - pressure glue applicator (a), pneumatic coil nailer (b), and drill (c).

The pneumatic coil nailer from MORE® is used to execute the nailing process on the simple laminate joint, laminate joint with junction alignment, and double strap joint. The pneumatic coil nailer is a heavy-duty pneumatic coil nailer designed for applications such as framing, pallet construction, and wooden crate assembly. It operates with wire-collated nails set at a 16° angle, supporting nail lengths from 50 mm to 90 mm. The nails used have a body diameter between 2.8 mm and 3.3 mm, and head diameters from 6.7 mm to 7.2 mm, ensuring strong and secure fastening. Nails are driven with a working pressure of up to 8 bar, providing deep and consistent penetration even in dense wood materials. However, as shown in Figure 53, some defects can occur due to pressure. For the other joints, a fastener driver is used for bolting.

Figure 53 - Visible defect on a nail.

The simplified laminated joint fabrication process is illustrated in Figure 54. The process is initiated by cutting the wooden beams and plywood into the required dimensions. After the preparation of all components, the adhesive is initially applied to one face of the longest wooden beam. No surface preparation is made, once NEFAB do not do it in their fabrication procedure. The adhesive is applied in a wave-like pattern using a pressure adhesive applicator to ensure uniform distribution. Subsequently, the plywood is positioned on the surface that has been glued previously and is then nailed to the beam using a pneumatic coil nailer. This step ensures a strong initial bond between the plywood and the wooden beam through both adhesive and mechanical fastening. A second layer of adhesive is then applied to the plywood surface in preparation for the final assembly stage. The remaining wooden components are positioned on this glued surface, and then nailed into the desired position, thus forming the complete laminated joint. This technique is extensively employed at NEFAB, particularly in the assembly of large beams, as it enables operators to complete the joint without the need to rotate the beam, thereby simplifying the process and ensuring the integrity of the joint is maintained.

Figure 54 - Fabrication procedure of the simple laminate joint.

The laminated joint with junction alignment fabrication is illustrated in Figure 55. The process initiated with the cutting process. Differently to the preceding joint, this version employs four wooden beams of equal length. After cutting all components to the specified dimensions, the adhesive is applied to the upper surfaces of two wooden beams, in accordance with the identical procedure as the simple laminated joint do not present a surface preparation. After the application of the adhesive, the plywood is positioned on the surface and rapidly nailed to the beams by averages of the pneumatic coil nailer. In accordance with the previously established protocol, a secondary layer of adhesive is applied onto the plywood surface. The final step in the process is the positioning of the two remaining wooden beams on top of the glued plywood, followed by nailing them into place. This procedure results in a joint constructed using the same basic process as the simple laminated joint, but with aligned junctions.

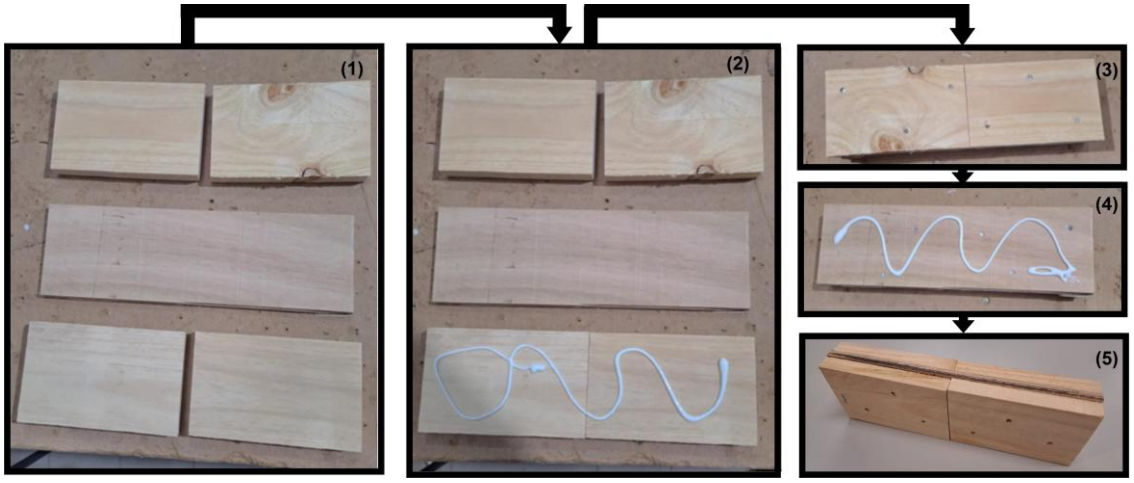

Figure 55 - Fabrication procedure of the laminated joint with junction alignment.

The double strap joint fabrication process is illustrated in Figure 56. The process starts by cutting of the wood to the final dimensions. This joint is essentially made of wood. After the cutting process, adhesive is applied in the central wooden beams, as for the other joint, no surface preparation is made Then a third wooden part is nailed to the central beams. After the strap wood being nailed, the joint is turn over and the process is repeated.

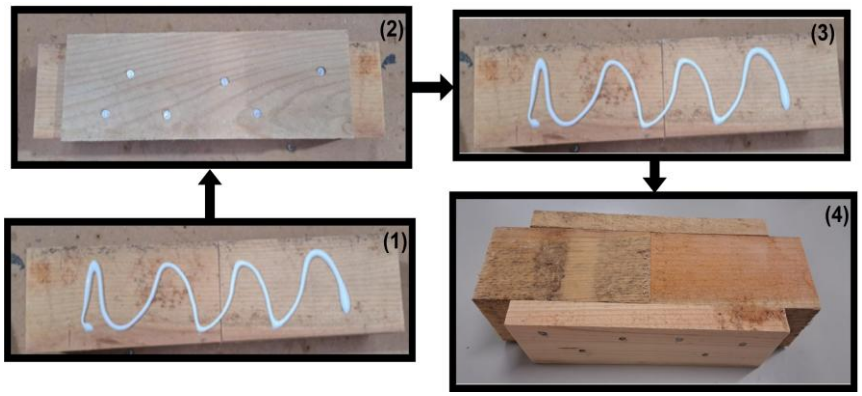

Figure 56 - Fabrication procedure of the double strap joint.

The fastened double strap joint fabrication process is illustrated in Figure 57. This joint follows the same fabrication process of the previous one. Starting by cutting the wood to the final dimensions and then a third wooden part is fastened, with M4 or M6 wooden fasteners depending on the version, to the central beams. After the strap wood being fastened, the joint is turned over and the process is repeated.

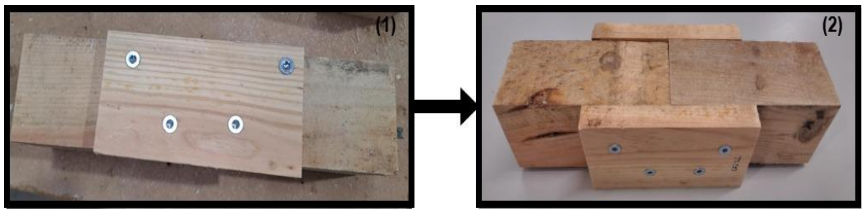

Figure 57 - Fabrication procedure of the fastened double strap joint.

The bolted double strap joint fabrication process is illustrated in Figure 58. The fabrication process for this geometry was particularly difficult, due to the required plywood drilling before fastening. To expedite this process, initially small nails were applied to maintain all components together and then the holes could be drilled. However, a second idea of using corrugated fasteners was used instead, since these have a smaller impact on the joint strength. After that, the holes were drilled for the threaded rods to be positioned and bolted on both sides.

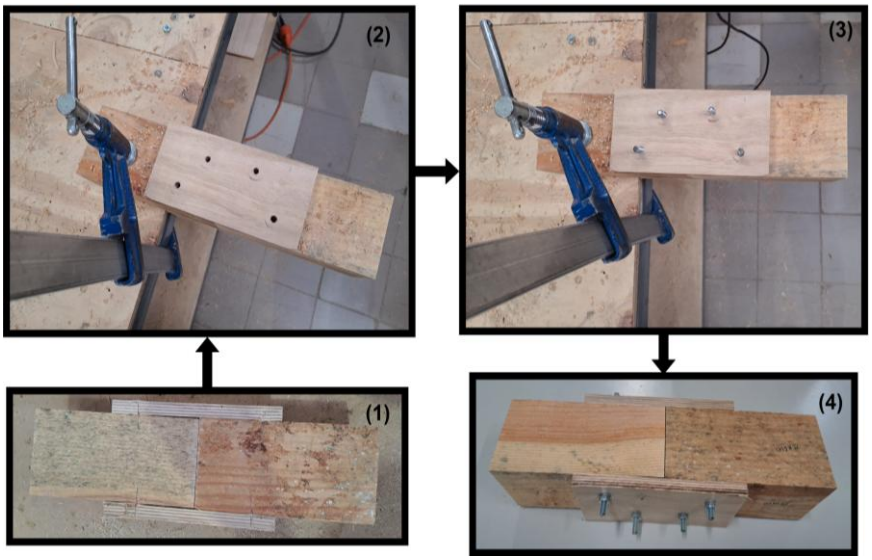

Figure 58 - Fabrication procedure of the bolted double strap joint.

The double strap joint with a chamfer on the main beams' fabrication process is illustrated in Figure 59. The fabrication process is like the first geometries, but without using adhesive, i.e. the straps are directly fastened to the central beams.

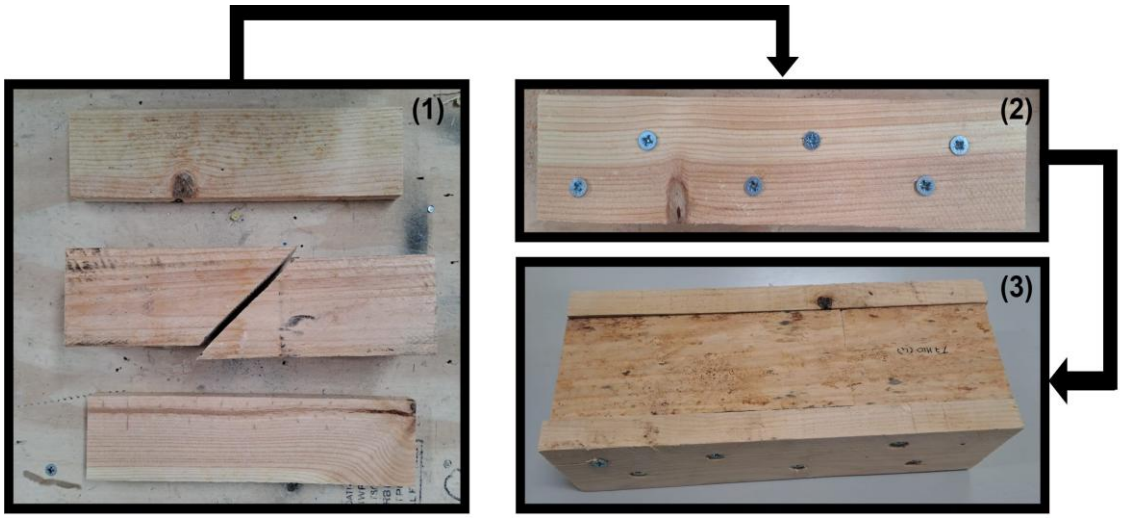

Figure 59 - Fabrication procedure of the double strap joint with a chamfer on the main beams.

3.3.3. Testing

The tests were conducted at the ISEP laboratory, in a universal testing machine (UTM). This testing machine is a Shimadzu Autograph AG-X 100 kN, which as a maximum load capacity (P_{max}) of 100 kN. This machine supports various types of tests, including tensile, compression, bending, shear, and peel. However, as referred previously, the joints studied do not have defined testing standards. Thus, a 3-point bending setup was considered to evaluate the testing conditions, which is presented in Figure 60.

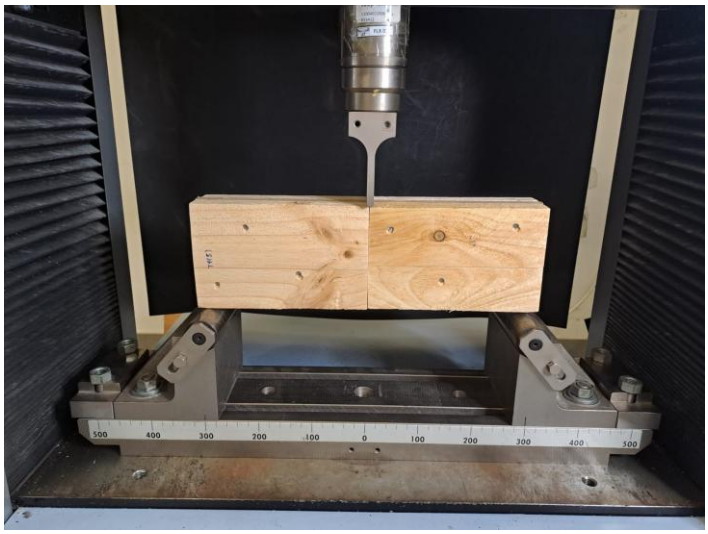

Figure 60 - First setup for a 3-point bending test.

The main problem encountered with this setup was the radius of the punching part, which has a small dimension. Due to the small radius of the loading punch, the punch penetrates the wood (Figure 61) due to the resulting high stress concentrations.

Figure 61 - Penetration of the punch in the wood.

To avoid wood penetration, a bigger radius needs to be used. However, only the reported punch was available at ISEP laboratory. To prevent indentation, a semi-cylindrical with 25 mm radius was inserted between the loading punch and the beam, as shown in Figure 62. This setup decreases tension concentrations, aiming to decrease wood penetration.

Figure 62 - Second setup for a 3-point bending test.

The realization of this 3-point bending test needs to be quasistatic, to simulate the most critical scenarios of pallet elevation by the forklift with the fork exactly in the joint. Table 12 presents all the parameters of the testing setup.

Table 12 - Parameters used in the setups

Parameter	Setup 1	Setup 2
Distance between supports	300 mm	
Support radius	15 mm	
Punch radius	2.5 mm	25 mm
Testing speed	5 mm/s	

In the other hand, five specimens of each geometry are tested. The dimensions of all specimens are presented in Table 13. The dimensions were taken using a digital calliper with a resolution of 0.01 mm.

Table 13 - Specimens dimensions

Case	Geometry	Specimen	Width [mm]	Thickness [mm]
Wooden beams (70x80/80x100)	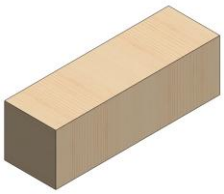	1	72.77/80.40	82.47/99.52
		2	73.24/80.13	83.87/100.6
		3	73.33/79.49	82.19/98.40
		4	76.15/79.30	82.06/100.77
		5	72.94/82.79	81.81/100.02
Simple laminate joint		1	97.83	54.22
		2	100.29	51.98
		3	101.89	53.15
		4	101.83	53.36
		5	100.03	52.11
Laminate joint with junction alignment		1	100.03	51.93
		2	99.85	51.92
		3	101.72	52.08
		4	99.06	52.83
		5	99.15	52.49
Double strap joint		1	82.66	120.80
		2	82.23	122.69
		3	82.62	121.91
		4	82.44	118.65
		5	81.90	121.63
Fastened double strap joint (M4/M6)	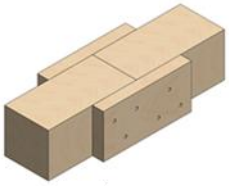	1	78.08/86.95	120.33/122.73
		2	83.24/87.27	121.93/120.84
		3	78.11/83.53	122.12/121.04
		4	85.95/86.15	123.42/120.40
		5	84.58/85.11	122.45/120.72
Bolted double strap joint (M6/M10)		1	101.89/102.34	80.58/80.03
		2	102.32/100.77	80.11/79.41
		3	100.85/102.81	79.62/80.07
		4	101.75/101.50	80.81/79.14
		5	101.16/101.00	82.10/79.28
Double strap joint with chamfer (M4/M6)		1	122.78/123.28	77.68/82.38
		2	121.76/119.74	76.45/80.40
		3	122.54/123.88	76.71/78.49
		4	121.40/118.79	78.56/79.79
		5	120.55/121.68	82.89/82.44

3.3.4. Results

3.3.4.1. Failure mode

To better understand the efficiency of the joint geometry, it is necessary to examine how failure occurs. Consequently, each specimen of every geometry type is analysed, and a global conclusion about the joint's failure mode is drawn. Figure 63 presents the first tested specimen of the 80x70 mm^2 wooden beams following the execution of the 3-point bending test. The results of all specimens of the 80x70 mm^2 wooden beam are presented in Appendix A, in Table A.1. Specimens that do not exhibit significant knots demonstrate similar failure modes, which are typically characterised by fibre separation along the grain direction.

(a) **(b)**

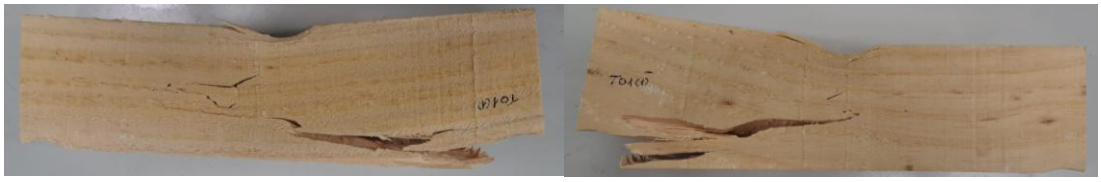

Figure 63 – First tested specimen of the 80x70 mm^2 wooden beams front (a) and back (b) view.

However, knots with large dimensions significantly influenced both the failure mode and the mechanical strength of the wood. For instance, Figure 64 illustrates the bottom view of the fourth specimen, which contains a prominent knot. This knot has been shown to induce crack propagation perpendicular to the fibre direction, thereby considerably reducing the structural efficiency of the wood.

Figure 64 - Bottom view of the fourth specimen of the 80x70 mm^2 wooden beams.

As with the 80x70 mm^2 wooden beams, the first tested specimen of the 100x80 mm^2 wooden beams is shown in Figure 65. The results of all specimens of the 80x70 mm^2 wooden beam are presented in Appendix A, in Table A.2. Most of the observed cracks demonstrate a tendency to align with the fibre direction, a finding that is consistent with the failure modes identified in the preceding specimens of the 80x70 mm^2 wooden beams. However, the third specimen contains a knot and exhibits a failure mode identical to the fourth 80x70 mm^2 specimen, with crack propagation occurring perpendicular to the fibre direction due to the knot's influence.

(a) **(b)**

Figure 65 – First tested specimen of the 100x80 mm^2 wooden beams front (a) and back (b) view.

Figure 66 presents the first tested specimen of the simple laminate joints. The results of all specimens of the simple laminate joint are presented in Appendix A, in Table A.3. In this configuration, the plywood first manifest delamination between layers which, after all the accumulated stress in the plywood, followed by wood damage. Due to that, the wood immediately fails, displaying fissures oriented perpendicularly to the fibre direction and aligned with the direction of the applied force.

Figure 66 - First tested specimen of the simple laminate joint front (a) and back (b) view.

Finally, in certain specimens, it was possible to identify the type of failure that occurred at the adhesive level. The Figure 67 a), adhesive is visible in the red-marked area at the centre of the joint. However, the corresponding area that was bonded to the central part shows no adhesive residue, as can be seen in Figure 67 b) in the red-marked zone. This observation indicates that the adhesive failure mode can be classified as interface failure, enhancing that the adhesive itself could support higher loads if a good surface preparation was made.

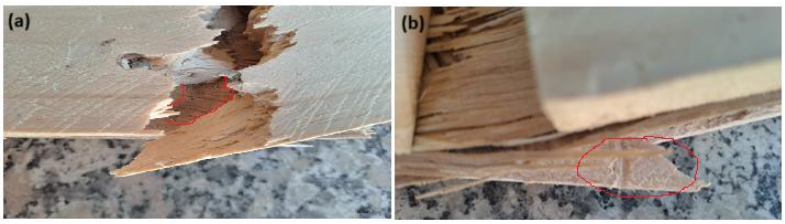

Figure 67 - Front view (a) and back view (b) of the fourth case of the simple laminate joint.

Figure 68 presents the first tested specimen corresponding to the laminate joints with junction alignment geometry. The results of all specimens of the laminate joint with junction alignment are presented in Appendix A, in Table A.4. These specimens demonstrate an identical behaviour to the previous configuration, showing delamination between the layers of the plywood. However, no failure was observed in either the wood or the adhesive.

Figure 68 - First tested specimen of the laminate joint with junction alignment front (a) and back (b) view.

Figure 69 presents the first tested specimen corresponding to the double strap joint geometry. The results of all specimens of the double strap joint are presented in Appendix A, in Table A.5. It is noteworthy that the fissures manifest along the direction of the wood fibre. As anticipated, it is evident that the cracks propagate through the nail holes, due to the discontinuities introduced by the nails. About the adhesive, as with the simple laminated joint, the transparency of the adhesive when dry presents a challenge in identifying the failure mode.

Figure 69 - First tested specimen of the double strap joint front (a) and back (b) view.

However, in certain specimens, it was possible to identify the nature of the failure that occurred at the adhesive level. As illustrated in Figure 70 a), the presence of adhesive material is observable within the red-marked area of the central portion of the joint. However, the corresponding area that was previously bonded to this central section shows no adhesive residue, as can be seen in Figure 70 b) in the red-marked region. This observation indicates that the adhesive failure mode can be classified as an interface failure.

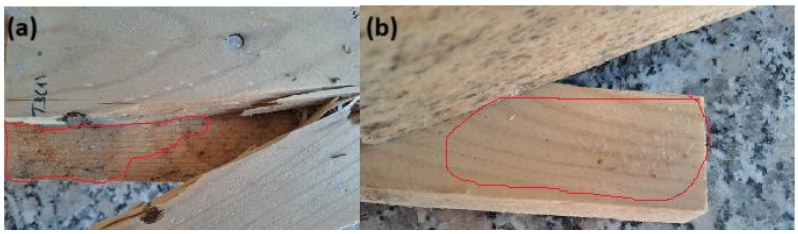

Figure 70 - Front view (a) and back (b) view of the fourth case of the double strap joint.

Figure 71 presents the first tested specimen related to the fastened double strap joint assembled with M4 fasteners. The results of all specimens of the fastened double strap joint (M4) are presented in Appendix A, in Table A.6. It can be observed that failures primarily occurred at the edges along the fastener lines. In instances where no wood failure was observed, the fasteners were deformed, indicating the inadequacy of this fastener size for this type of joint when compared to previous configurations.

Figure 71 - First tested specimen of the fastened double strap joint (M4 fasteners) front (a) and back (b) view.

Figure 72 presents the first tested specimen related to the double strap joint assembled with M6 fasteners. The results of all specimens of the fastened double strap joint (M6) are presented in Appendix A, in Table A.7.Increasing the fastener size led to failure occurring more frequently in the wood than in the fasteners. However, it is noteworthy that the failure of the wood was primarily observed around the edge fasteners, with no evidence of failure of the fasteners themselves. Less pronounced signs of deterioration were evident in the central area, where the fasteners exhibited visible signs of twisting, while the wood displayed minimal indications of degradation.

(a) **(b)**

Figure 72 - First tested specimen of the fastened double strap joint (M6 fasteners) front (a) and back (b) view.

Figure 73 presents the first tested specimen corresponding to the bolted double strap joint geometry with M6 bolts. The results of all specimens of the bolted double strap joint (M6) are presented in Appendix A, in Table A.8. In most specimens, the threaded connection failed without causing significant damage to the plywood that had been used as the connecting element. However, in the first tested specimen, failure occurred within the plywood itself, which may be attributed to a weaker plywood plate or to different positioning of the bolts. It is notable that most of failures occurred at the level of the threaded connection.

(a) **(b)**

Figure 73 - First tested specimen of the bolted double strap joint (M6 bolts) front (a) and back (b) view.

Figure 74 presents the second tested specimen corresponding to the bolted double strap joint geometry using M10 bolts. The results of all specimens of the bolted double strap joint (M6) are presented in Appendix A, in Table A.9. In contrast to the use of M6 bolts, the use of M10 bolts has been found to result in failure occurring primarily in the plywood. It is noteworthy that, the second tested specimen, failure occurred in the wood, which may indicate the presence of a defect, such as a knot or the creation of a crack during the fabrication process. In general, the use of M10 bolts has been demonstrated to result in failure occurring in the plywood rather than in the threaded connection.

Figure 74 - Second tested specimen of the bolted double strap joint (M10 bolts) front (a) and back (b) view.

Figure 75 presents the first tested specimen for the double strap joint with chamfer geometry using M4 fasteners. The results of all specimens of the double strap joint with chamfer (M4) are presented in Appendix A, in Table A.10. In this geometry, failure occurs in the wood of the straps, with cracks propagating through the fastener holes. For this geometry, when using M4 fasteners, the cracks tend to be small.

Figure 75 - First tested specimen of the double strap joint with chamfer (M6 fasteners) front (a) and back (b) view.

Figure 76 presents the first tested specimen for the double strap joint with chamfer using M6 fasteners. The results of all specimens of the double strap joint with chamfer (M6) are presented in Appendix A, in Table A.11. Equally to the specimens with M4 fasteners, failure occurs in the side wood plates, with cracks propagating along the fasteners. In this case, the cracks are larger in size compared to those observed when using M4 fasteners.

Figure 76 - First tested specimen of the double strap joint with chamfer (M6 fasteners) front (a) and back (b) view.

In general, for the double strap joint with chamfer, the fasteners size does not influence the failure mode but affects the extent of damage to the wood, which is greater when M6 fasteners are used.

3.3.4.2. *P-δ* curves

Figure 77a) presents the compilation of the *P-δ* curves from the five tested specimens for the 80x70 mm^2 wooden beams. As previously mentioned, the fourth specimen contains a significant knot, which may explain the much lower P_{max} compared to the other specimens. Consequently, the fourth specimen can be excluded on the basis that it presents a notable defect. The remaining specimens demonstrate similar maximum values of approximately 32 kN and show a high similarity in the elastic regime even for the fourth specimen. Figure 77b) presents the compilation of the *P-δ* curves from the five tested specimens for the 100x80 mm2 wooden beams. It is notable that all specimens exhibit a P_{max} of approximately 39 kN and present a high similarity in the elastic regime, enhancing a small variation of *E* between the specimens. Comparing the effect of increased dimensions, the enlargement of the cross-section resulted in a P_{max} increase and a slight increase in the failure displacement (δ_{max}).

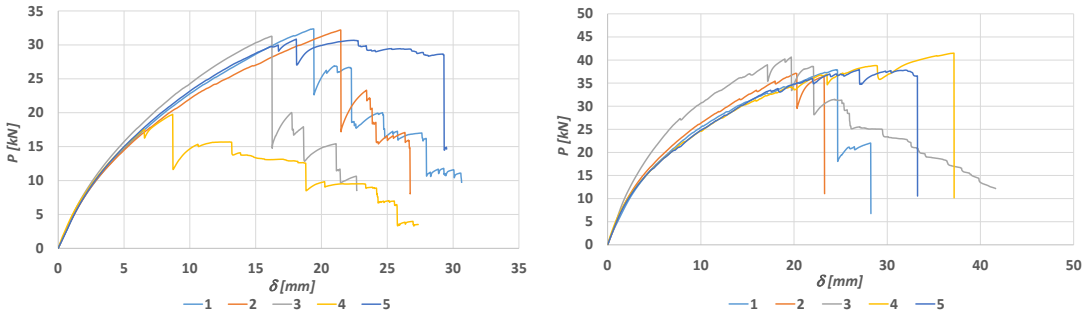

Figure 77 - *P-δ* curves of the 80x70 mm^2 (a) and of the 100x80 mm^2 wooden beams (b).

Figure 78a) presents the compilation of the *P-δ* curves from the five tested specimens of the simple laminate joint. As shown, all specimens exhibit a P_{max} around 29 kN and present a higher dispersion of *E* between specimens comparing to the previous geometries. Figure 78b) presents the compilation of the *P-δ* curves from the five tested specimens of the laminate joint with junction alignment. It is notable that this geometry exhibits greater linearity up to failure. As can be seen, the specimens have a P_{max} approximately 28 kN and *E* demonstrates less dispersion between specimens compared to the simple laminate joint, although a more significant P_{max} variation between specimens.

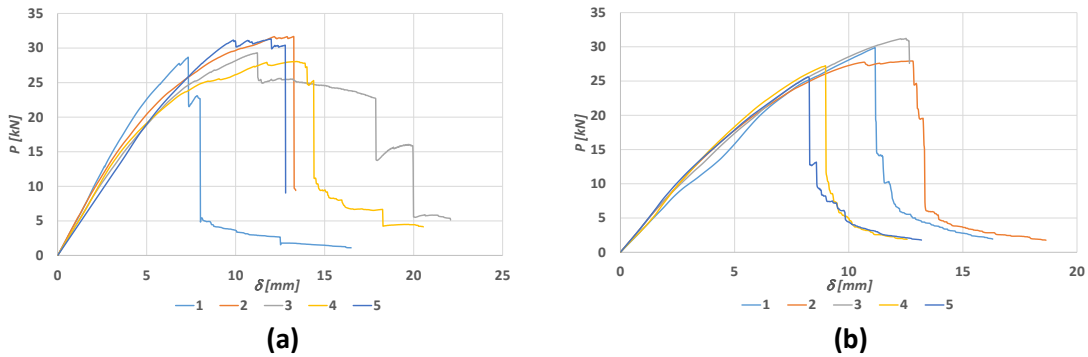

Figure 78 - *P-δ* curves of the simple laminate joint (a) and of the simple laminate joint with junction alignment (b).

Comparing the effect of joint alignment, it can be stated that it does not have a significant influence on P_{max} or δ_{max}. However, the presence of alignment leads to an abrupt collapse once P_{max} is reached. In contrast, the absence of alignment demonstrates a residual resistance after P_{max} is attained, delaying the collapse.

Figure 79 presents the compilation of the *P*-δ curves from the five tested specimens of the double strap joint. These joint exhibits a P_{max} around 22 kN, a δ_{max} that is lower than in the previous geometries and a reasonable dispersion of *E* between specimens.

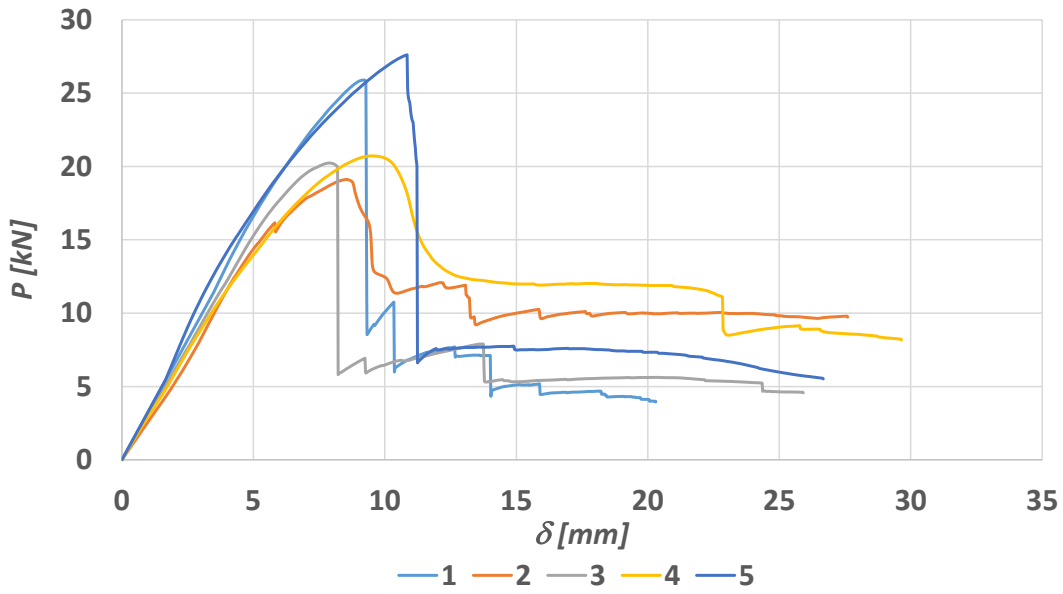

Figure 79 - *P*-δ curves of the double strap joint.

Figure 80a) presents the compilation of the *P*-δ curves from the five tested specimens of the fastened double strap joint using M4 fasteners. The results exhibit low consistency and an overall low P_{max}, averaging approximately 7.3 kN, and present significant dispersion in the measured *E* between specimens. Figure 80b) presents the compilation of the *P*-δ curves from the five tested specimens of the fastened double strap joint using M6 fasteners. In this case, the results show greater consistency of *E* between the specimens, yet P_{max} remains relatively low, at approximately 8.6 kN, especially when compared to previous joint geometries.

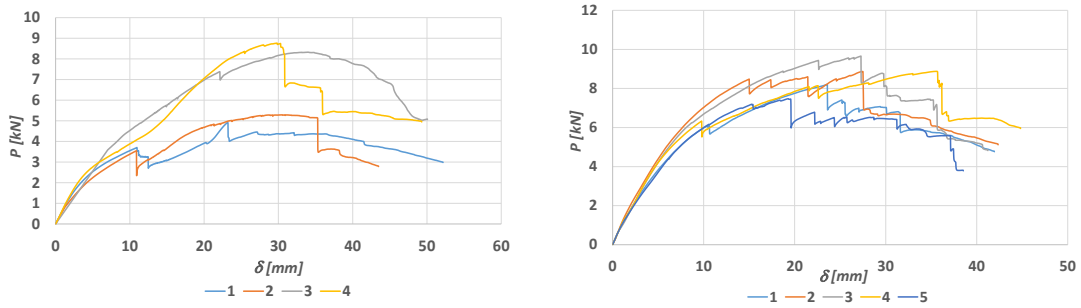

Figure 80 - *P*-δ curves of the fastened (M4) double strap joint (a) and of the fastened (M6) double strap joint (b).

Comparing the effect of using fasteners of different sizes, it can be stated that the main impact of using M6 instead of M4 fasteners lies in the improved P_{max} and *E* consistency, although the load values remain relatively low. The results for this joint geometry also highlight the significant effect of using adhesive. When comparing the double strap joint using nails and adhesive with the fastened double strap joint without adhesive, it is evident that the use of adhesive has an important impact, since it increases P_{max} by approximately 55%.

Figure 81a) and b) presents the compilation of the *P*-δ curves for the bolted strap joints with M6 and M10 bolts, respectively. P_{max} is quite similar in both cases, i.e., are approximately 22 kN for M6 bolts and approximately 24 kN for M10 bolts, representing a small increase of 9%. The most notable difference due to bolt size is in δ_{max}, which is greater when using M6 bolts. However, the joints assembled with M6 bolts exhibit higher consistency in *E* compared to those with M10 bolts.

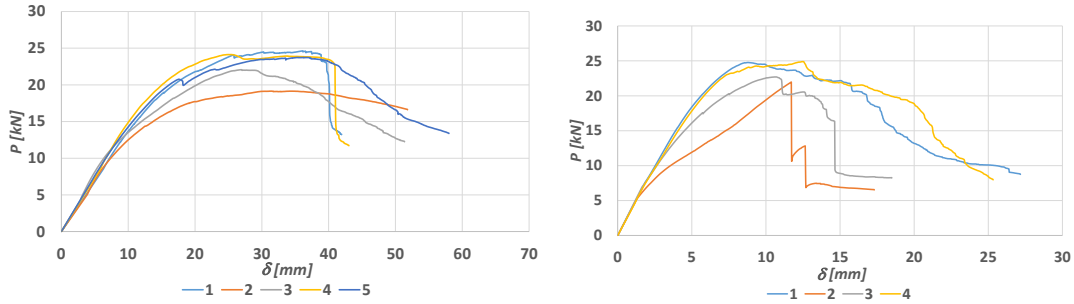

Figure 81 - *P*-δ curves of the bolted (M6) double strap joint (a) and of the bolted (M10) double strap joint (b).

Figure 82a) and b) presents the compilation of the *P*-δ curves for the double strap joint with chamfer, using M4 and M6 fasteners, respectively. For this geometry, the fastener size appears to have little influence on P_{max}, which is approximately 26 kN with M4 fasteners and 28 kN with M6 fasteners. However, in both cases, it is noteworthy that the joint exhibits consistency of *E* between specimens and presents multiple stages of behaviour indicating that, even after failure, it does not collapse immediately due to the chamfer.

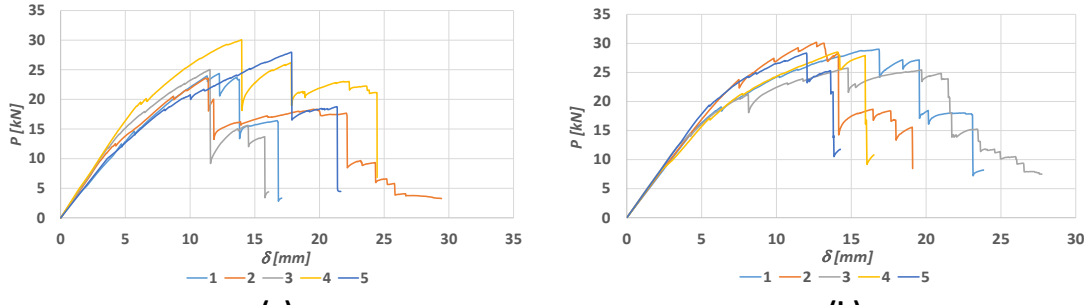

Figure 82 - *P*-δ curves of the double strap joint with chamfer (M4) (a) and of the double strap joint with chamfer (M6) (b).

3.3.4.3. Mechanical properties

Based on the *P*-δ curves analysed, this section addresses the mechanical properties of the joints, such as *E*, P_{max}, δ_{max}., and maximum stress (σ_{max}). For each geometry, the average and deviation are calculated based on the values of each specimen. Additionally, the coefficient of variation (COV) is computed to assess the dispersion of the results and determine whether the average can be considered a representative value, which is acceptable when equal or below to 10% as a good engineering practice.

To determine *E*, a trend line to the linear region of the *P–δ* curve is added, as illustrated in Figure 83. The *E* is then given by the slope of this line, and then after multiple by 1000 to give the *E* in MPa. To evaluate how well the trend line represents the data's linearity, the coefficient of correlation (R^2) is used. An R^2 value as close as possible to 1 indicates a reliable trend line.

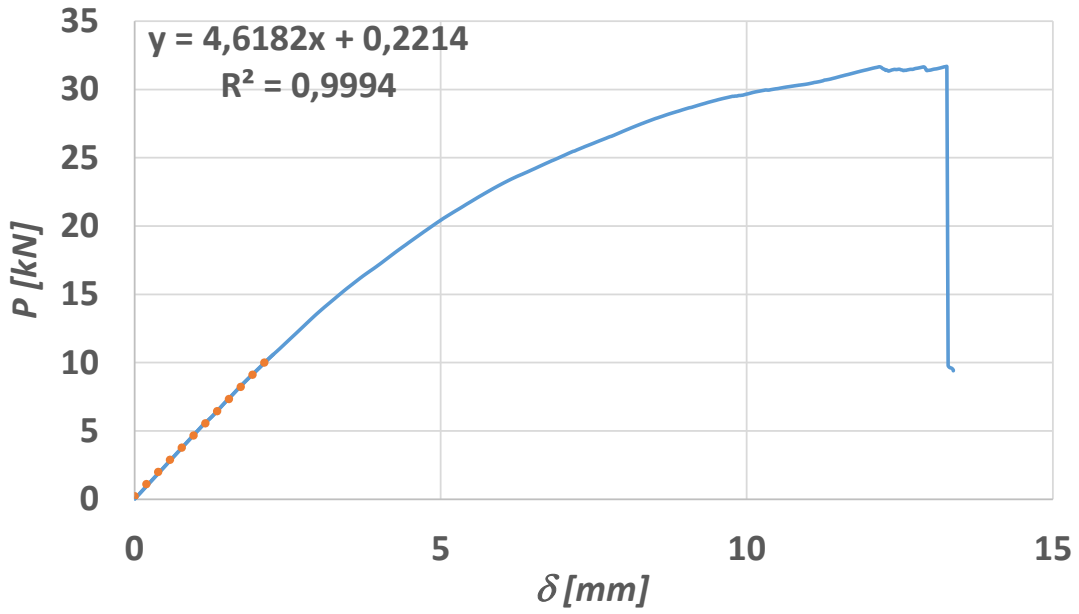

Figure 83 - *P–δ* curve of the first specimen of the simple laminate joint.

Subsequently, P_{max} and the δ_{max} are directly extracted from the experimental data. Finally, the determination of the σ_{max} for all specimens is carried out by the calculation of the maximum bending moment (M_f^{max}), based on equation 5, which incorporates the P_{max} and the distance between supports (L).

$$M_f^{max} = \frac{P_{max}}{2} \cdot \frac{L}{2} \qquad (5)$$

Next, the moment of inertia (I_i) for rectangular sections of each component of a joint is calculated with equation 6, which incorporates the width (h) and the thickness (b) of each component. After that, once all parts have same the distance to the neutral axis (y), which is $\frac{h}{2}$, I_i of each component are sum up, resulting in the global moment of inertia (I_g). But not every part of a joint is considered (i.e., parts with discontinuity), and only the parts that increase the

E of the joint are. Figure 84 presents the simple laminate joint, where the red parts are used for the stress calculation and blue parts are not. Finally, σ_{max} can be calculated using equation 7.

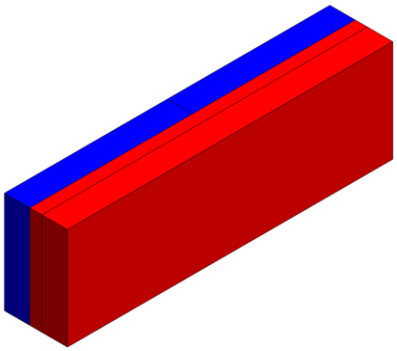

Figure 84 - Simple laminate joint, identification of the parts used for the global moment of inertia.

$$I_i = \frac{bh^3}{12} \tag{6}$$

$$\sigma_{max} = \frac{M_f^{max} \cdot y}{I_g} \tag{7}$$

Having established this procedure, Table 14 presents the values of *E*, P_{max}, δ_{max}, and σ_{max} for the specimens of 80×70 mm^2 wooden beams, while Table 15 presents the corresponding values for the 100×80 mm^2 wooden beams. In both cases, since the COV for *E*, P_{max}, and σ_{max} is below 10%, the average values can be used to characterize the beams. This is not the case for δ_{max} at failure, which exhibits a COV greater than 10%. For this and subsequent analyses, whenever the COV is higher than 10%, the measured quantities are established as an interval of minimum and maximum values.

Table 14 - Mechanical properties of 80x70 mm^2 wooden beams

	**Properties**			
	***E* [MPa]**	**P_{max} [N]**	**δ_{max} [mm]**	**σ_{max} [MPa]**
1	3712.8	32356.8	20.58	33.34
2	3834.5	32198.2	23.09	32.21
3	4139.7	31264.4	16.94	31.83
4	4246.4	19757.1	9.41	18.68
5	3601.1	30849.6	19.11	31.90
Average	3822.0	31667.3	19.93	32.32
Deviation	201.1	630.1	2.24	0.61
COV	5.3%%	2.0%	11.2%	1.9%

Table 15 - Mechanical properties of 100x80 mm² wooden beams

	**Properties**			
	***E* [MPa]**	**P_{max} [N]**	**δ_{max} [mm]**	**σ_{max} [MPa]**
1	5393.2	37918.6	25.46	26.52
2	5229.1	37125.1	21.57	25.86
3	5455.5	40635.7	20.93	29.41
4	5433.1	41487.4	37.56	29.46
5	5263.6	37932.4	27.86	24.90
Average	5354.9	39019.8	26.68	27.23
Deviation	91.5	1713.8	6.01	1.87
COV	1.7%	4.4%	22.5%	6.9%

Comparing the values resulting from the increased dimensions, the 100×80 mm² wooden beams generally exhibit higher mechanical properties than the 80×70 mm² wooden beams. *E* for the 100×80 mm² beams is 28.2% higher compared to the 80×70 mm² beams. Additionally, P_{max} of the 100×80 mm² beams are 23.2% higher than that of the 80×70 mm² beams. On the other hand, the 100×80 mm² beams show a reduction in σ_{max} of approximately 18.7% compared to the σ_{max} observed in the 80×70 mm² beams.

Table 16 presents the values of *E*, P_{max}, δ_{max}, and σ_{max} for the specimens of the simple laminate joint, while Table 17 presents the values for the laminate joint with junction alignment. Since, for both geometries, the COV for *E*, P_{max}, and σ_{max} is equal or below 10%, the average values can be used to characterize the joints. This is not the case for the δ_{max}, which exhibits a COV greater than 10%.

Table 16 - Mechanical properties of the simple laminate joint

	**Properties**			
	***E* [MPa]**	**P_{max} [N]**	**δ_{max} [mm]**	**σ_{max} [MPa]**
1	4817.5	28681.1	8.44	37.98
2	4618.2	31678.2	13.27	42.16
3	4267.8	29304.8	14.43	41.65
4	4287.7	28069.7	16.09	36.40
5	3811.0	31326.6	13.5	43.27
Average	4360.4	29812.1	13.15	40.29
Deviation	393.8	1438.6	2.55	2.64
COV	7.9%	4.8%	19.4%	6.5%

Table 17 - Mechanical properties of the laminate joint with junction alignment

	**Properties**			
	***E* [MPa]**	**P_{max} [N]**	**δ_{max} [mm]**	**σ_{max} [MPa]**
1	3417.8	29873	11.87	108.78
2	3879.7	27932.5	13.57	105.41
3	3737.5	31223.7	13.02	112.04
4	3760.6	27232.9	11.18	95.84
5	4107.7	25609.6	9.31	93.71
Average	3780.7	28374.4	11.79	103.16
Deviation	223.9	1975.16	1.50	7.19
COV	5.9%	7.0%	12.7%	7.0%

Comparing the values obtained for the two geometries, it is evident that there are no significant differences in terms of P_{max}, since it shows a decrease of 5.1%. On the other hand, *E* and σ_{max} show a more pronounced difference, with a reduction of 13.3% and an increase of 156%, respectively, indicating that the junction alignment provides a more compliant behaviour but is also prone to higher stresses.

Table 18 presents the values of *E*, P_{max}, δ_{max}, and σ_{max} for the specimens of the double strap joint. Since the COV for *E* is below 10%, the average value can be used to characterize the joint. This is not the case for P_{max}, δ_{max}, and σ_{max}, as their COV values exceed 10%.

Table 18 - Mechanical properties of the double strap joint

	**Properties**			
	***E* [MPa]**	**P_{max} [N]**	**δ_{max} [mm]**	**σ_{max} [MPa]**
1	3322.3	25889.1	13.43	23.08
2	2772.0	19107.4	9.93	16.48
3	3061.6	20237.5	12.29	18.61
4	2935.7	20719.7	11.03	17.80
5	3577.7	27607.8	13.29	24.72
Average	3133.9	22712.3	11.99	20.14
Deviation	285.6	3380.8	1.34	3.19
COV	9.1%	14.9%	11.2%	15.8%

Comparing this geometry with the previous ones, *E* decreased by approximately 34.2% relatively to the simple laminate joint and about 18.5% relatively to the laminate joint with junction alignment, making it a less attractive geometry. However, this geometry presents a significant decrease in the σ_{max} (50%) compared to the simple laminate joint and approximately 80.6% compared to the laminate joint with junction alignment.

Table 19 presents the values of *E*, P_{max}, δ_{max}, and σ_{max} for specimens of the fastened double strap joint using M4 fasteners, while Table 20 shows the same data for specimens using M6

fasteners. When M4 fasteners are used, a high COV is observed. However, upon closer examination, two specimens show notably lower P_{max} values than the others, which may indicate slight differences in nail placement, which enhance the importance of the nails. Focusing on the specimens with M6 fasteners, their COV values are below 10%, except for δ_{max}.

Table 19 - Mechanical properties of fastened double strap with M4 fasteners

	**Properties**			
	***E* [MPa]**	**P_{max} [N]**	**δ_{max} [mm]**	**σ_{max} [MPa]**
1	704.13	4914.9	23.73	7.21
2	643.88	5288.7	32.01	7.04
3	508.86	8323.4	45.96	12.06
4	693.50	8755.9	30.62	12.95
5	680.20	9559.2	32.89	13.92
Average	646.11	7368.4	33.04	10.64
Deviation	71.58	1896.4	7.22	2.93
COV	11.1%	25.7%	21.8%	27.5

Table 20 - Mechanical properties of fastened double strap joint with M6 fasteners

	**Properties**			
	***E* [MPa]**	**P_{max} [N]**	**δ_{max} [mm]**	**σ_{max} [MPa]**
1	976.4	8207.3	26.73	11.65
2	1052.4	8871.4	28.39	11.81
3	967.7	9656.6	29.05	12.34
4	1009.8	8878.6	38.05	12.27
5	1044.4	7472.1	19.90	10.56
Average	1010.1	8617.2	28.42	11.79
Deviation	34.36	733.9	5.81	0.53
COV	3.4%	8.5%	20.4%	4.5%

Based on the COV, it is evident that fastener size influences the consistency of the joint. Comparing the obtained values, *E* is higher when using M6 fasteners, and σ_{max} is also higher for the geometry with M6 fasteners. Analysing the P_{max} values, it is more difficult to determine which of the two options performs better, as their values are similar. However, compared to previous geometries, these values are considerably lower, which emphasizes the importance of the adhesive in the joints.

Table 21 presents the values of *E*, P_{max}, δ_{max}, and σ_{max} for specimens of the bolted double strap joint with M6 bolts, while Table 22 presents the values when M10 bolts are used. Since, for both geometries, the COV for *E*, P_{max}, and σ_{max} is below 10%, the average values can be used to characterize the joints. This is not the case for the δ_{max}, which exhibits a COV greater than 10%.

Table 21 - Mechanical properties of bolted double strap joint with M6 bolts

	**Properties**			
	***E* [MPa]**	**P_{max} [N]**	**δ_{max} [mm]**	**σ_{max} [MPa]**
1	1382.6	24630.3	38.91	43.42
2	1380.4	19144.9	36.56	33.15
3	1548.2	22068.2	27.95	42.32
4	1470.5	24131.5	26.87	42.80
5	1365.1	23727.5	39.37	43.34
Average	1429.4	22740.5	33.93	41.01
Deviation	70.04	1993.03	5.42	3.95
COV	4.9%	8.8%	16.0%	9.6%

Table 22 - Mechanical properties of bolted double strap joint with M10

	**Properties**			
	***E* [MPa]**	**P_{max} [N]**	**δ_{max} [mm]**	**σ_{max} [MPa]**
1	4085.1	24771.5	11.82	43.24
2	4034.9	21972.0	13.95	40.25
3	4213.3	22696.1	14.92	40.94
4	4019.5	24896.5	14.33	45.77
Average	4088.2	23584.0	13.76	42.55
Deviation	76.19	1276.7	1.17	2.16
COV	1.9%	5.4%	8.5%	5.1%

Comparing the influence of increasing bolts size, it is observed that P_{max} using M10 bolts shows a slight increase of 3.7%, with a σ_{max} very similar to the geometry using M6 bolts. On the other hand, there is a significant increase of 286% in *E*, showing that the use of M10 bolts highly decrease the ductility of the joint.

Table 23 presents the values of *E*, P_{max}, δ_{max}, and σ_{max} for specimens of the double strap joint with chamfer using M4 fasteners, while Table 24 presents the values for specimens with M6 fasteners. Since, for both geometries, the COV for *E* and P_{max} is below 10%, it is considered that the average values can be used to characterize the joints. This is not the case for the δ_{max} and σ_{max} when using M4 fasteners, which exhibits a COV greater than 10%.

Table 23 - Mechanical properties of double strap joint with chamfer with M4 fasteners

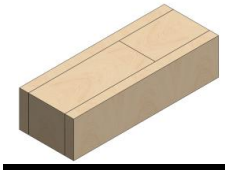	**Properties**			
	***E* [MPa]**	**P_{max} [N]**	**δ_{max} [mm]**	**σ_{max} [MPa]**
1	3259.1	24368	13.95	15.81
2	3158.8	23605.3	14.89	15.19
3	3270.7	25031.8	14.26	17.88
4	3286.5	30054.8	18.12	20.44
5	2769.7	27962.7	20.33	20.21
Average	3148.9	26204.5	16.31	17.91
Deviation	194.8	2425.7	2.50	2.17
COV	6.2%	9.3%	15.3%	12.1%

Table 24 - Mechanical properties of double strap joint with chamfer with M6 fasteners

	**Properties**			
	***E* [MPa]**	**P_{max} [N]**	**δ_{max} [mm]**	**σ_{max} [MPa]**
1	3339.0	29001.6	21.85	20.49
2	3449.2	30180.2	19.05	19.42
3	3666.5	25758.9	16.92	16.54
4	3397.3	28507.5	17.4	20.93
5	3604.5	28336.5	15.11	20.81
Average	3491.3	28356.9	18.07	19.64
Deviation	124.4	1450.02	2.27	1.64
COV	3.6%	5.1%	12.6%	8.3%

In this case, it is evident that increasing the fastener size from M4 to M6 does not significantly influence the mechanical properties of the joint. Specifically, the transition from M4 to M6 results in an increase of 10.9% in *E*, 8.2% in P_{max}, and 9.66% in σ_{max}.

3.3.5. Results discussion

To compare the geometries as well as the manufacturing processes required for their realization, Table 25 presents the average values when the COV of the property was equal or below 10%. When the COV exceeded this threshold, the range between the minimum and maximum values is exposed.

Table 25 - Mechanical properties of the different joints

Properties	E [MPa]	P_{max} [N]	δ_{max} [mm]	σ_{max} [MPa]
80x70 mm^{2}wooden beams	3822.0	29285.2	16.94-23.09	29.59
100x80 mm^2 wooden beams	5354.9	39019.8	20.93-37.56	27.23
Simple laminate joint	4360.4	29812.1	8.44-16.09	40.29
Laminate joint with junction alignment	3780.7	28374.4	9.31-13.57	103.2
Double strap joint	3133.9	19107.4-27607.8	9.93-13.43	16.48-24.72
Fastened (M4) double strap joint	508.9-704.1	4914.9-9559.2	23.73-45.96	7.04-13.91
Fastened (M6) double strap joint	1010.1	8617.2	19.9-38.05	11.79
Bolted (M6) double strap joint	1429.4	22740.5	26.87-39.37	41.01
Bolted (M10) double strap joint	4088.2	23584.0	11.82-14.92	42.55
Double strap joint with chamfer (M4)	3148.9	26204.5	13.95-20.33	15.19-20.44
Double strap joint with chamfer (M6)	3491.3	28356.9	15.11-21.85	19.64

Based on the obtained values, it is evident that the geometry exhibiting the highest E and P_{max} is the 100x80 mm^2 wooden beams. This geometry is representative of the ideal case, i.e. one in which there is no discontinuity. Table 26 presents a comparison between the joints and the 100x80 mm^2 wooden beams.

Table 26 - Variation of properties of the joints compared to the 100x80 mm^2 wooden beams

Variation of:	E	P_{max}	δ_{max}	σ_{max}
Simple laminate joint	-18.6%	-23.6%	-50.7%	+47.9%
Laminate joint with junction alignment	-29.4%	-27.3%	-55.8%	+279.1%
Double strap joint	-41.5%	-41.8%	-55.1%	-26.05%
Fastened (M4) double strap joint	-87.9%	-81.1%	+23.9%	-60.9%
Fastened (M6) double strap joint	-81.1%	-77.9%	+6.5%	-56.7%
Bolted (M6) double strap joint	-73.3%	-41.7&	+27.1%	+50.6%

Table 26 - Variation of properties of the joints compared to the 100x80 mm^2 wooden beams (Continued)

Bolted (M10) double strap joint	-23.7%	-39.6%	-48.4%	+56.3%
Double strap joint with chamfer (M4)	-41.2%	-32.9%	-38.9%	-34.2%
Double strap joint with chamfer (M6)	-34.8%	-27.3%	32.3%	-27.9%

Based on the obtained percentual variations, it is evident that the joint presenting greater proximity with the 100x80 mm^2 wooden beams properties, is the simple laminate joint using. This joint present a very small variation of the *E* (-18.6%) compared to the others.

To better understand the influence of each type of connection and geometry, the comparison between similar joints is made. Comparing the **simple laminate joint** with the **laminate joint with junction alignment**, it is notable that the junction alignment does not significantly influence the *E*, P_{max}, δ_{max}, but highly increase the σ_{max}.

The double strap joint can be compared to the **fastened double strap** joint to highlight the significant impact of adhesive in the joints. From this comparison, adhesive primarily contributes to the joint's strength. Regarding the fastened double strap joints, the transition from M4 to M6 fasteners brings improvements in mechanical properties as well as greater consistency in the values obtained from each specimen. As mentioned, this geometry underscores the importance of using adhesive in these joints. A notable parameter for the fastened double strap joints is that the displacement at failure is much greater compared to joints using adhesive, thus demonstrating higher ductility.

The bolted double strap joint comparing the bolts size, it can be observed that increasing the bolt size from M6 to M10 does not influence the load capacity, but significantly affects the joint *E*. This behaviour indicates that using M6 bolts results in a more ductile joint, given the lower *E* and much higher δ_{max}. When comparing the bolted double strap joint with M10 bolts to the double strap joint, it is show that the use of M10 bolts and plywood on the sides provides similar P_{max} to the double strap joint, making an analysis of the manufacturing process is necessary to determine the most viable joint. Another point can be the tightening torque in the bolts, which can highly influence the geometry performance.

The double strap joint with chamfer once again demonstrates that increasing fastener size has little effect on the mechanical properties. On the other hand, this geometry, which does not use adhesive, presents P_{max} values like those of adhesive based geometries. Therefore, the addition of a chamfer allows for a small increase in *E* and P_{max} compared to the standard double strap joint.

Overall, the experimental test demonstrated that the use of adhesive is essential to achieve high *E* and P_{max} when no chamfer is present on the central beams. On the other hand, the

increase in fastener size has not a significant influence on the mechanical properties of the joints. But the bolts can have a high impact in the joint performance, depending on the Tightening torque impose.

To conduct a complete comprehensive analysis of the joints, it is necessary to consider the manufacturing process, since an overly complex process or the use of more expensive materials can make a joint industrially less attractive. Accordingly, Table 27 presents a qualitative analysis using the 9-point Likert scale from Table 1. For the 'Material acquisition' column, both the cost and market availability of the materials present in the joint are considered. Thus, geometries incorporating plywood, bolts, fasteners, and/or adhesive are regarded as having a higher final cost. Next, the 'Fabrication procedure' column considers the ease of joint fabrication in terms of required tools, the quantity of materials needed, and the time required for realization. Finally, 'Joint quality' column refers to the consistency of producing a high-quality joint and the extent to which the manufacturing process avoids causing defects in the materials. At the end, a score is assigned to each joint, calculated by summing the intensity of agreement values. This analysis does not differentiate fastener/bolts sizes but considers only the joint type, and it also excludes the 80x70 mm^2 and 100x80 mm^2 wooden beams, since they are only for properties comparison.

Table 27 - Qualitative analysis of overall fabrication process of the geometries

Geometry	Material acquisition	Fabrication procedure	Joint quality	Overall classification
Simple laminate joint	7	9	8	24
Laminate joint with junction alignment	7	8	8	23
Double strap joint	8	7	8	23
Fastened double strap joint	8	7	8	23
Bolted double strap joint	6	1	4	11
Double strap joint with chamfer	9	7	8	24

Finally, it is possible to gain a more general overview of each joint and its industrial viability. It is notable that the bolted double strap joint is complex to manufacture and exhibits geometric defects, making it less viable given the manufacturing method used. On the other hand, the inclusion of a chamfer makes the fabrication of the joint more challenging compared to the simple laminate joint but involves a smaller variety of materials. Therefore, the simple laminate

joint and the double strap joint with chamfer are the geometries with highest potential and thus recommended to use in the studied pallet at this point.

3.4. Numerical analysis

Along with the experimental tests, numerical analyses are performed to support and validate the experimental results. This section introduces the chosen software and explains the reasons behind its selection. It also outlines the overall modelling process, illustrated using the simple laminated joint. A key aspect of the modelling involves the mechanical properties of the materials. Since most of the materials used are orthotropic, a literature review was carried out and adjustments were made to obtain properties that best reflect the experimentally observed behaviour. Finally, as in the experimental section, the numerical results are presented and directly compared with the experimental data.

3.4.1. Choice of software

Choosing the most suitable software for FEA depends on several technical and practical criteria. One of the main factors to consider is the software's ability to control the mesh modelling and the complex materials models, which is essential for high-precision simulations. For instance, software such as ANSYS® and Abaqus® are often favoured for their wide range of features, such as damage and fracture mechanics, and their ability that enable simulating real-world operating conditions with high accuracy. The bases of that software have common aspects, including parametric modelling or the possibility to import geometries from others software.

Due to the fact most of the materials used on the studied pallet are anisotropic, it is more convenient the use of Abaqus®, which accounts for material formulations to model those types of materials. As shown in Figure 85a), an anisotropic material is a material whose properties vary depending on the direction in which they are measured. In other words, the material behaves differently along different axes or directions. In the other hand isotropic material have the same properties in all directions (Figure 85b)).

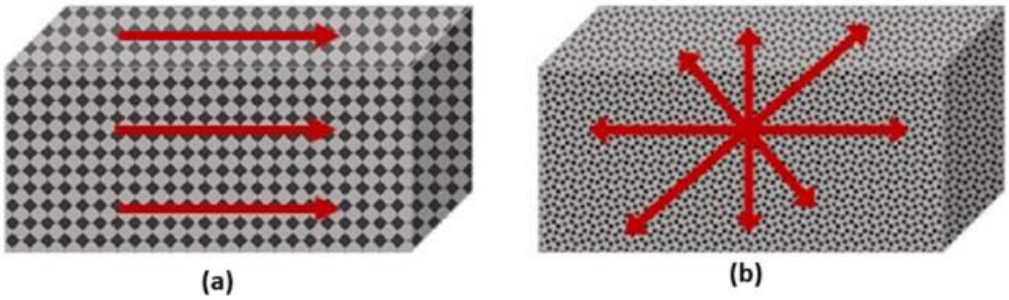

Figure 85 – Anisotropic (a) and Isotropic material (b) [119].

Abaqus® is a widely chosen software for advanced simulations due to its ability to model complex constitutive models, including cohesive models, supported by a dedicated cohesive materials library. These models are essential to represent the behaviour of interfaces, adhesives, and brittle materials prone to delamination or interfacial fracture [120]. Abaqus® enables accurate modelling and prediction of crack growth and structural response. By

enhancing the realism of numerical analysis, it provides more reliable assessments of component structural integrity, making Abaqus® an ideal tool for this type of study [121], and justifying its choice.

3.4.2. Pre-processing

The accuracy and reliability of FEA results are heavily dependent on the initial phase of the simulation process, known as pre-processing. This stage involves the preparation of the computational model. This is achieved through the definition of its geometry, the assignment of material properties, the assembly of components, the setting up of analysis steps and interactions, the application of boundary conditions, the generation of the mesh, and the creation of the job for analysis. Pre-processing constitutes a critical step, as errors or oversimplifications introduced at this stage can compromise the accuracy of the results to a significant degree. It is imperative to exercise meticulous attention during this phase to ensure that the numerical model closely mirrors the real-world behaviour of the system, whilst also ensuring the efficient utilisation of computational resources. The subsequent section provides an overview of the general methodology employed in the development of the various models. To illustrate the process, a simple laminate joint is used as an example. As previously mentioned, the FEA simulations are performed using Abaqus®, with the goal of modelling a three-point bending scenario. The development of the numerical model necessitates navigation through several key modules within the software. The following modules must be considered: part, property, assembly, step, interaction, load, mesh, job and visualisation.

The simulation process is initiated by the first module, which involves the creation of parts. Two main components are modelled for this analysis, namely the joint (Figure 86a)) and a separate part representing the supports and the punch (Figure 86b)). The joint is modelled as a three-dimensional deformable solid, as its geometry is width-dependent, allowing for an accurate representation of its mechanical response under loading conditions.

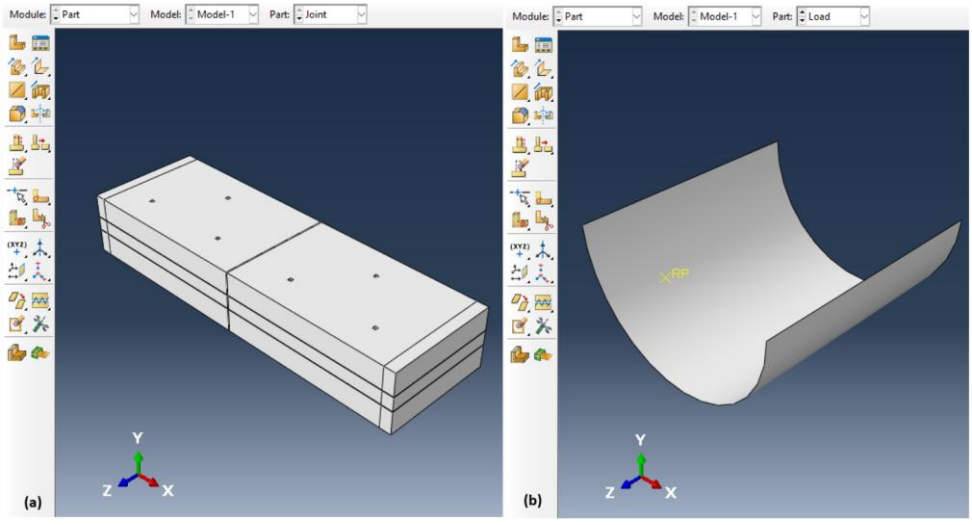

Figure 86 - 3D model of the joint part (a) and support/punch part (b).

The initial phase of the process involves the delineation of the joint outline (Figure 87), which is then extruded to the appropriate depth to form the three-dimensional geometry.

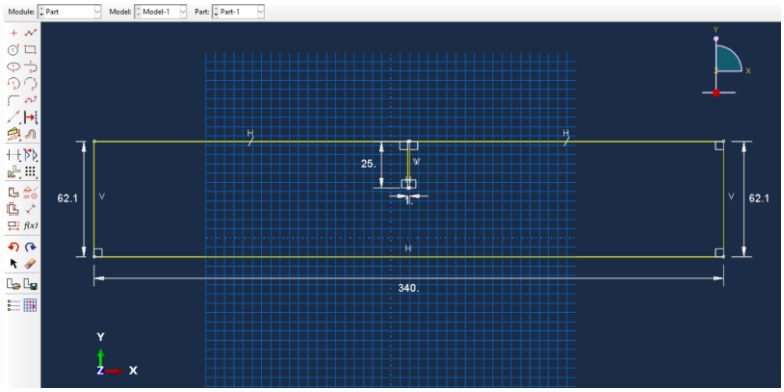

Figure 87 - 2D sketch of the general outline of the joint part.

Subsequently, partitions are created within the geometry (Figure 88) to define the regions corresponding to the various materials. The introduction of additional partitions in the support and loading areas is a key element in facilitating mesh refinement in critical zones. With these steps, the joint geometry is fully defined and ready for the next stage.

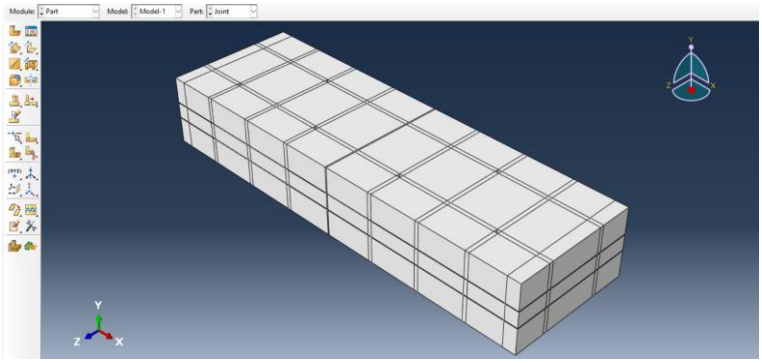

Figure 88 - 3D model of the joint part with the partitions.

The part used to simulate the supports, and the punch is created by first sketching a semi-circular profile in a 2D plane, which is then extruded to form a 3D solid. This component is defined as an analytical rigid body, as it is not expected to undergo deformation during the simulation. As demonstrated in Figure 89, a reference point (RP) is created and linked to this rigid component. The RP functions as the location at which loads, and boundary conditions can be applied with precision.

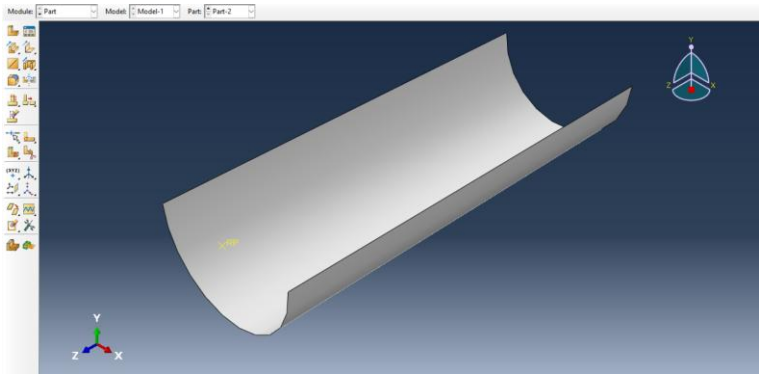

Figure 89 - 3D model of the support/punch part.

After the creation of all constituent components, the next step is to define and assign materials to the appropriate partitions within the joint component. The material definition process is initiated with the selection of constitutive models that most accurately represent the behaviour of the real materials. Based on these models, materials and corresponding sections are created. The constitutive models and their associated properties are detailed in the following two sections. It is important to note that, given that the support/punch component is modelled as a rigid body, no material is assigned to it.

Following the delineation of all requisite materials, the creation of sections occurs through the establishment of links between each material and its respective constitutive model. These sections are then allocated to the respective partitions of the 3D joint model (Figure 90), thereby ensuring that each region reflects the intended mechanical behaviour.

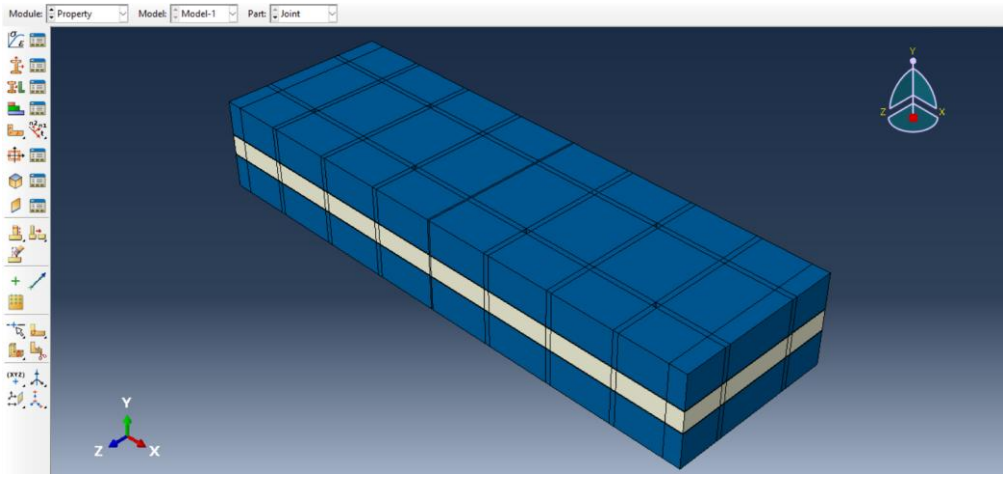

Figure 90 - Joint part with defined materials.

Upon the conclusion of the property module, the subsequent step is the assembly module. It is imperative to acknowledge that the model is composed of numerous constituent parts. Consequently, it is necessary to formulate an assembly that encompasses both the joint and the support/punch components. The distance between the supports is set to match the configuration used in the experimental tests (300 mm), and the punch is positioned directly above the joint, as illustrated in Figure 91.

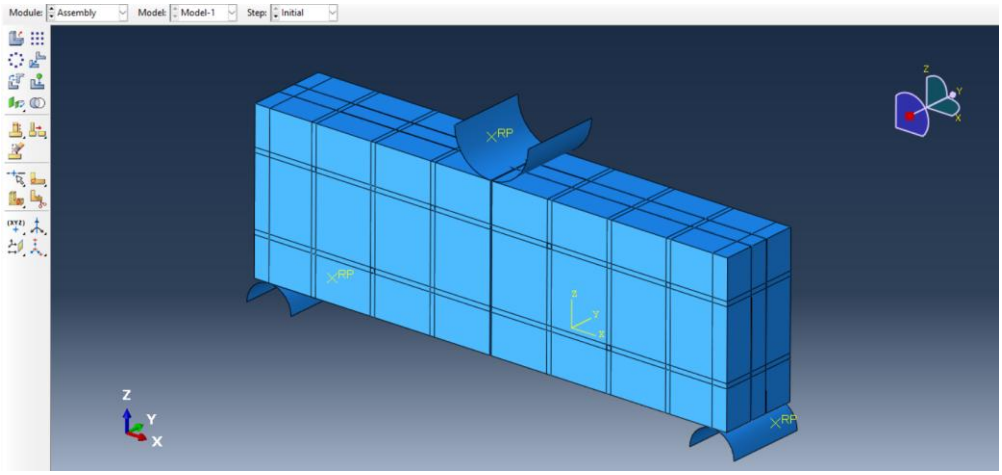

Figure 91 - Assembly of the joint with the supports/punch.

After the assembly of the final structure, the simulation progresses to the step module. This module is employed to delineate the analysis type and steps that govern the simulation's temporal evolution, including the application and evolution of loads and boundary conditions. Additionally, it enables the selection of output variables to be documented during the simulation process. To create the P-δ curves, the displacement (U3) of the punch and the reaction force (RF3) are outputted.

Once having the step module configure, it is possible to go to the interaction module, which defines the contacts between the various parts of the model. In this study a surface-to-surface contact and tie interaction are used. Surface-to-surface is used between the joint parts that are not bonded but are in contact, and the support/punch part to prevent interpenetration during loading, thereby ensuring realistic physical behaviour. In this contact definition, the tangential behaviour is set to frictionless, allowing free sliding between the contacting surfaces without resistance. The normal behaviour is defined using the pressure-overclosure relationship with hard contact, which prevents penetration under compression while allowing separation under tension. This configuration captures the essential contact mechanics during loading, ensuring both stability and accuracy in the simulation results. The tie interaction is used between the bolts/fasteners/nails and the parts of the joint directly in contact, so that the bolts/fasteners/nails are bonded to the parts. With this procedure, the interaction module is complete.

After the configuration of interactions, the simulation advances to the load module (Figure 93). To replicate a three-point bending test, it is necessary to fully constrain the supports, while restricting the punch to move only in the vertical (z) direction. The application of these boundary conditions is performed on the RP that has been previously defined on the rigid support/punch part. A displacement-controlled approach is employed, whereby the value of the vertical displacement is based on the experimental one. However, using only those loading constrains could cause a rigid body behaviour of the specimen. As presented in Figure 92, during the first modelling iterations, the part presented a rotation around the loading axis. To prevent this undesirable behaviour, a constraint for the rotation around the loading axis and a displacement constraint in the perpendicular direction are implemented. With these modifications, the joint can only present a displacement in the load direction.

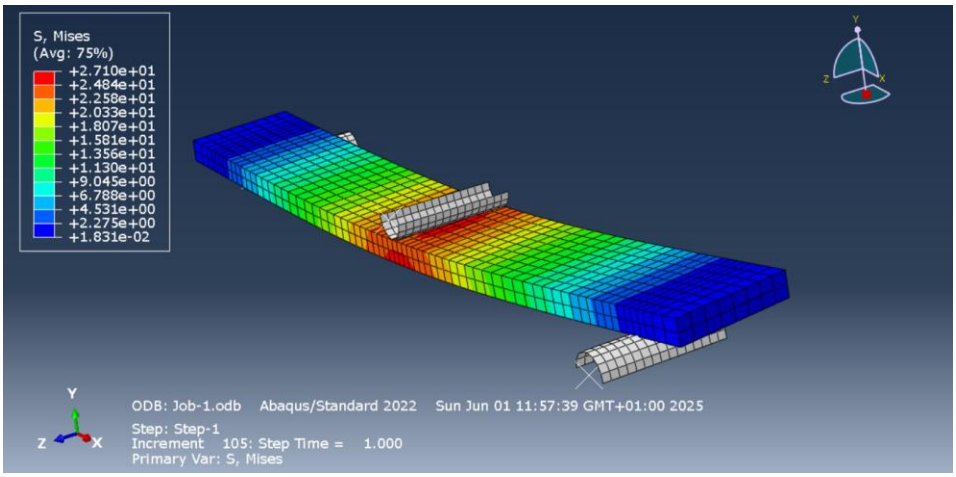

Figure 92 - Undesirable behaviour of the part.

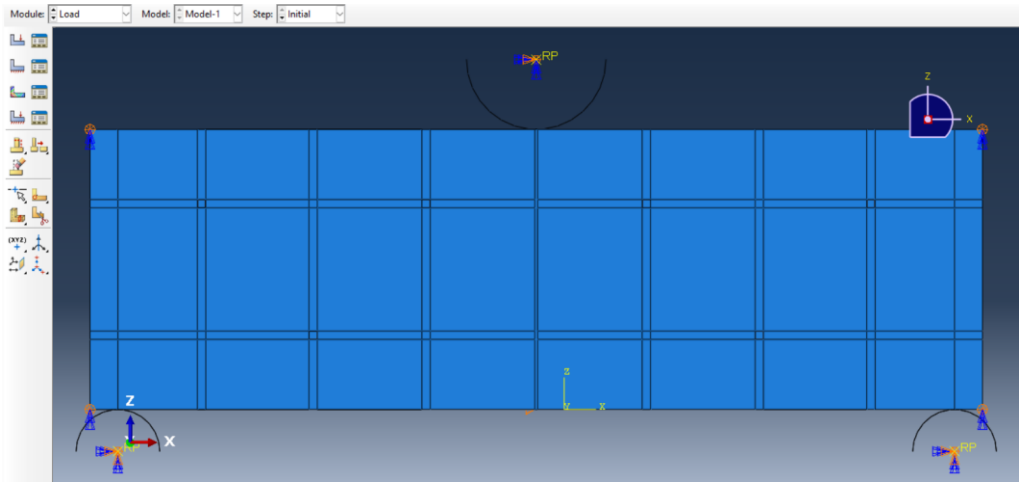

Figure 93 - Boundary conditions.

The mesh module represents the final stage preceding the execution of the simulation. The primary function of this module is to define and assign the mesh to each partition of the model. To accurately capture the behaviour of the different materials within the joint, two meshing strategies are employed. For the orthotropic and isotropic materials, a structured hexagonal mesh is applied. As demonstrated in Figure 94, mesh refinement is employed in critical areas where stress concentrations are expected, by reducing the element size. In less critical regions, larger elements are used. This mesh variation allows for optimized computational efficiency by reducing the total number of elements without compromising accuracy in key zones. In the context of the adhesive layer, the implementation of a sweep mesh technique is imperative when cohesive elements are employed. This method establishes a direct connection between the two adherend interfaces using a single element through the thickness, thereby ensuring correct representation of the cohesive behaviour while maintaining a simplified mesh. However, despite numerous attempts using the recommended method for the adhesive, the analysis remained unsuccessful. Therefore, to further simplify the process, the adhesive was treated as a solid and meshed using the same technique as the other materials. This simplification was justified by the attained experimental results, which showed no evidence of adhesive failure.

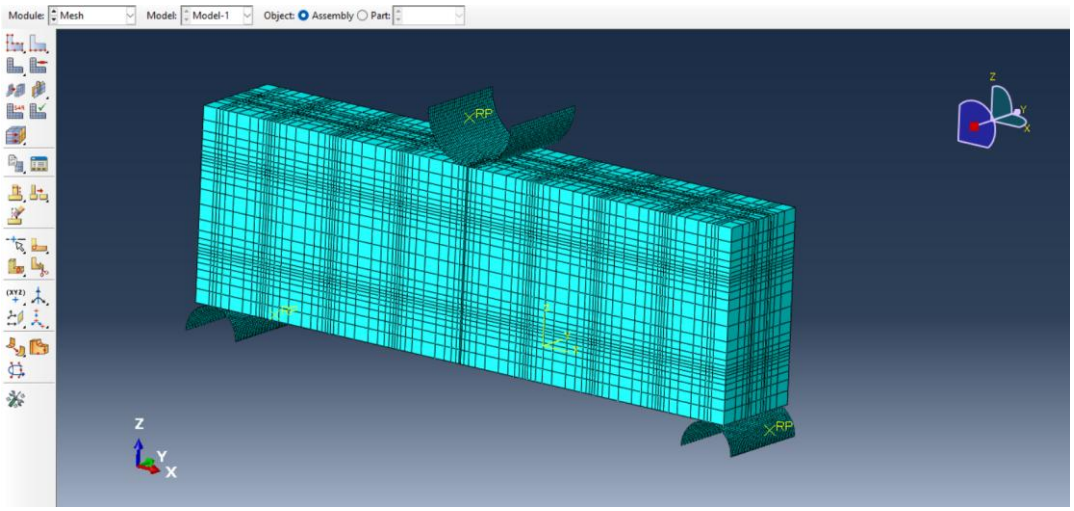

Figure 94 - Mesh used in the model.

Following the assignment of the mesh to the various sections of the model, the subsequent step is to specify the type of elements to be utilised. For the hexagonal structured mesh, an 8-node 3D stress element is selected, with reduced integration deactivated to enhance the simulation's precision.

Additionally, a viscosity parameter of 10^{-5} is applied to hexagonal structured elements to help stabilize the model during the simulation and to prevent numerical instabilities. Table 28 provides a summary of the meshing strategy and element types utilised for each material.

Table 28 - Mesh summarizing

Material type	Mesh geometry	Mesh type	Viscosity	Mesh designation
Orthotropic	Hexagonal structured	3D stress	10^{-5}	C3D8
Isotropic	Hexagonal structured	3D stress	10^{-5}	C3D8
Adhesive	Hexagonal structured	3D stress	10^{-5}	C3D8

Finally, the job module is employed for the creation and configuration of the simulation. This module enables the definition of the computer memory allocation that Abaqus® will utilise during the analysis, ensuring optimal resource management. After the configuration of the task, its submission is required to initiate the simulation process. Following the conclusion of the simulation, the results are obtained and presented visually through the visualization module (Figure 95). This module permits the analysis of diverse outputs, thereby enabling the evaluation of the model's behaviour.

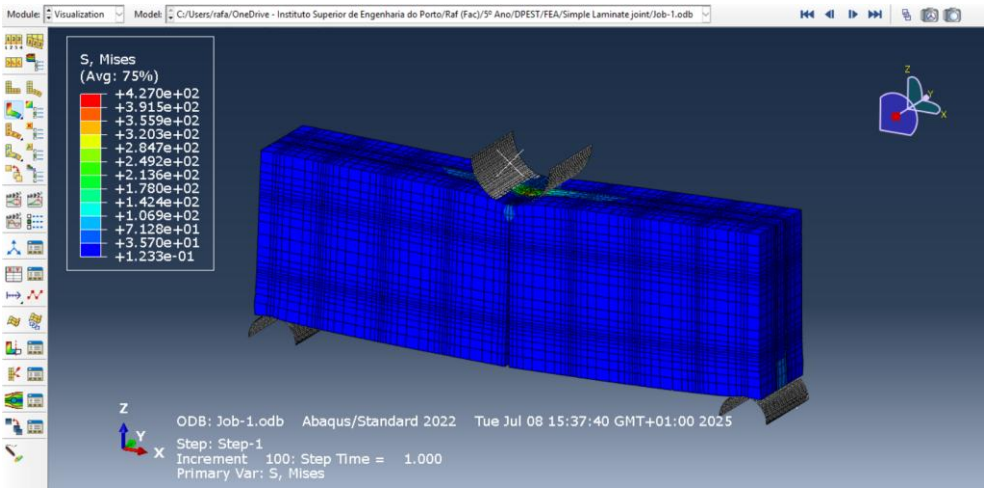

Figure 95 - Visualization module.

3.4.3. Constitutive model

To carry out a numerical analysis, it is necessary to choose the constitutive models for each material present in the study. A constitutive model is a mathematical description of how a

material responds to external loads, such as forces, deformations, or temperature changes. The effectiveness of constitutive models plays a key role in the predictive capabilities of computational models of structures [122]. Thus, it is necessary to understand the type of material being modelled to better relate each material to his respective constitutive model.

The wood and plywood components in the joint are modelled as orthotropic elastic materials to accurately reflect their direction-dependent mechanical behaviour. Wood exhibits significant anisotropy due to its fibrous cellular structure, with distinct properties along the longitudinal, radial, and tangential directions. Plywood, being a layered composite of wood veneers oriented in alternating directions, is also treated as an orthotropic material, but with more balanced in-plane properties depending on the lay-up configuration [115]. The constitutive model for these materials is defined by Hooke's law for orthotropic elasticity, using nine independent material constants, including three E, G, and ν. This formulation enables the simulation to capture the E variation and directional response of the wooden elements under mechanical loading [123].

On the other hand, the adhesive layer in the wood joint is initially modelled using a cohesive zone model (CZM) to accurately capture the initiation and evolution of damage at the bonded interface. This approach allows for the simulation of progressive failure mechanisms such as micro-crack formation, debonding, and eventual separation of the adherends. By incorporating the CZM, the model provides a more realistic representation of the adhesive behaviour under mechanical loading, especially in capturing the non-linear response and potential delamination within the joint [120]. However, as previously mentioned, the adhesive was not modelled using this constitutive model. A more detailed investigation could be carried out to identify the reasons behind the model's unsuccessful application to the joints.

For isotropic materials, such as bolts, nails and fasteners, are modelled as isotropic elastoplastic material, reflecting its uniform mechanical properties in all directions and its ability to undergo plastic deformation. Initially, the material follows a linear elastic response characterized by E and ν [124]. If necessary, beyond the yield point, plastic deformation is captured using a Von Mises yield criterion with isotropic hardening, allowing the simulation to represent both the onset of yielding and the subsequent strain hardening behaviour under continued loading [125].

3.4.4. Material properties

Along with a suitable constitutive model, material properties permit to carry out a FEA analysis to simulate how a material behaves when subject to mechanical forces. Thus, it is necessary to assign accurate properties for each constitutive model. However, the supplier of the material used to fabricate the specimens does not provide all the needed properties to realize the numerical analysis. Consequently, a literature review was conducted to identify the desired material properties. It is important to note that some of the considered properties do not fully reflect the actual behaviour of the joints, as the characteristics of wood and plywood can vary significantly. Consequently, adjustments to literature-based properties are necessary to obtain numerical results that are consistent with experimental data. To achieve this objective, an inverse method is employed to ascertain the properties of the various materials. This process involves the comparison of the experimentally obtained E with the numerical one, with the

objective of ensuring that they are reasonably close. Figure 96 illustrates the complete process used to determine the material properties.

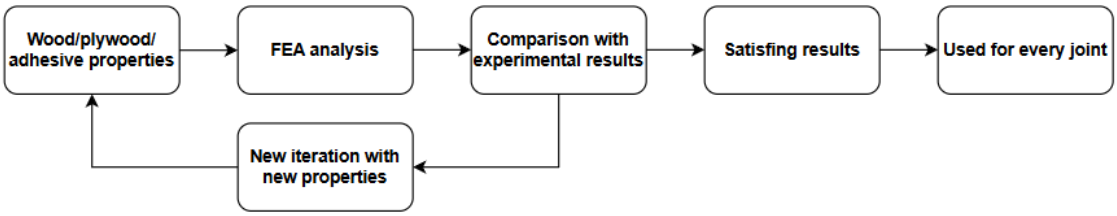

Figure 96 - Determination of the materials properties.

The process is initiated with the determination of the wood properties, as specimens of different cross-sections are tested, enabling direct comparison. In the initial phase, a simulation was conducted for the 80x70 mm^2 beam utilising properties taken from reference [116], which are presented in Table 29. The numerical *E* obtained is 5460.8 MPa, representing a 42% deviation from the experimental value of 3845.1 MPa. To reduce this discrepancy, a series of iterations was performed by gradually lowering the property values until those shown in the table were obtained. Consequently, a numerical *E* value of 3901.2 MPa was attained for the 80x70 mm^2 beam, with a deviation of 1.46%. After the adjustment, a simulation was conducted for the 100x80 mm^2 beam using the adjusted properties, to validate the feasibility of the adjusted properties. The simulation provides a *E* of 5497.4 MPa, corresponding to a deviation of 2.66% from the experimental value of 5354.9 MPa. Following the establishment of a close alignment between the numerical and experimental values, it can be concluded that the adjusted properties can be reliably utilised for all subsequent joints composed of wood.

Table 29 - Orthotropic properties for radiata pine wood [116]

Property	Value	Adjusted value
E_L [MPa]	2810	2000
E_T [MPa]	190	200
E_R [MPa]	300	200
G_{LT} [MPa]	210	400
G_{TR} [MPa]	20	300
G_{LR} [MPa]	30	50
ν_{LT}	0.16	0.4
ν_{TR}	0.33	0.4
ν_{LR}	0.47	0.4

Next, it is possible to evaluate the adhesive properties taken from reference [126] for the PVA adhesive, which are presented in Table 30. To enable a direct comparison of *E*, the double strap joint is used. As demonstrated in the fabrication procedure, the double strap joint is composed exclusively of wood, adhesive, and nails. It was determined through experimental analysis of the fastened double strap joint (which does not present adhesive) that the adhesive plays a primary role in the joint's stiffness. A simulation of the double strap joint can be conducted, since nails do not impact the joint stiffness. The modified wood properties were utilised, and the literature values for the adhesive were considered. This procedure resulted in *E* of

3844.1 MPa, corresponding to a 22.7% deviation from the experimental value. In consideration of the simplifications implemented within the model, as previously delineated, the obtained value is adjudged satisfactory. Consequently, no adjustments were made to the adhesive properties taken from literature [126].

Table 30 - Adhesive properties [126]

Property	Value
E [MPa]	2000
ν	0.40
G [MPa]	800
Tensile strength, σ_t [MPa]	40
Shear strength, τ [MPa]	20
Tensile fracture toughness, G_{IC} [MPa m$^{1/2}$]	1
Shear fracture toughness, G_{IIC} [MPa m$^{1/2}$]	2

Following the determination of the properties of the wood and adhesive, the focus shifted to the plywood properties. For direct comparison between experimental and numerical results, the simple laminate joint was utilised. An initial simulation of the simple laminate joint was conducted, employing the wood properties that had been previously adjusted, the adhesive properties, and the plywood properties taken from the literature [118], which are presented in Table 11. This simulation resulted in a numerical value of E of 9942.9 MPa, which represents a deviation of 127.6% compared to the experimental value. As previously conducted for the wood, multiple iterations were executed to calibrate the plywood properties until a numerical E value near the experimental one was attained. The final adjusted values, as presented in the Table 31, result in a E of 4935.3 MPa, with a deviation of 13.2% relative to the experimental result. It is important to note that the adjusted properties differ significantly from those taken from reference [118], which may be attributed to the modelling simplifications.

Table 31 - Adjusted orthotropic properties for plywood

Property	Adjusted value
E_L [MPa]	8000
E_T [MPa]	600
E_R [MPa]	800
G_{LT} [MPa]	800
G_{TR} [MPa]	100
G_{LR} [MPa]	700
ν_{LT}	0.426
ν_{TR}	0.451
ν_{LR}	0.697

Subsequent to the definition of the properties of all materials, it was possible to carry out all simulations for the different geometries using the adjusted properties for wood and plywood, along with the adhesive properties taken from literature [126].

3.4.5. Results and comparison with experiments

3.4.5.1. Stress analysis

To evaluate the precision and reliability of the numerical model, a direct comparison with the experimental results is necessary. However, prior to conducting this comparison, it is imperative to describe the methodology employed in the estimation of the key parameters, namely P_{max} and *E*, for each joint under analysis.

The numerical models used in this study do not incorporate damage or failure criteria. Consequently, the analysis persists in a linear form, with the stresses extending beyond the true capacity limit of the materials. Consequently, the model may persist in predicting stress increases that are unrealistic, even after the physical collapse point of the structure. To address this limitation and enable a consistent comparison with experimental data, it is necessary to define the strength limits of the materials used. The σ_{max} values adopted for the various materials in the models are presented in Table 32. The adhesive's σ_{max} is taken from reference [126] and the σ_{max} for wood and plywood correspond to those used by NEFAB. The bolts are of strength class 8.8; therefore, according to EN 1993-1-8, the σ_{max} is 640 MPa. Regarding the nails and wooden fasteners, they exhibit a σ_{max} of 300 MPa based on supplier data. As can be observed, the σ_{max} values for the metallic components are significantly higher compared to those of wood, plywood, and adhesive. Both experimental and numerical analyses confirmed that no failure occurred in the metallic components. The limits of strength that have been defined serve as a basis for identifying, in the simulation results, the load increments that correspond to the occurrence of failure, thus allowing a direct comparison with the values obtained from the experiments.

Table 32 - σ_{max} of the different joint materials

Material	$\boldsymbol{\sigma_{max}}$
Wood	80 MPa
Plywood	20 MPa
Adhesive	50 MPa
Bolts	640 MPa
Nails/Wooden fasteners	300 MPa

Given that the case under study corresponds to a three-point bending test, the main stress component generated in the specimen is axial. Thus, it can be concluded that the σ_{max} of the materials are the most appropriate criteria to estimate the moment of collapse. This methodology facilitates the identification, within the numerical analysis, of the load increment at which the stress exceeds the material's strength, thereby indicating the initiation of failure. In Abaqus®, the load is applied incrementally, i.e., in small successive steps. By identifying the increment at which the stress surpasses the material's tensile strength, it becomes possible to estimate the collapse point predicted by the simulation and directly compare it to the experimental results.

3.4.5.2. Failure mode

It is possible to determine the failure mode in the simulation by considering the experimental results and the σ_{max} presented in Table 32. It is important to note that the P_{max} value is dependent on the specific load increment at which material failure is reached in the model. Consequently, depending on the geometry under analysis, the failure mode considered may vary, as joint collapse can result from the failure of different materials. Given the implementation of a σ_{max}, the numerical comparison is conducted through the evaluation of stress along the fibre direction, which is the main stress component under three-point bending.

The 80x70 mm^2 and 100x80 mm^2 wooden beams were used to calibrate wood properties in the numerical model and are considered the most suitable for comparing joint performance. A criterion based on the region where 80 MPa is reached in terms of Von Mises stress was defined. The employment of the Von Mises criterion facilitates the consideration of the combined stress state. As demonstrated in Figure 97, it is assumed that failure occurs in the compression zone, and only when the entire cross-section of the beam exceeds 80 MPa. In this and further figures, the grey represents stresses exceeding the specified stress limit.

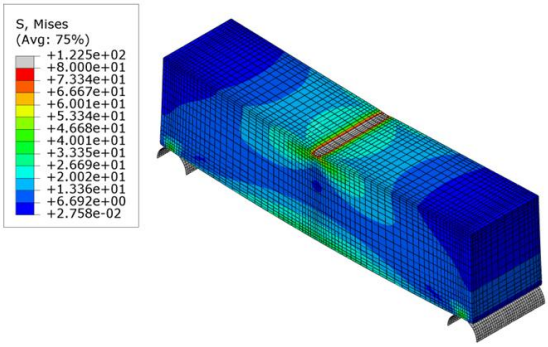

Figure 97 - Increment of failure of the 80x70 mm^2 wooden beam.

Employing this criterion for wood, the failure is identified at increment 46, corresponding to a P_{max} of 36.5 kN, which is close to the 32 kN obtained experimentally. It is evident that the 100x80 mm^2 beam must be analysed using the same second criterion as the 80x70 mm^2 beam. This analysis results in a P_{max} of 49 kN at increment 29 (Figure 98). Based on the obtained results, it is recommended that the criterion be adopted as the standard for identifying failure in the wooden elements.

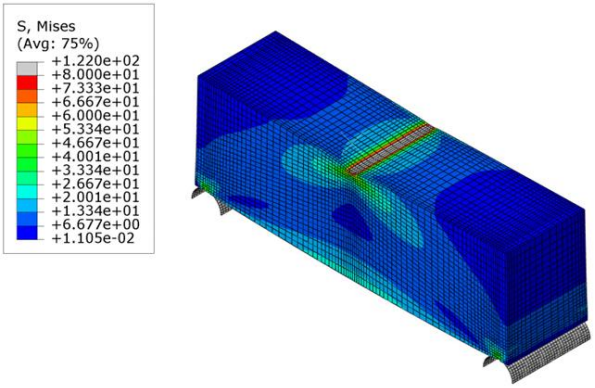

Figure 98 - Increment of failure of the 100x80 mm^2 wooden beam using the second criteria.

In the subsequent geometries, it will be necessary to analyse the different materials present in the joint. Accordingly, Table 33 presents the criteria used, based on the previously established σ_{max} from Table 32. When comparing the numerical results with the values presented in Table 32, it is observed that the type of stress considered varies according to the mechanical behaviour of each material. For the adhesive, the equivalent Von Mises stress is used, as it exhibits a multi-axial stress state. Solid wood is also evaluated using Von Mises stress, due to the localized multi-axial stress condition caused by the punch compression. In contrast, for the plywood, only the S11 component is considered, since this element is predominantly subjected to pure tensile stress, and its reduced thickness limits the development of significant stresses in the other directions. These criteria have been derived from experimental tests and earlier simulations conducted for the wood components. In joints composed of multiple materials, the increment considered to be the point of failure is equivalent to the lowest increment at which any individual material will fail. Next, each joint type is described separately.

Table 33 - Criteria used for each material

Material	Failure mode	Tensile comparison
Wood	σ_{max} in all thickness	Von Mises
Plywood	σ_{max} from bottom to mid-height	S11
Adhesive	σ_{max} appear in the bottom zone	Von Mises

The simple laminate joint includes wood, plywood, and adhesive, thus necessitating analysis of all three materials. Figure 99a) illustrates the meshed geometry, along with the load increments at which each material in the joint reaches its failure criterion. In this geometry, the wood (Figure 99b) never achieves 80 MPa. In the other hand, the plywood (Figure 100a) achieves is stress limit (20 MPa) at increment 66. Finally, the adhesive (Figure 100b) achieves 50 MPa at increment 87. Thus, once plywood fail first, it can be deduced that the failure of the joint is attributable to the plywood failure. Consequently, the failure of the structure is predicted to occur at increment 66, corresponding to a P_{max} of 33.6 kN. A comparison of the predicted P_{max} with the experimental results reveals a high degree of similarity, as does the failure mode, since in the experimental tests, failure occurred in the plywood when a crack formed and propagated to halfway through its height. Consequently, it can be deduced that failure occurred in the plywood when a crack developed up to mid-height.

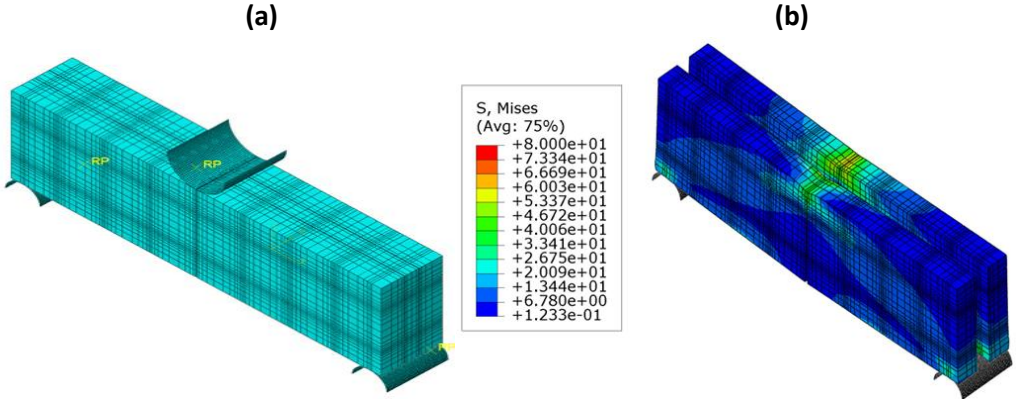

Figure 99 - Stresses in the simple laminate joint: meshed geometry (a), and wood elements (b).

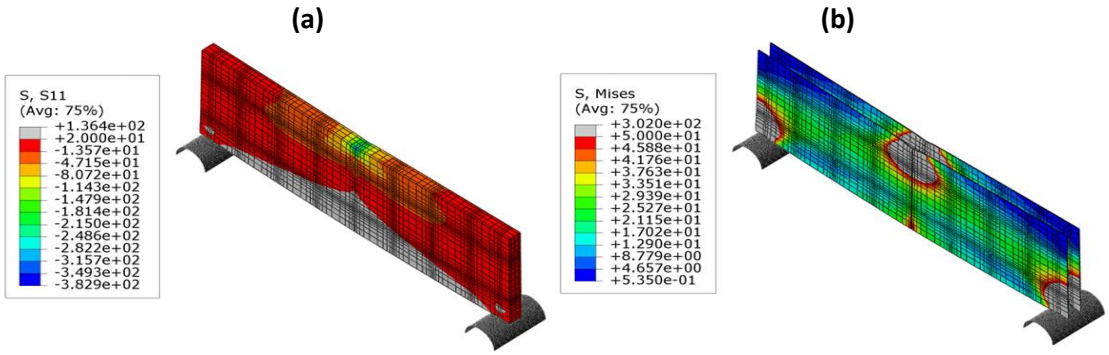

Figure 100 - Stresses in the simple laminate joint: plywood elements (a), and adhesive elements (b).

Laminate joint with junction alignment features the same materials as the simple laminate joint, requiring analysis of all three: wood, plywood, and adhesive. Figure 101a) illustrates the meshed geometry, along with the load increments at which each material in the joint reaches its failure criterion. Once again, wood (Figure 101b) never achieves 80 MPa. On the other hand, the plywood (Figure 101c) achieves 20 MPa in the mid-height at the increment 70. Finally, the adhesive (Figure 101d) achieves 50 MPa at increment 97. Identically to the previous joint, it has been demonstrated that the material responsible for the joint failure is plywood. Consequently, the failure of the structure is theorised to occur at increment 70, corresponding to a P_{max} of 34.3 kN. A comparison of the predicted P_{max} with the experimental results reveals a high degree of similarity, as does the failure mode, since in the experimental tests, failure occurred in the plywood when a crack formed and propagated halfway through its height. Consequently, it can be deduced that the failure of the plywood occurred because of the emergence of a crack that traversed the mid-height of the material.

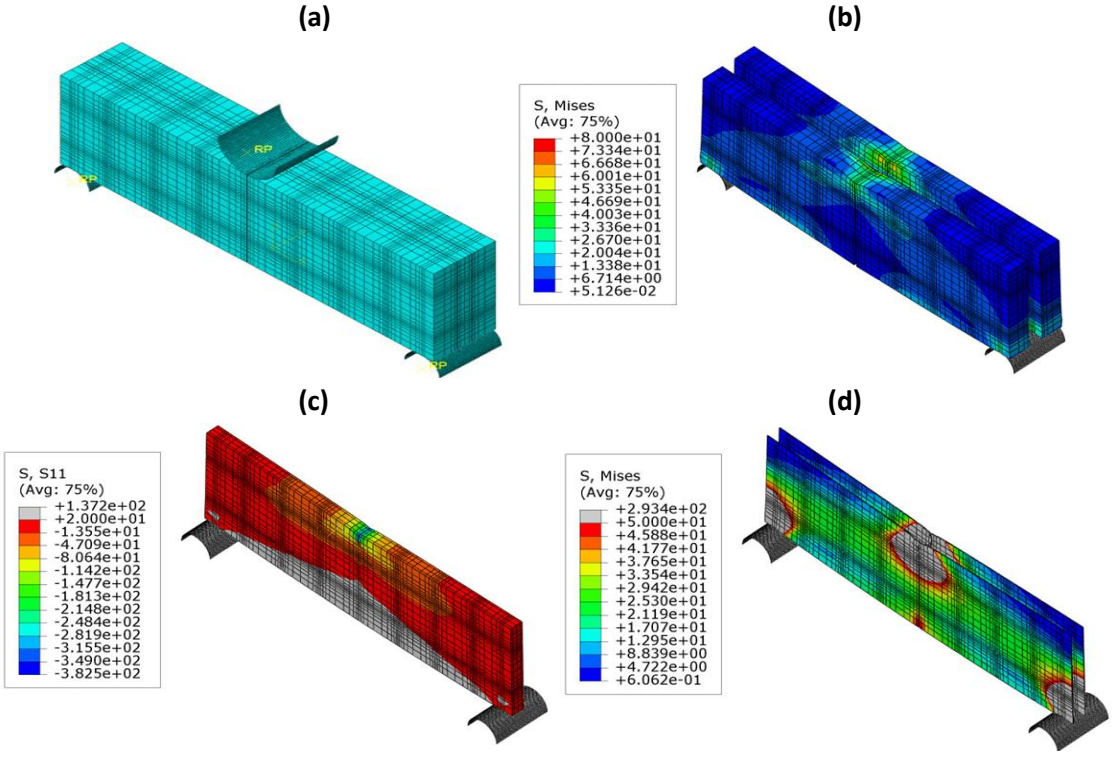

Figure 101 - Stresses in the laminate joint with junction alignment: meshed geometry (a), wood elements (b), plywood element (c), and adhesive elements (d).

The double strap joint incorporates both wood and adhesive components, necessitating a comprehensive analysis of both materials. Figure 102a) illustrates the meshed geometry, along with the load increments at which each material reaches its respective failure criterion. In this case, it can be observed that the wood (Figure 102b) does not reach maximum stress across the full thickness of the lateral sections, which are responsible for holding the central wood element. On the other hand, the adhesive (Figure 102c) exhibits stress above 50 MPa in the lower region at increment 75, corresponding to a P_{max} of 28.6 kN. The numerical P_{max} is close to the experimental value and, moreover, the failure mode agreed by taking place in the adhesive, specifically in the region most distant from the punch.

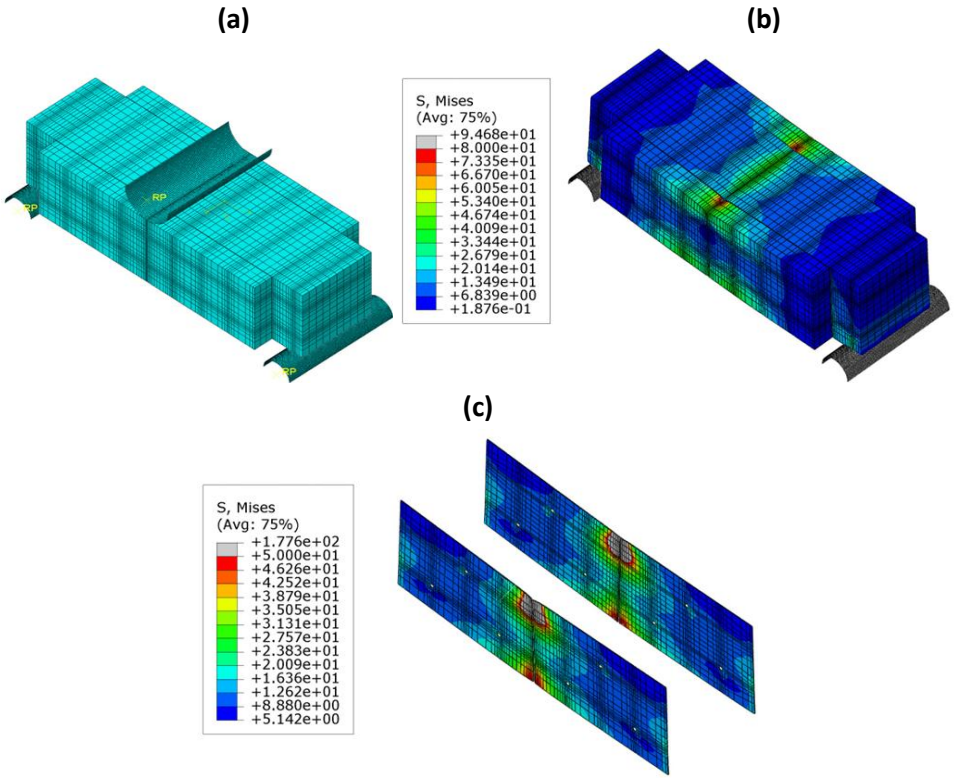

Figure 102 - Stresses in the double strap joint: meshed geometry (a), wood elements (b), and adhesive elements (c).

Fastened double strap joint includes two variants using M4 and M6 wooden fasteners. Given that wood is the only material present in both cases, it is the primary focus for determining the joint's failure increment. Figure 103a) and Figure 103c) illustrates the meshed geometries, along with the failure increments for both the M4 and M6 configurations. Based on the experimental test and as referred before, failure consistently occurs in the fastener hole regions, more specifically the ones close to joint centre. As a result, only the fastener holes regions are analysed in the model. The results indicate that failure occurs at increment 83 for M4 wooden fasteners (Figure 103b) and increment 69 for M6 wooden fasteners (Figure 103b), corresponding to P_{max} values of 10.3 kN and 12.1 kN, respectively. The numerical P_{max} obtained are proximal to the experimental values, and, moreover, the failure mode agreed by taking place in the wood near the fasteners closest to the joint centre.

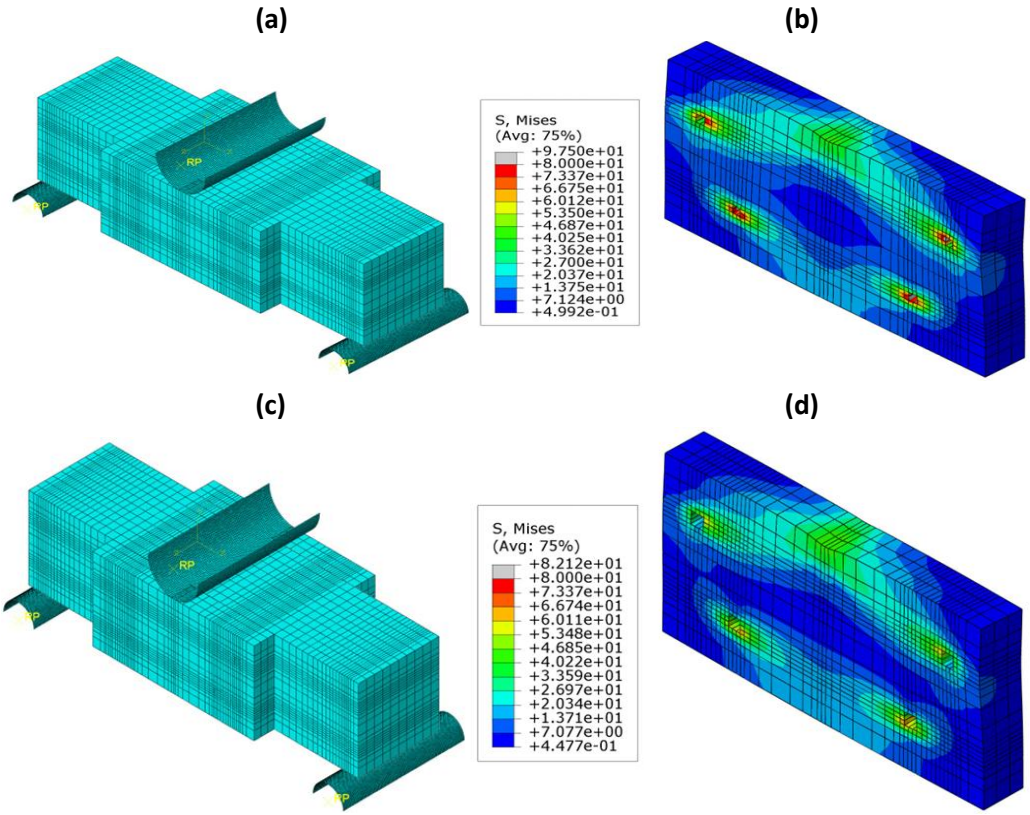

Figure 103 - Stresses in the fastened double strap joint: meshed geometry for M4 fasteners (a), wood elements for M4 fasteners (b), meshed geometry for M6 fasteners (a), and wood elements for M6 fasteners (b).

The bolted double strap joint includes wood and plywood, with two variants using M6 or M10 bolts. Given that the wood in the joint does not experience significant tensile stress, the analysis is confined to the plywood. Figure 104a) and Figure 105a) illustrates the meshed geometries, along with the failure increments of the plywood for both M6 and M10 configurations. It can be observed that failure occurs at increment 70 for M6 bolts (Figure 104b)) and increment 64 for M10 bolts (Figure 105b), corresponding to P_{max} values of 20.2 kN and 23.1 kN, respectively. The numerical P_{max} obtained are in close agreement with the experimental results, and, moreover, the failure mode agreed by taking place in the plywood, specifically in the regions proximate to the bolts closest to the centre of the joint.

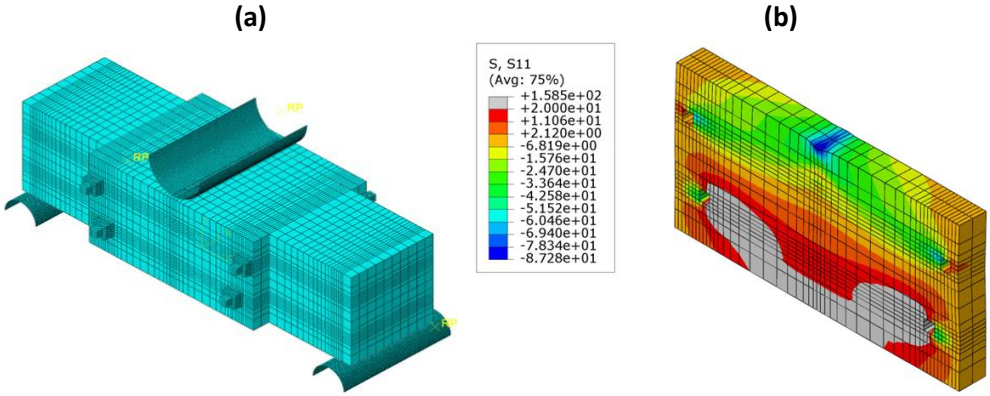

Figure 104 - Stresses in the bolted double strap joint: meshed geometry for M6 bolts (a), and plywood elements for M6 bolts (b).

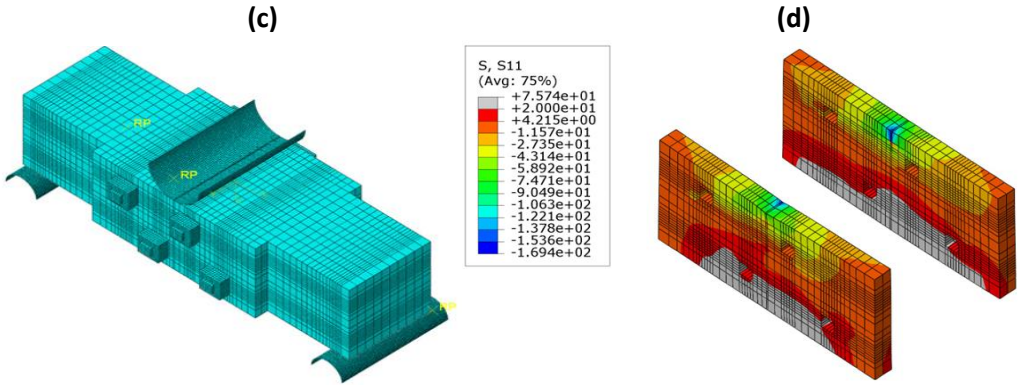

Figure 105 - Stresses in the bolted double strap joint: meshed geometry for M6 bolts (a), plywood elements for M6 bolts (b), meshed geometry for M10 bolts (c), and wood elements for M10 bolts (d).

The double strap joint with chamfer incorporates wood as the primary material, with two variants: one employing M4 wooden fasteners and the other M6 wooden fasteners. Figure 106a) and c) presents the meshed geometries, along with the failure increments for both fastener types. It can be observed that failure occurs at increment 86 for the M4 wooden fasteners (Figure 106b) configuration and at increment 93 for the M6 wooden fasteners (Figure 106d) configuration, corresponding to P_{max} values of 28.3 kN and 33.0 kN, respectively. The numerical results obtained are in close agreement with the experimental values. Based on the results and failure mode obtained experimentally and numerically, and, moreover, the failure mode agreed by taking place in the wood, specifically in the regions around the fasteners closest to the centre of the joint.

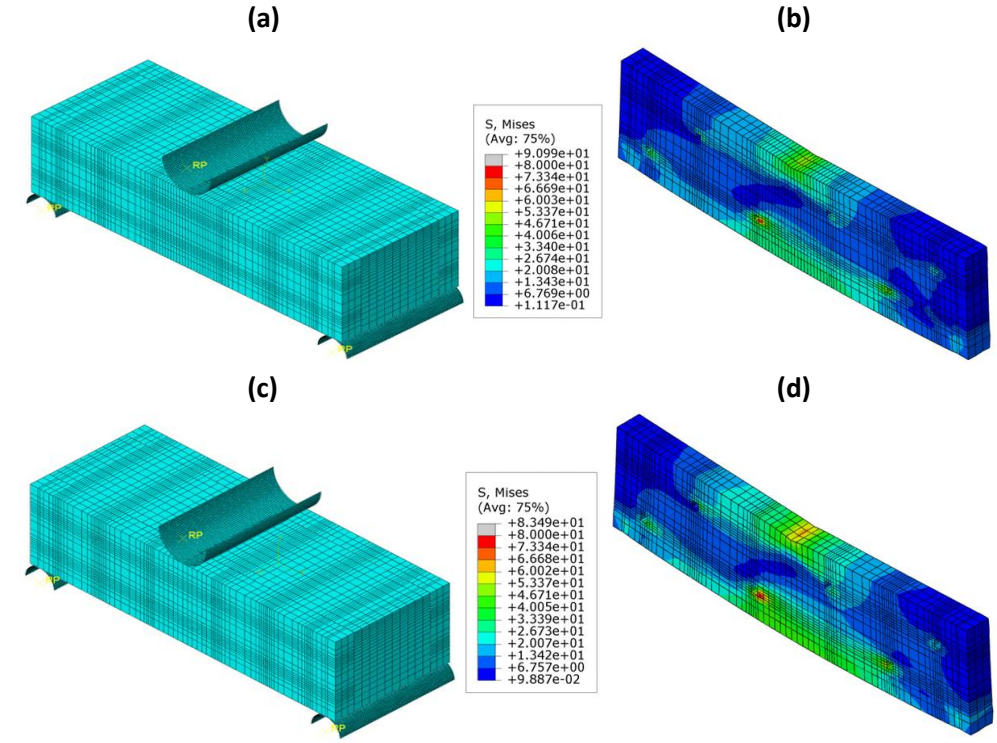

Figure 106 - Stresses in the double strap joint with chamfer: meshed geometry for M4 fasteners (a), wood elements for M4 fasteners (b), meshed geometry for M6 fasteners (c), and wood elements for M6 fasteners (d).

3.4.5.3. *P-δ* curves

Figure 107 presents the experimental *P-δ* curves alongside with the numerical response of the 80x70 mm^2 (Figure 107a) and 100x80 mm^2 (Figure 107b) wooden beams. The numerical lines are presented only up to the failure increment that was discussed in the previous section. It can be observed that, for both cases, the numerically obtained behaviour closely matches the initial portions of the experimental curves. The reduction in the *E* value observed in the experimental curves is a consequence of progressive damage to the wood, a factor that has not been incorporated into the numerical model. Furthermore, numerical analysis demonstrates a superior P_{max} in the numerical analysis, attributable to the idealised depiction of the wood in the model.

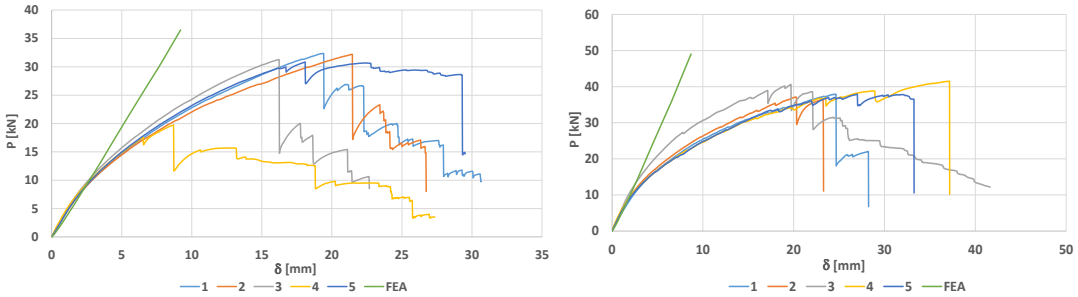

Figure 107 - *P-δ* curves of the 80x70 mm^2 (a) and of the 100x80 mm^2 wooden beams (b).

Figure 108 presents the experimental *P-δ* curves, alongside the linear response obtained from the numerical analysis of the simple laminate joint (Figure 108a) and the laminate joint with junction alignment (Figure 108b). The numerical curves are displayed exclusively up to the failure increment that was the subject of discussion in the preceding section. It is evident that, in both instances, the numerically obtained lines demonstrate a strong correlation with the initial segments of the experimental graphs. The observed reduction in the *E* values, as evidenced by the experimental curves, can be attributed to the progressive damage incurred by the orthotropic materials, a phenomenon that has not been incorporated into the numerical model. Furthermore, a superior P_{max} is evident in the numerical analysis, which can be due to the idealised depiction of the orthotropic materials in the model.

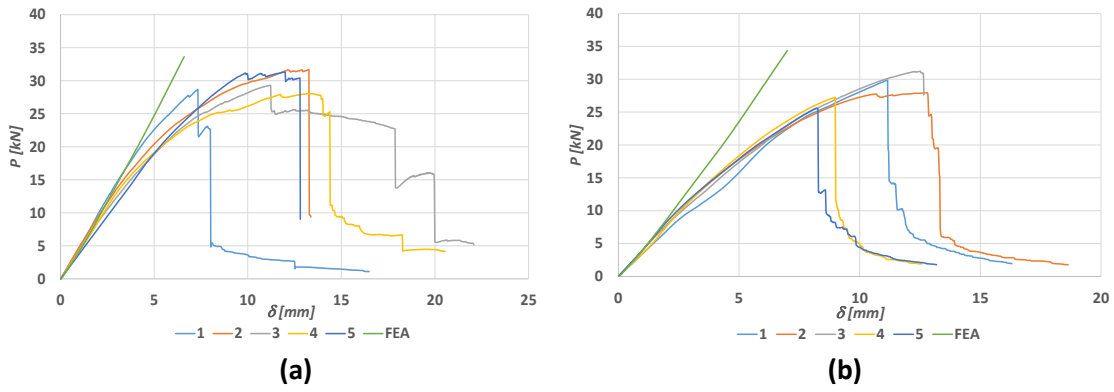

Figure 108 - *P-δ* curves of the simple laminate joint (a) and of the simple laminate joint with junction alignment (b).

Figure 109 presents the experimental *P*-δ curves, alongside the numerical response of the double strap joint. The numerical curve is displayed exclusively up to the failure increment that has been previously discussed in the preceding section. It is evident that, in both instances, the numerically obtained line demonstrates a strong correlation with the initial segments of the experimental graphs. In the numerical model, a slight increase in the *E* value is observed towards the end of the curve, which can be explained by the compression of the central wooden blocks. Conversely, the decline in the *E* value observed in the experimental curves is attributable to progressive damage in the wood, a factor that has been omitted from the numerical model. Nevertheless, the P_{max} predicted numerically is very similar to the experimental value.

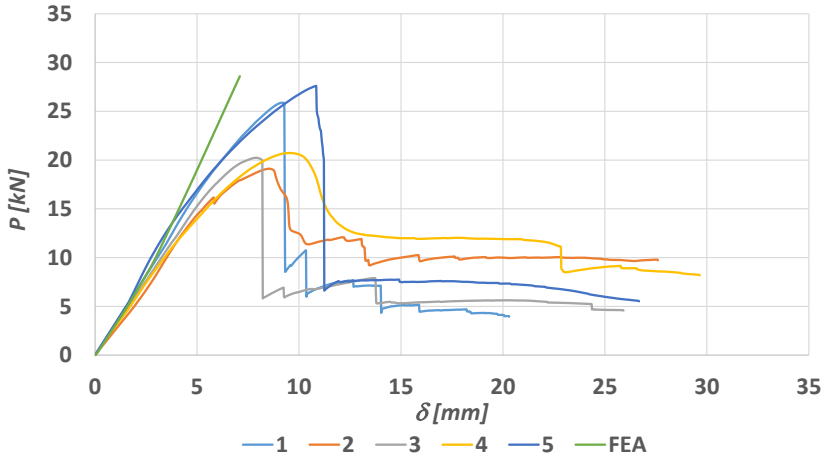

Figure 109 - *P*-δ curves of the double strap joint.

Figure 110 presents the experimental *P*-δ curves, alongside the numerical response of the fastened double strap joints with M4 (Figure 110a) and M6 (Figure 110b) fasteners. The numerical curves are displayed exclusively up to the failure increment previously discussed in the preceding section. For the configuration with M4 fasteners, the initial *E* value is comparable between the numerical and experimental results. However, in the same M4 configuration, the experimental the *E* value demonstrates a significant decrease shortly after the test onset, an effect not captured in the numerical curve. This discrepancy is attributed to the absence of damage modelling in the numerical simulation. About the configuration with M6 fasteners, there is a stronger correlation between the experimental and numerical results in terms of joint stiffness. Conversely, the P_{max} predicted by the numerical model further deviates from the experimental value when compared to the M4 fastener configuration.

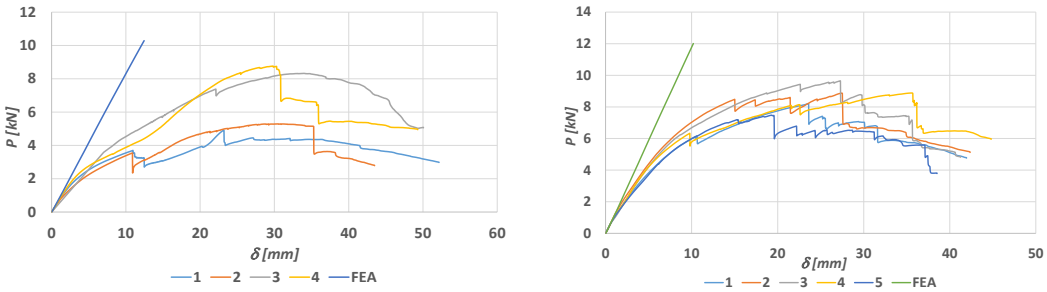

(a) **(b)**

Figure 110 - *P*-δ curves of the fastened (M4) double strap joint (a) and of the fastened (M6) double strap joint (b).

Figure 111 presents the experimental *P*-δ curves, alongside the numerical response of the bolted double strap joints with M6 bolts (Figure 111a) and M10 bolts (Figure 111b). The numerical curves are displayed exclusively up to the failure increment previously discussed in the preceding section. In the joint using M6 bolts, the numerically obtained line demonstrates slightly lower *E* and P_{max} compared to the experimental results. This discrepancy can be attributed to the bolt torque tightening, as the applied torque was not recorded and, therefore, no pre-tension could be included in the numerical model. Conversely, for the configuration with M10 bolts, the numerical curve demonstrates a greater proximity to the experimental results.

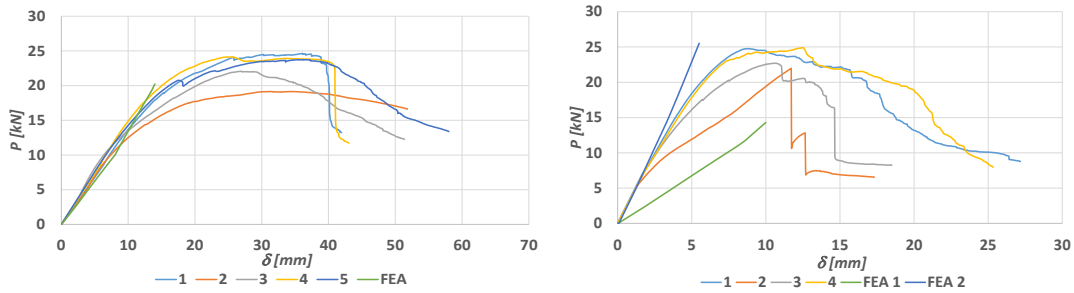

(a) **(b)**

Figure 111 - *P*-δ curves of the bolted (M6) double strap joint (a) and of the bolted (M10) double strap joint (b).

Figure 112 presents the experimental results, along with two simulation attempts aimed at achieving results consistent with the experimental data of the bolted double strap joint using M10 bolts. The initial attempt (FEA 1) is predicated on the assumption that no compressive forces are transmitted between the plywood and the wood. As demonstrated, the resulting curve displays significantly reduced *E* and a substantially P_{max} in comparison to the experimental results. An increase in the *E* of the FEA 1 curve is observed at higher displacements, which can be due to the development of compressive forces between the two central wooden beams upon their contact, enhancing the overall stiffness of the connection. Consequently, a second iteration (FEA 2) was conducted under the opposite assumption: the plywood and wood were fully bonded to each other. In this instance, the numerical outcomes demonstrate a robust correlation with the experimental data, particularly on *E* and P_{max}. This finding indicates that the torque applied to the bolts is sufficient to effectively clamp the plywood to the wood, thereby enabling the interface to behave as if it were bonded together. Consequently, it can be deduced that joint failure is not attributable to bolt failure, but rather to failure in the plywood on the lateral faces.

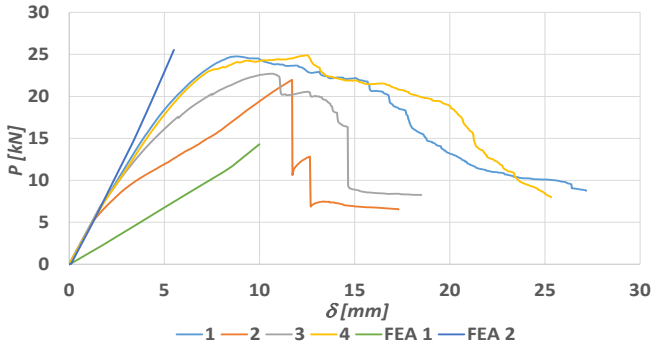

Figure 112 - *P*-δ curves of the bolted (M10) double strap joint with two FEA iterations.

Figure 113 presents the experimental *P*-δ curves, alongside the numerical results for the double strap joints with chamfered ends using M4 wooden fasteners (Figure 113a) and M6 wooden fasteners (Figure 113b). The numerical curves are displayed exclusively up to the failure increment that was the focus of the preceding section. For both configurations, the numerical *E* is comparable to that observed in the experimental curves. In both cases, M4 and M6 fasteners configuration, the P_{max} is higher than the average experimental values.

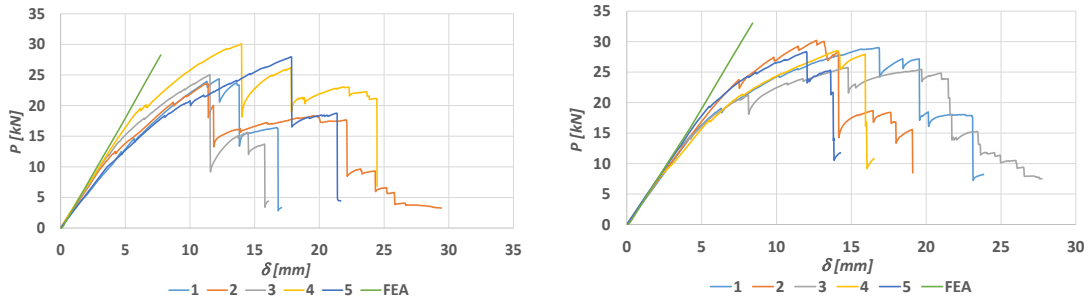

Figure 113 - *P*-δ curves of the double strap joint with chamfer (M4) (a) and of the double strap joint with chamfer (M6) (b).

3.4.5.4. Mechanical properties

In this section, the numerically obtained values of *E* and P_{max} are presented for the geometries of Table 7. As previously mentioned, *E* is determined as the slope of the *P*–*δ* curve extracted from the Abaqus® software. About P_{max}, as previously demonstrated, it was necessary to determine the material's ultimate stress limits, as well as to analyse and compare with real failure mode tests, so that the numerically obtained values more accurately represent reality.

To facilitate a comparison between the experimental and numerical results, both the numerically obtained values and the experimental average values are presented in tabular form. This procedure facilitates the calculation of the percentile variation between numerical and experimental values, thereby enabling a direct comparison.

Table 34 presents the values of *E* and P_{max} that have been obtained through experimental and numerical analysis for the 80×70 mm^2 wooden beam. Conversely, Table 35 presents the corresponding values for the 100×80 mm^2 wooden beam. It can be observed that, in both cases, the numerical values of *E* are close to the experimental ones, which reinforces the suitability of the adjusted material properties. Conversely, a more substantial discrepancy was observed in P_{max}, with the model demonstrating an overestimation of the material's capacity. This discrepancy is attributed to the lack of implementation of wood damage evolution in the numerical model.

Table 34 - Mechanical properties of 80x70 mm^2 wooden beams

Properties	***E* [MPa]**	**P_{max} [N]**
Experimental	3845.1	31667.3
Numerical analysis	3901.2	36494.9
Variation	+1.46%	+15.24%

Table 35 - Mechanical properties of 100x80 mm^2 wooden beams

Properties	***E* [MPa]**	$\boldsymbol{P_{max}}$ **[N]**
Experimental	5354.9	39019.8
Numerical analysis	5497.4	49035.8
Variation	+2.66%	+25.66%

Table 36 presents the values of *E* and P_{max} through experimental and numerical analysis of the simple laminate joint. Table 37 shows the corresponding values for the laminate joint with junction alignment. It can be observed that the simple laminate joint exhibits a smaller variation between experimental and numerical values compared to the laminate joint with junction alignment. It is also noteworthy that the simple laminate joint demonstrates a higher *E* value in both the experimental and numerical results. However, this is not the case for P_{max}, as the numerical results indicate that the laminate joint with junction alignment present a P_{max} value higher than the simple laminate joint, a difference that is not reflected in the experimental results. In consideration of the experimental and numerical results, which demonstrate comparable P_{max} values for both geometries.

Table 36 - Mechanical properties of the simple laminate joint

Properties	***E* [MPa]**	$\boldsymbol{P_{max}}$ **[N]**
Experimental	4360.4	29812.1
Numerical analysis	4935.3	33634.9
Variation	+13.18%	+12.82%

Table 37 - Mechanical properties of the laminate joint with junction alignment

Properties	***E* [MPa]**	$\boldsymbol{P_{max}}$ **[N]**
Experimental	3780.7	28374.4
Numerical analysis	4736.7	34332.4
Variation	+25.28%	+21.00%

Table 38 presents the values of *E* and P_{max} that have been obtained through experimental and numerical analysis of the double strap joint. As was evidenced in preceding results, the numerical value exceeds the average experimental one. This discrepancy can be attributed primarily to the omission of damage evolution in the model, in conjunction with the potential for minor variations resulting from the positioning of the nails. When compared to the previously analysed geometries, thus joint exhibits lower numerical values of *E* and P_{max} than both the simple laminate joint and the laminate joint with junction alignment, which is consistent with the experimental findings.

Table 38 - Mechanical properties of the double strap joint

Properties	***E* [MPa]**	$\boldsymbol{P_{max}}$ **[N]**
Experimental	3133.9	22712.3
Numerical analysis	3844.1	28589.6
Variation	+22.67%	+25.88%

Table 39 presents the values of *E* and P_{max} that were obtained through experimentation and numerical analysis for the fastened double strap joint with M4 wooden fasteners. Table 40 presents the corresponding values for the fastened double strap joint with M6 wooden fasteners. Equally to the preceding instances, the numerical values exceed the experimental values. This overestimation of joint capacity is primarily attributable to the absence of damage evolution in the model. However, a similar conclusion can be drawn from the numerical results as was previously determined from the experimental data, i.e. in the absence of adhesive, this joint configuration exhibits a substantial decrease in mechanical performance in comparison to the previously analysed geometries.

Table 39 - Mechanical properties of the fastened double strap joint with M4 fasteners

Properties	***E* [MPa]**	**P_{max} [N]**
Experimental	646.11	7368.4
Numerical analysis	830.12	10284.3
Variation	+28.48%	+39.56%

Table 40 - Mechanical properties of the fastened double strap joint with M6 fasteners

Properties	***E* [MPa]**	**P_{max} [N]**
Experimental	1010.1	8617.2
Numerical analysis	1175.4	12007.3
Variation	+16.36%	+39.35%

Table 41 presents the values of E and P_{max} that have been obtained through experimental and numerical analysis for the bolted double strap joint with M6 bolts. Table 42 shows the corresponding values for the bolted double strap joint with M10 bolts. In contrast to the preceding cases, the numerical values for the M6 bolt configuration are lower than the experimental results. This discrepancy may be attributed to the torque applied to the bolts during the fabrication process, which was not recorded. Consequently, the assumptions employed in the numerical model, particularly the absence pre-tightening in the bolts, may have resulted in an underestimation of the joint's capacity. Conversely, as previously discussed, for the geometry utilising M10 bolts, the assumption that the outer straps are bonded to the central beams results relatively close values to the experimental ones. This finding indicates that the torque applied during the fabrication process was likely to have been high. However, a similar conclusion can be drawn from the numerical results as was observed from the experimental data, according to which the implementation of M10 bolts results in a significant increase in joint stiffness. Nevertheless, this does not result in a substantial enhancement in its load capacity.

Table 41 - Mechanical properties of the bolted double strap joint with M6 bolts

Properties	***E* [MPa]**	**P_{max} [N]**
Experimental	1429.4	22740.5
Numerical analysis	1230.9	20219.1
Variation	-13.89%	-11.09%

Table 42 - Mechanical properties of the bolted double strap joint with M10 bolts

Properties	*E* [MPa]	P_{max} [N]
Experimental	4088.2	23584.0
Numerical analysis	4177.3	23149.1
Variation	+2.18%	-1.85%

Table 43 presents the values of *E* and P_{max} that have been obtained through experimental and numerical analysis for the double strap joint with M4 fasteners. Table 44 presents the corresponding values for the double strap joint with M6 fasteners. For both geometry variants, there is a high degree of correlation between the experimental and numerical results. As previously mentioned, the numerical values of *E* and P_{max} tend to exceed experimental ones to a slight degree, primarily due to the absence of damage evolution in the model. A comparison of the numerical results indicates that the utilisation of M6 fasteners results in an enhancement of the mechanical properties of the joint. In addition, numerical and experimental data demonstrate that this configuration provides comparable properties to those of adhesive-based joints, despite the absence of any adhesive.

Table 43 - Mechanical properties of the double strap joint with chamfer using M4 fasteners

Properties	*E* [MPa]	P_{max} [N]
Experimental	3148.9	26204.5
Numerical analysis	3615.0	28257.7
Variation	+14.80%	+7.83%

Table 44 - Mechanical properties of the double strap joint with chamfer using M6 fasteners

Properties	*E* [MPa]	P_{max} [N]
Experimental	3491.3	28356.9
Numerical analysis	3821.6	33014.9
Variation	+9.46%	+16.43%

Finally, based on the experimental and numerical results, the simple laminate joint, laminate joint with junction alignment, and the double strap joint with chamfer are recommended for implementation in the studied pallet and for future applications.

3.5. Cost and sustainable analysis

Cost analysis

Once the experimental and numerical analysis provided the best geometries joint referring to the mechanical properties and the fabrication procedure, a more advanced cost analysis is conducted. The cost analysis follows the NEFAB's standard, which divides the cost in two parts:

- Direct material (DM), which determines the cost of the material used, based on the volume (m^3) produced;

- Direct labour (DL), which is divided into cutting process, assembly process, and it also includes the setup, which is divided by the five specimens of each joint.

To undertake the requisite cost calculations, NEFAB provides the constants (Table 45) related to the cost of wood and plywood per cubic metre, in addition to the labour and setup costs. The processes involved in the production of the specimens are cutting and assembly, expressed respectively in m^3/h and h/board. It is important to note that the cost of connection elements, such as bolts, wooden fasteners and adhesives, is not considered, as their impact on the overall cost is negligible. Another salient point is the average material waste. This value is utilised in the calculation of the necessary material quantity to produce the specimen, as it is inevitable that a certain amount of waste will be generated.

Table 45 - Constants for the cost analysis

Constants	Wood	Plywood
Cost [€/m^3]	280	690
Cutting time [m^3/h]	1	0.25
Average waste	15%	
Assembly time [h/board]	0.025	0.042
Labour cost [€/h]	23.5	
SETUP time [h]	0.17	
SETUP cost [€]	7.99	

Starting with the determination of the DM cost, it is necessary to calculate the cost of the different materials used in the joints. Based on the dimensions of the various components presented in Table 7, the volume of wood and plywood in each joint can be determined. Subsequently, using equation 8, a waste factor is applied, since the volume required for production is greater than that of the final joint

$$Production\ volume = \frac{Joint\ material\ volume}{1 - Average\ waste} \quad (8)$$

After the determination of the production volume for each material, the material cost can be multiplied by the respective material cost. Consequently, Table 46 presents both the production volume and the final cost of a joint, with the total value calculated by summing the individual costs of each material.

Table 46 - Production volumes per material and DM cost per specimen

Geometry	Wood	Plywood	DM cost per specimen
	Production volume [mm^3]	Production volume [mm^3]	
80x70 mm^2 wooden beam	0.0105	-	0.59 €
100x80 mm^2 wooden beam	0.0151	-	0.84 €

Table 46 - Production volumes per material and DM cost per specimen (Continued)

Simple laminate joint	0.00753	0.00226	0.73 €
Laminate joint with junction alignment	0.00753	0.00226	0.73 €
Double strap joint	0.0179	-	1.00 €
Fastened double strap joint	0.0316	-	0.89 €
Bolted double strap joint	0.0241	0.00452	0.99 €
Double strap joint with chamfer	0.0452	-	1.26 €

Following the calculation of the DM cost, the subsequent step is to determine the DL cost. The cost of the DL is divided into three constituent parts: cutting, assembly, and setup cost. The calculation of cutting cost is achieved by using equation 9, in which the previously calculated production volume is used. In the subsequent step of the process, the assembly cost is determined using equation 10. This equation is based on the joint component quantities listed in Table 7, which are then multiplied by the number of specimens produced. Finally, the setup cost is obtained by summing the setup values for cutting and assembly from Table 45, and then dividing this total by the number of specimens produced.

$$Cutting\ cost = \frac{Production\ volume}{Cutting\ time} \cdot Labour\ cost \quad (9)$$

$$Assembly\ cost = Part\ quantity \cdot Number\ of\ specimens \cdot Assembly\ time \cdot Labour\ cost \quad (10)$$

Following the calculation of the cutting, assembly, and setup costs, the total DL cost can be obtained by summing these values. To determine the DL cost per joint, it is necessary to divide the total by the number of specimens produced. Table 47 presents the DL cost per specimen.

Table 47 - DL cost per specimen

Geometry	DL cost per specimen
80x70 mm^2	0.96 €
100x80 mm^2	0.98 €
Simple laminate joint	3.14 €
Laminate joint with junction alignment	3.73 €
Double strap joint	2.75 €
Fastened double strap joint	2.50 €
Bolted double strap joint	3.31 €
Double strap joint with chamfer	1.95 €

Following the determination of the material, labour, and process costs per specimen, the total cost can be calculated. Table 48 presents the final cost per specimen for each geometry.

Table 48 - Final cost per specimen

Case	Final cost per specimen
80x70 mm^2	1.55 €
100x80 mm^2	1.82 €
Simple laminate joint	3.87 €
Laminate joint with junction alignment	4.46 €
Double strap joint	3.76 €
Fastened double strap joint	3.39 €
Bolted double strap joint	4.30 €
Double strap joint with chamfer	3.21 €

Finally, once having the overall cost per specimen for each geometry, the most financially viable option can be identified. The 80x70 mm^2 and 100x80 mm^2 wooden beams are not included in this analysis, as they do not constitute joint configurations. As previously mentioned, connectors such as nails, bolts, and adhesive are excluded from the cost analysis due to their negligible impact. It is evident, upon consideration of the aforementioned factors, that the double strap joint with chamfer demonstrates the most cost-effective solution when compared to other geometries. Meanwhile, the most used joint geometry at NEFAB, the simple laminate joint, is the third most economical option. Consequently, the double strap joint with chamfer is identified as the most financially viable geometry and recommended to the company for implementation in the large dimension pallet.

Sustainable analysis

Following a cost analysis of each joint, a sustainability assessment was conducted utilising the GreenCalc® software. In this instance, the global pallet illustrated in Figure 40 is taken into consideration, with the type of joint being the only variable altered, with the objective of isolating the environmental impact of the pallet based on the different types of joints. It is hypothesised that the transportation of two pallets from Portugal to France (1350 km) is undertaken exclusively by truck, with both pallets being shipped simultaneously. To proceed with the project, it is necessary to determine the mass of each material used in the pallet. Table 49 presents the mass of each material, as well as the total mass of the pallet, which were determined using IRON CAD® functionalities. It is important to note that nails are excluded from the calculation due to their negligible mass compared to the other components. Furthermore, the analysis is confined to joints that utilise M6 wooden fasteners and M6 bolts, as these are the most prevalent sizes within the NEFAB range.

Table 49 - Mass per joint and total mass of the palette per joint

Case	Wood	Plywood	Steel	Total
Simple laminate joint	506 kg	6 kg	-	512 kg
Laminate joint with junction alignment	506 kg	6 kg	-	512 kg
Double strap joint	666 kg	-	-	666 kg
Fastened double strap joint	664 kg	-	1 kg	665 kg

Table 49 - Mass per joint and total mass of the palette per joint (Continued)

Bolted double strap joint	660 kg	6 kg	4 kg	670 kg
Double strap joint with chamfer	668 kg	-	2 kg	670 kg

It is therefore possible to utilise GreenCalc® to ascertain the most sustainable joint geometry. In this context, geometries with lower mass are hypothesised to have a lower environmental impact. Consequently, the following geometries are compared to the simple laminate joint, as it consistently demonstrated robust performance throughout the study and possesses the least mass. It should be emphasized that the laminate joint with junction alignment possesses equivalent mass to that of the simple laminate joint. Thus, a joint analysis is performed with these two cases. Figure 114 thus provides a comparison between the simple laminate joint/laminate joint with junction alignment and the double strap joint. The results demonstrate that the simple laminate joint results in an CO_2e reduction of approximately 29% compared to the double strap joint.

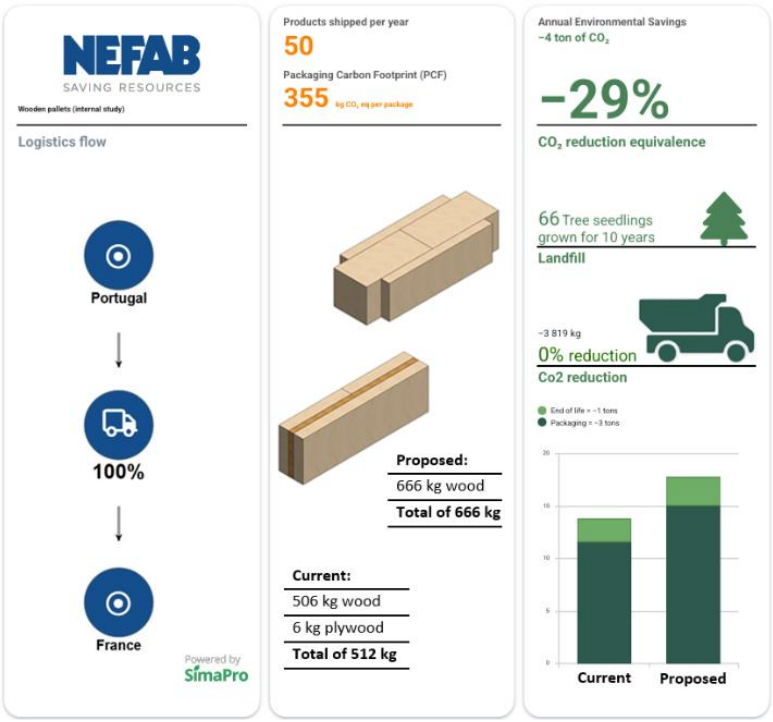

Figure 114 – GreenCalc® comparison between simple laminate joint/laminate joint with junction alignment and double strap joint.

Figure 115 presents a comparison between the simple laminate joint/laminate joint with junction alignment and the fastened double strap joint. It can be observed that, in this case, the fastened double strap joint presents an increase in CO_2e of 31%, when compared to the simple laminate joint/laminate joint with junction alignment. This outcome serves to further substantiate the finding that the simple laminate joint remains the most sustainable options.

Figure 116 presents a comparison between the simple laminate joint/laminate joint with junction alignment and the bolted double strap joint. It can be observed that, in this case, the bolted double strap joint presents an increase in CO_2e of 39%, when compared to the simple laminate joint/laminate joint with junction alignment. This finding provides further evidence

that the simple laminate joint/laminate joint with junction alignment remains the most sustainable options.

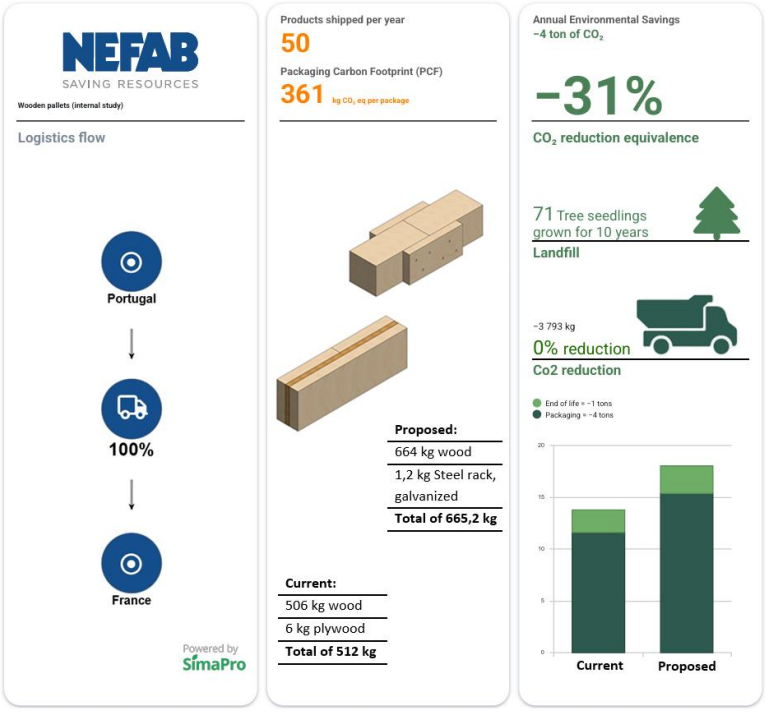

Figure 115 – GreenCalc® comparison between simple laminate joint/laminate joint with junction alignment and fastened double strap joint.

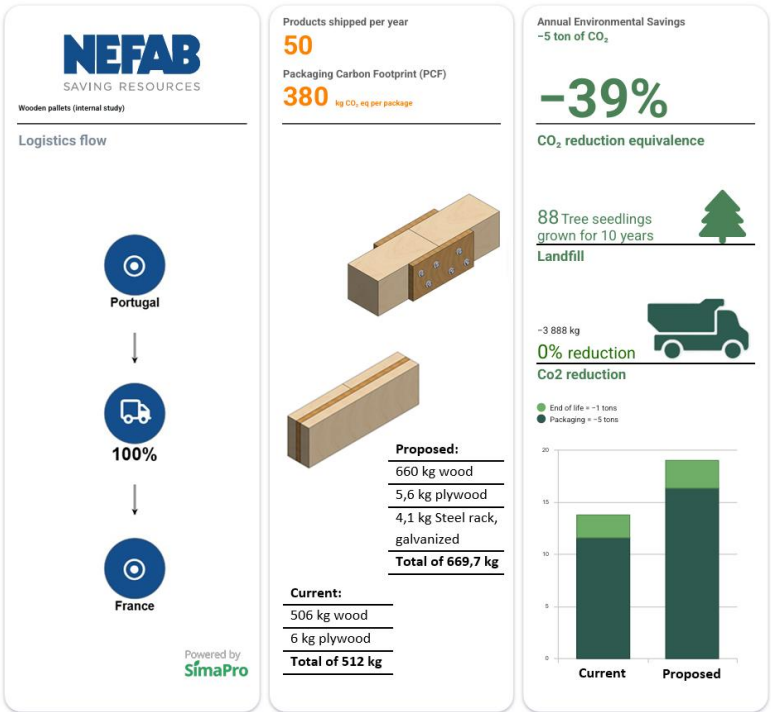

Figure 116 – GreenCalc® comparison between simple laminate joint/laminate joint with junction alignment and bolted double strap joint.

Figure 117 presents a comparison between the simple laminate joint/laminate joint with junction alignment and the double strap joint with chamfer. It can be observed that, in this case, the double strap joint with chamfer presents an increase in CO_2e of 34%, when compared to the simple laminate joint/laminate joint with junction alignment. This further demonstrates that the simple laminate joint/laminate joint with junction alignment continues to be the most sustainable options.

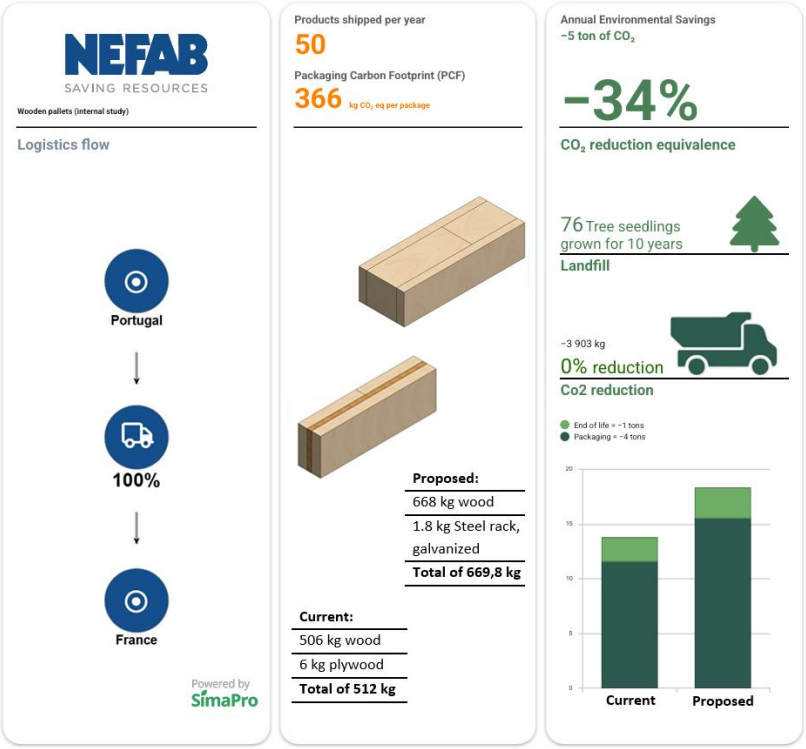

Figure 117 – GreenCalc® comparison between simple laminate joint and double strap joint with chamfer.

As demonstrated by the sustainability analysis of the joints, it can be concluded that the simple laminate joint and the laminate joint with junction alignment exhibit significantly lower values of CO_2e emissions. This result makes these geometries the most sustainable options. Conversely, the joint exhibiting the highest CO_2e emissions is the bolted double strap joint.

3.6. Final proposal

Having completed the cost and sustainable analysis, the next step is to synthesise all the information obtained from the experimental, numerical, cost, and sustainable analyses to identify the optimal option for the pallet under study, as well as for future pallet designs. To facilitate the comparison, Table 50 presents the properties obtained from both experimental and numerical analyses, along with the cost determined in the previous section.

Table 50 - Summary of the experimental and numerical results and the cost per specimen of each geometry

Case		Geometry	Experimental		Numerical		Cost
			E [MPa]	P_{max} [N]	E [MPa]	P_{max} [N]	
80x70 mm^2 wooden beam		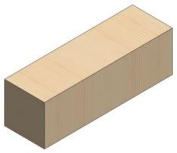	3822.0	31667	3901.2	36495	1.55 €
100x80 mm^2 wooden beam			5354.9	39020	5497.4	49036	1.82 €
Simple laminate joint			4360.4	29812	4935.3	33635	3.87 €
Laminate joint with junction alignment			3780.7	28374	4736.7	34332	4.46 €
Double strap joint			3133.9	22712	3844.1	28590	3.76 €
Fastened double strap joint	M4		646.11	7368	830.11	10284	3.39 €
	M6		1010.1	8617	1175.4	12007	
Bolted double strap joint	M6		1429.4	22741	1230.9	20219	4.30 €
	M10		4088.2	23584	4177.3	23149	
Double strap joint chamfer	M4		3148.9	26205	3615.0	28258	3.21 €
	M6		3491.3	28357	3821.6	33015	

A comparison of the different geometries reveals that the simple laminate joint offers good mechanical properties at an acceptable cost and presents a low environmental impact compared to the other geometries. The laminate joint with junction alignment demonstrates enhanced ductility, attributable to the joint alignment. However, this characteristic is accompanied by a marginal reduction in load capacity and an increase in manufacturing cost of approximately 15.2% in comparison with the simple laminate joint. Among the other

geometries, the double strap joint with chamfer is distinguished by its cost-effectiveness, as it is the most economical to manufacture, but presents an increase of 34% of CO_2e during transportation, as seen before. It also exhibits commendable mechanical properties and a load capacity that is closely comparable to that of the simple laminate joint.

In conclusion, the study demonstrated that the simple laminate joint and the double strap joint with chamfer using M6 connectors were the two most relevant geometries, in terms of both mechanical performance and cost, but the laminate joint distinguish by his environmental impact. On the other hand, since the double strap joint with chamfer only presents one type of material (wood) and no adhesive, disassembly and recycling at the end of its life cycle is easier. Furthermore, the double strap joint with chamfer can potentially present higher mechanical properties if combined with adhesive. Thus, the double strap with chamfer can become the most advantageous geometry if the use of adhesive brings higher mechanical properties. Once this option is not one the cases of the study, the simple laminate is the recommended joint for the studied pallet and for possible future nonstandard pallets.

4. Conclusion

4.1. Final conclusions

The main objective of this work was to respond to the large pallet's problems, due to the dimensional constrains of the wood-based components. The focus was the study of different geometries and methods to join two wooden components, to create the desired length.

Initially, a comprehensive literature review was conducted, forming a robust foundation by abording key aspects of the packaging industry, product development, and sustainable pallet design. This review was imperative in guiding subsequent experimental and numerical phases of the research. Moreover, NEFAB Portugal faces practical challenges related to standard wood beam dimensions, which frequently exceed market standards. These dimensional constraints necessitated investigating joint geometries as a practical solution to produce large dimensions pallet structures. Thus, the study specifically focusses on a 10 m long pallet currently under development by NEFAB Portugal.

The experimental phase consisted of static bending tests (three-point bending tests) carried out on six distinct joint configurations. Each configuration was prepared according to realistic production standards at NEFAB Portugal, closely simulating actual pallet conditions rather than idealised laboratory conditions. The mechanical performance, including *E*, P_{max} and failure mode, was evaluated and then compared between the different geometries. Among all tested configurations, the simple laminate joint exhibited the greatest mechanical strength, demonstrating the highest *E*, P_{max}, and consistent reliability under test conditions, clearly surpassing the other configurations.

After, a FEA was conducted to support the experimental results. One of the most important parts of the modelling procedure is the correct definition of the materials properties. However, a literature review was first conducted to find the materials properties of the wood, plywood and adhesive, since the supplier do not present enough information about the mechanical properties. An inverse method was used of the different materials, which will allow to more accurately represent the real material behaviour. After the property's determination, the FEA for all the geometries can be conducted. The results from the FEA, such as *E* and P_{max}, are then directly compared to the experimental ones. As for the experimental results, the simple laminate joint presents the best mechanical properties and is the recommended joint for large dimension pallets at this point. It is noteworthy that the double strap joint with chamfer also presented good mechanical properties without the use of adhesive, which can be an advantage.

Finally, cost and sustainability analyses were conducted using the GreenCalc® tool providing essential information into the economic and environmental implications of each joint geometry. As previously referred, the double strap joint with chamfer does not have an adhesive layer, which simplifies the disassembly process for recycling. But, based on the GreenCalc® results, the double strap joint with chamfer presented an increase in the CO_2e of 34% compared to the simple laminate joint. Thus, the simple laminate joint again emerged as the optimal solution, offering substantial advantages in terms of cost-effectiveness, ease of manufacture, efficient material use, and reduced environmental impact. Consequently, this joint represents a highly viable and sustainable option for large dimensions pallet production.

4.2. Limitations and future work

Following the conclusion of the study, its limitations and opportunities for future research could be identified.

The initial major challenge was related to the use of orthotropic materials and adhesive in the numerical model. It is evident that both solid wood and plywood exhibit orthotropic behaviour, which complicates the accurate determination of their material properties. It is noteworthy that even wood from the same tree can exhibit divergent properties depending on the region of the trunk and the moisture content. Furthermore, given the lack of linearity exhibited by these materials, the employment of more advanced modelling approaches, such as damage evolution, is necessary to more accurately capture their mechanical response. About the adhesive, cohesive behaviour was initially considered in this study. However, due to convergence issues in the numerical model, simplifications had to be made, and the adhesive was ultimately modelled as a solid, homogeneous material.

In consideration of these limitations, a study could focus on the joint geometries that demonstrated optimal performance in the present study, namely the simple laminate joint, the laminate joint with junction alignment, the double strap joint, and the double strap joint with chamfer. For these joints, a more detailed FEA could be carried out, incorporating advanced damage modelling techniques.

A subsequent study could be the chamfers impact in the joints. Based on this study, it is evident that the double strap joint with chamfer exhibited satisfactory mechanical performance when utilising wood exclusively and employing no adhesive. Consequently, it would be interesting to investigate alternative types of chamfers, incorporating both adhesive and non-adhesive applications, with the objective of expanding the NEFAB database.

Finally, a study could be carried out to replicate the joints analysed in this study but using laminated veneer lumber (LVL) instead of solid wood and plywood, since LVL presents higher structural strength and stiffness compared to plywood, although it is more expensive. As a result, it would be possible to directly compare this solution with the current results and assist in evaluating the potential of LVL in such applications.

References

1. Hook, P. and Heimlich, J.E. (2017). *A History of Packaging*. Ohioline. [cited 2024 October]; Available from: https://ohioline.osu.edu/factsheet/cdfs-133.
2. U.S. PACKAGING & WRAPPING (2024). *The History of Packaging Products*. U.S. Packaging & Wrapping LLC. [cited 2024 October]; Available from: https://uspackagingandwrapping.com/blog/the-history-of-packaging.html.
3. Pandey, D. (2024). *Packaging Market Size, Growth and Industry Developments (2023 - 2032)*. Towards Packaging. [cited 2024 October]; Available from: https://www.towardspackaging.com/insights/packaging-market-sizing.
4. STATISTA (2024). *Distribution of packaging materials market volume worldwide in 2020, by material type*. STATISTA. [cited October 2024]; Available from: https://www.statista.com/statistics/1428026/global-packaging-materials-type-market-volume-share/.
5. Graham, M. (2024). *Packaging Waste Facts and Statistics*. [cited 2024 October]; Available from: https://www.businesswaste.co.uk/your-waste/packaging-waste-recycling/packaging-waste-facts-and-statistics/.
6. OURWORLDINDATA (2022). *Annual global plastic use, 2019*. OUR WORLD IN DATA. [cited 2024 October]; Available from: https://ourworldindata.org/grapher/plastic-waste-by-sector.
7. EUROSTAT (2023). *Packaging waste*. EUROSTAT. [cited 2024 October]; Available from: https://ec.europa.eu/eurostat/statistics-explained/SEPDF/cache/10547.pdf.
8. EUROPEAN ENVIRONMENT AGENCY (2022), *Early warning assessment related to the 2025 targets for municipal waste and packaging waste*. European Environment Agency. Copenhagen, Denmark.
9. Silva, N. and Pålsson, H. (2022). *Industrial packaging and its impact on sustainability and circular economy: A systematic literature review.* Journal of Cleaner Production, Vol. **333**, 130165.
10. APAENGINEERING 2023. *Essential guide on packaging regulations*. APA ENGINEERING. [cited 2024 October]; Available from: https://apaengineering.com/compliance-blog-packaging-regulations-essential-guide-for-industry-professionals.
11. ASTM (2022). *Standard Practice for Performance Testing of Shipping Containers and Systems.*(ASTM D4169-22). West Conshohocken, Pensilvânia: American Society for Testing and Materials
12. ISTA (2018). *Series General Simulation Performance Test procedure.*(ISTA 3A). East Lansing, Michigan: Internacional Safe Transit Association
13. NEFAB (2023). *NEFAB's GreenCalc*. NEFAB. [cited 2024 October]; Available from: https://www.nefab.com/news-insights/2023/nefabs-greencalc-tool/.
14. Filho, W.L., Salvia, A.L., Bonoli, A., Saari, U.A., Voronova, V., Klõga, M., Kumbhar, S.S., and Olszewski, K. (2021). *An assessment of attitudes towards plastics and bioplastics in Europe.* Science of The Total Environment, Vol. **755**, 142732.
15. Monteiro, J., Silva, F.J.G., Ramos, S.F., Campilho, R.D.S.G., and Fonseca, A.M. (2019). *Eco-Design and Sustainability in Packaging: A Survey.* Procedia Manufacturing, Vol. **38**, 1741-1749.
16. UNITEDNATIONS (2015), *The 2030 Agenda for Sustainable Development*.
17. Fofana, O. (2024). *Packaging: How the industry can adapt to changing regulations*. Packaging Gateway. [cited 2024 October]; Available from: https://www.packaging-

gateway.com/features/packaging-how-the-industry-can-adapt-to-changing-regulations/?cf-view.
18. Grafström, J. and Aasma, S. (2021). *Breaking circular economy barriers.* Journal of Cleaner Production, Vol. **292**, 126002.
19. Rejish, R., Jun Tae, K., R., S., and Aswathy, J. (2024). *Recent advances in carboxymethyl cellulose-based active and intelligent packaging materials: a comprehensive review.* International Journal of Biological Macromolecules, Vol. **259**, 129194.
20. Witek-Krowiak, A., Szopa, D., and Anwajler, B. (2024). *Advanced Packaging Techniques—A Mini-Review of 3D Printing Potential.* Materials, Vol. **17**(12), 2997.
21. Sani, M.A., Khezerlou, A., and McClements, D.J. (2024). *Zeolitic imidazolate frameworks (ZIFs): Advanced nanostructured materials to enhance the functional performance of food packaging materials.* Advances in Colloid and Interface Science, Vol. **327**, 103153.
22. Nida, S., Moses, J., A., and Anandharamakrishnan, C. (2022). *Emerging applications of 5D and 6D printing in the food industry.* Journal of Agriculture and Food Research, Vol. **10**, 100392.
23. Ulrich, K.T. and Eppinger, S.D. (2019), *Product design and development*. McGraw Hill: Columbus, Ohio.
24. Gastaldello, G. (2024). *From concept to market: A step-by-step to the new product development process*. In the loop. [cited 2024 November]; Available from: https://maze.co/collections/product-development/new/.
25. Raeburn, A. (2024). *Le processus de développement produit en 6 étapes, exemples inclus*. asana. [cited 2024 November]; Available from: https://asana.com/fr/resources/product-development-process.
26. ANSYS (2023). *What is Design for Excellence (DfX)?* ANSYS. [cited 2024 October]; Available from: https://www.ansys.com/blog/what-is-dfx.
27. Velling, A. (2021). *Design for X (DFX) methods*. Fractory. [cited 2024 November]; Available from: https://fractory.com/design-for-x-dfx/.
28. Ulrich, K.T., Eppinger, S.D., and Yang, M.C. (2019), *Product Design and Development*. McGraw Hill: Columbus, Ohio.
29. Ulrich, K.T., Eppinger, S.D., and Yang, M.C. (2020), *Product Design and Development*. McGraw Hill: Columbus, Ohio.
30. Željko, S., Dragan, P., Adis, P., and Prasenjit, C. (2020). *Sustainable supplier selection in healthcare industries using a new MCDM method: Measurement of alternatives and ranking according to Compromise solution (MARCOS).* Computers & industrial engineering, Vol. **140**, 106231.
31. Aarushi, S. and Sanjay, K.M. (2014). *Major MCDM Techniques and their application-A Review.* IOSR Journal of Engineering, Vol. **4**(5), 15-25.
32. Ming-Chyuan, L., Chen-Cheng, W., Ming-Shi, C., and C Alec, C. (2008). *Using AHP and TOPSIS approaches in customer-driven product design process.* Computers in industry, Vol. **59**(1), 17-31.
33. Atef M, G., Husam, K., Ali, A., Syed, H., M. , and Lotfi, H. (2020). *Assessment and comparison of various MCDM approaches in the selection of manufacturing process.* Advances in Materials Science and Engineering, Vol. **2020**(1), 4039253.
34. Dean, E. and Yunus, K. (1997). *An overview of benchmarking process: a tool for continuous improvement and competitive advantage.* Benchmarking for Quality Management & Technology, Vol. **4**(4), 229-243.
35. Ashby, M.F. (2005), *Materials Selection in Mechanical design*. Butterworth-Heinemann: Oxford, UK.

36. Carraher, J. and Charles, E. (2017), *Carraher's polymer chemistry*.(10th ed.). CRC press: Boca Raton, Florida.
37. SWIFTGLASS (2022). *Properties of Glass Materials: A Guide*. [cited 2024 November]; Available from: https://www.swiftglass.com/blog/glass-materials-properties.
38. Jan, K. (2017), *Basics cad*. Birkhäuser: Basel, Switzerland.
39. Avallone, E., A. , Baumeister III, T., and Sadegh, A., M. (2007), *Mark's Standard Handbook for Mechanical Engineers*.(11th ed.). McGraw Hill: Columbus, Ohio.
40. AUTODESK (2024). *CAD software for designers, drafters, and creators*. AUTODESK. [cited 2024 November]; Available from: https://www.autodesk.com/asean/solutions/cad-software.
41. Janssen, P. and Stouffs, R. (2015). *Types of parametric modelling*. in *Proceedings of the 20th International Conference of the Association for Computer-Aided Architectural Design Research in Asia (CAADRIA)*. Hong-Kong, China.
42. Campilho, R.D.S.G. (2012), *Método de elementos finitos*. Publindústria: Porto, Portugal.
43. SIMSCALE (2024). *What is FEA | Finite Element Analysis?* SIMSCALE. [cited 2024 November]; Available from: https://www.simscale.com/docs/simwiki/fea-finite-element-analysis/what-is-fea-finite-element-analysis/.
44. LeBacq, C., Brechet, Y., Shercliff, H.R., Jeggy, T., and Salvo, L. (2002). *Selection of joining methods in mechanical design.* Materials & design, Vol. **23**(4), 405-416.
45. Silva, F.J.G. (2022), *Tecnologia da Soldadura uma abordagem técnico-didática*.(3th ed.). Publindústria: Porto, Portugal.
46. Groover, M.P. (2021), *Fundamentals of Modern Manufacturing: Materials Processes and Systems. SI Version*.(7th ed.). Wiley: Hoboken, New Jersey.
47. Pramanik, A., Basak, A., Dong, Y., Sarker, P., Uddin, M., Littlefair, G., Dixit, A., and Chattopadhyaya, S. (2017). *Joining of carbon fibre reinforced polymer (CFRP) composites and aluminium alloys–A review.* Composites Part A: Applied Science and Manufacturing, Vol. **101**, 1-29.
48. Speck, J.A. (2015), *Mechanical Fastening, joining, and Assembly*.(2nd ed.). CRC Press: Boca Raton, Florida. 384.
49. Varma, A. (2013), *Chapter 5. Bolted Connection*, in *CE 405: Design of Steel Structures* Catanduanes, Philippines.
50. Budynas, R.G. and Nisbett, K.J. (2011), *Shigley's Mechanical Engineering Design*.(9th ed.). McGraw Hill: Columbus, Ohio.
51. CEN 2005. *Eurocode 3: Design of steel structures - Part 1-8 Design of joints*.(EN 1993-1-8). Brussels, Belgium: EUROPEAN COMMITTEE FOR STANDARDIZATION
52. Ravichandran, B. and Balasubramanian, M. (2024). *Joining methods for Fiber Reinforced Polymer (FRP) composites – a critical review.* Composites Part A: Applied Science and Manufacturing, Vol. **186**, 108394.
53. Comyn, J. (2021), *Adhesion Science*. ROYAL SOCIETY OF CHEMISTRY: London, UK.
54. Baldan, A. (2012). *Adhesion phenomena in bonded joints.* International Journal of Adhesion and Adhesives, Vol. **38**, 95-116.
55. Lucas F. M. da Silva, C., R., and M., E. (2017), *Problemas e trabalhos práticos de juntas adesivas estruturais*. Publidústria: Porto, Portugal.
56. Jixing, C., Sen, X., Bo, W., Xiaofeng, F., Singh, D.J., and Weitao, Z. (2024). *Insights into the surface tension and superficial density peak of molten metals from molecular dynamics.* Acta Materialia, Vol. **276**, 120149.
57. Kupski, J. and De Freitas, S.T. (2021). *Design of adhesively bonded lap joints with laminated CFRP adherends: Review, challenges and new opportunities for aerospace structures.* Composite Structures, Vol. **268**, 113923.

58. Maggiore, S., Banea, M.D., Stagnaro, P., and Luciano, G. (2021). *A review of structural adhesive joints in hybrid joining processes.* Polymers, Vol. **13**(22), 3961.
59. Andreas, Ö., Lucas F. M. da Silva, and Holm, A. (2011), *Hybrid Adhesive Joints*. Vol. 6. SPRINGER: Berlin, Germany.
60. W., L. and Fisher, P.E. (2005), *Selection of Engineering Materials and Adhesives*. Taylo & Francis: Abingdon-on-Thames, UK.
61. Robert, A.D. (2021), *ADHESIVE BONDING SCIENCE, TECHNOLOGY AND APPLICATIONS*.(2nd ed.). ELSEVIER: Amsterdam, Netherlands.
62. Muciaccia, G., Khorasani, M., and Mostofinejad, D. (2022). *Effect of different parameters on the performance of FRP anchors in combination with EBR-FRP strengthening systems: A review.* Construction and Building Materials, Vol. **354**, 129181.
63. Budzik, M.K., Wolfahrt, M., Reis, P., Kozłowski, M., Sena-Cruz, J., Papadakis, L., Nasr Saleh, M., Machalicka, K.V., Teixeira de Freitas, S., and Vassilopoulos, A.P. (2022). *Testing mechanical performance of adhesively bonded composite joints in engineering applications: an overview.* The Journal of Adhesion, Vol. **98**(14), 2133-2209.
64. Flanigan, M.D. (2022), *Accelerated Aging of Adhesively Bonded Composite JOints for use in Material Screening and Selection During Development: A review and Case Study*, in *Aerospace Engineering*. Florida Institute of Technology: Florida, USA.
65. Adams, R.D. and Drinkwater, B.W. (1997). *Nondestructive testing of adhesively-bonded joints.* Vol. **30**, 93-98.
66. Pisani, D. and A., J. (2006). *Sustainable development–historical roots of the concept.* Environmental sciences, Vol. **3**(2), 83-96.
67. Zijp, M.C., Heijungs, R., Van der Voet, E., Van de Meent, D., Huijbregts, M.A., Hollander, A., and Posthuma, L. (2015). *An identification key for selecting methods for sustainability assessments.* Sustainability, Vol. **7**(3), 2490-2512.
68. Goodland, R. and Daly, H. (1995), *The concept of environmental sustainability*. Annual Reviews: San Mateo, California.
69. Lozano, R. (2008). *Envisioning sustainability three-dimensionally.* Journal of cleaner production, Vol. **16**(17), 1838-1846.
70. Tanguay, G.A., Rajaonson, J., Lefebvre, J.-F., and Lanoie, P. (2010). *Measuring the sustainability of cities: An analysis of the use of local indicators.* Ecological indicators, Vol. **10**(2), 407-418.
71. Brown, B.J., Hanson, M.E., Liverman, D.M., and Merideth, R.W. (1987). *Global sustainability: Toward definition.* Environmental management, Vol. **11**, 713-719.
72. Arushanyan, Y., Ekener, E., and Moberg, Å. (2017). *Sustainability assessment framework for scenarios–SAFS.* Environmental impact assessment review, Vol. **63**, 23-34.
73. Basiago, A.D. (1998). *Economic, social, and environmental sustainability in development theory and urban planning practice.* Environmentalist, Vol. **19**(2), 145-161.
74. Lehtonen, M. (2004). *The environmental–social interface of sustainable development: capabilities, social capital, institutions.* Ecological economics, Vol. **49**(2), 199-214.
75. Schoolman, E.D., Guest, J.S., Bush, K.F., and Bell, A.R. (2012). *How interdisciplinary is sustainability research? Analyzing the structure of an emerging scientific field.* Sustainability Science, Vol. **7**, 67-80.
76. Boyer, R.H., Peterson, N.D., Arora, P., and Caldwell, K. (2016). *Five approaches to social sustainability and an integrated way forward.* Sustainability, Vol. **8**(9), 878.
77. Purvis, B., Mao, Y., and Robinson, D. (2019). *Three pillars of sustainability: in search of conceptual origins.* Sustainability science, Vol. **14**, 681-695.

78. Carrano, A.L., Pazour, J.A., Roy, D., and Thorn, B.K. (2015). *Selection of pallet management strategies based on carbon emissions impact.* International Journal of Production Economics, Vol. **164**, 258-270.
79. Roy, D., Carrano, A.L., Pazour, J.A., and Gupta, A. (2016). *Cost-effective pallet management strategies.* Transportation Research Part E: Logistics and Transportation Review, Vol. **93**, 358-371.
80. INSIGHTS, F.B. (2024), *Pallets Market Size, Share and Industry Analysis By Material Type (Wood, Plastic, Composite Wood, and others), By Application (Pharmaceuticals, F&B, Manufacturing, and others), and Regional Forecast, 2019-2032*. FORTUNE BUSINESS INSIGHTS: Maharashtra, India.
81. Deviatkin, I., Khan, M., Ernst, E., and Horttanainen, M. (2019). *Wooden and plastic pallets: A review of life cycle assessment (LCA) studies.* Sustainability, Vol. **11**(20), 5750.
82. Giuseppe, S., Liotta, G., and Toshiya, K. (2013), *A Model to Realise Sustainability in Networked Production and Transportation (pp. 559-568)*, in *Collaborative Systems for Reindustralization*. Springer: Berlin, Germany.
83. Kim, S., Horvath, L., Russell, J.D., and Park, J. (2023). *Sustainable and Secure Transport: Achieving Environmental Impact Reductions by Optimizing Pallet-Package Strength Interactions during Transport.* Sustainability, Vol. **15**(17), 12687.
84. Arokiaraj, D. and Ramanarayan, S. (2019). *Recover, Recycle and Reuse: An Efficient Way to Reduce the Waste.* Interational Journal of Mechanical and Production Engineering Research and Development, Vol. **9**(3), 31-42.
85. Yu, K.H., Zhang, Y., Li, D., Montenegro-Marin, C.E., and Kumar, P.M. (2021). *Environmental planning based on reduce, reuse, recycle and recover using artificial intelligence.* Environmental Impact Assessment Review, Vol. **86**, 106492.
86. Bontempi, E., Sorrentino, G.P., Zanoletti, A., Alessandri, I., Depero, L.E., and Caneschi, A. (2021). *Sustainable materials and their contribution to the sustainable development goals (SDGs): a critical review based on an Italian example.* Molecules, Vol. **26**(5), 1407.
87. Bontempi, E. (2017), *Raw Materials Substitution Sustainability*. Springer: Berlin, Germany.
88. Matt (2024). *The Most Sustainable and Durable Material For Pallets*. ASSOCIATED PALLETS. [cited 2025 January]; Available from: https://associated-pallets.co.uk/blog/wood-sustainable-durable-material-pallets/.
89. Koop, C.M. (2024). *Product Life Cycle Explained: Stage and Examples*. INVESTOPEDIA. [cited 2025 January]; Available from: https://www.investopedia.com/terms/p/product-life-cycle.asp#toc-what-is-the-product-life-cycle.
90. TWI (2024). *WHAT IS A PRODUCT LIFE CYCLE? (DEFINITION, STAGES AND EXAMPLES)*. TWI. [cited 2025 February]; Available from: https://www.twi-global.com/technical-knowledge/faqs/what-is-a-product-life-cycle.
91. Tornese, F., Gnoni, M.G., Thorn, B.K., Carrano, A.L., and Pazour, J.A. (2021). *Management and logistics of returnable transport items: A review analysis on the pallet supply chain.* Sustainability, Vol. **13**(22), 12747.
92. Balfaqih, H., Saibani, N., and Nopiah, Z. (2016). *A conceptual Framework for Supply Chain Performance in Desalination Industry.* International Journal of Industrial Engineering and Management, Vol. **7**(2), 95-101.
93. Neri, A., Cagno, E., Lepri, M., and Trianni, A. (2021). *A triple bottom line balanced set of key performance indicators to measure the sustainability performance of industrial supply chains.* Sustainable Production and Consumption, Vol. **26**, 648-691.

94. Contini, G. and Peruzzini, M. (2022). *Sustainability and industry 4.0: definition of a set of key performance indicators for manufacturing companies.* Sustainability, Vol. **14**(17), 11004.
95. Giannakis, M. and Papadopoulos, T. (2016). *Supply chain sustainability: A risk management approach.* International journal of production economics, Vol. **171**, 455-470.
96. Aramyan, L.H., Lansink, A.G.O., Van Der Vorst, J.G., and Van Kooten, O. (2007). *Performance measurement in agri-food supply chains: a case study.* Supply chain management: an international Journal, Vol. **12**(4), 304-315.
97. Balfaqih, H., Al-Nory, M.T., Nopiah, Z.M., and Saibani, N. (2017). *Environmental and economic performance assessment of desalination supply chain.* Desalination, Vol. **406**, 2-9.
98. Pandey, D., Agrawal, M., Pandey, J., (2010). *Carbon Footprint: Current methods od estimation.* Springer Nature, Vol. **178**, 135-160.
99. BRIGHTLY (2023). *How to calculate Your Business's Carbon footprint*. BRIGHTLY. [cited 2025 February]; Available from: https://www.brightlysoftware.com/blog/calculate-carbon-footprint.
100. Borsos, G., lacob, C., and Calefariu, G. (2016). *The use KPI's to determine the waste in production process.* IOP Publishing Ltd, Vol. **161**, 012102.
101. Pappas, G., Papamichael, I., Zorpas, A., Siegel, J.E., Rutkowski, J., and Politopoulos, K. (2021). *Modelling key performance indicators in a gamified waste management tool.* Modelling, Vol. **3**(1), 27-53.
102. Blass, V. and Corbett, C.J. (2018). *Same supply chain, different models: Integrating perspectives from life cycle assessment and supply chain management.* Journal of Industrial Ecology, Vol. **22**(1), 18-30.
103. Geissdoerfer, M., Savaget, P., Bocken, N.M., and Hultink, E.J. (2017). *The Circular Economy–A new sustainability paradigm?* Journal of cleaner production, Vol. **143**, 757-768.
104. Basil-Jones, W. (2024). *A comprehensive overview of the best sustainability software on the market in 2025*. [cited 2025 February]; Available from: https://plana.earth/academy/sustainability-software.
105. Zhang, T., Wen, Z., Tan, Y., and Ekins, P. (2024). *Circular economy strategies for the booming industrial pallet use in China.* Sustainable Production and Consumption, Vol. **46**, 244-255.
106. Dakić, N., Jurošević, V., Reljić, V., Milenković, I., Dudić, S., and Šulc, J. (2024). *Augmented Reality System for Instructed and Visualized Pallet Loading.* Acta Polytechnica Hungarica, Vol. **21**(6), 263-284.
107. Franke, S., Bommert, A., Brandt, M.J., Kuhlmann, J.L., Olivier, M.-C., Schorning, K., Reining, C., and Kirchheim, A. (2024). *Smart pallets: Towards event detection using imus*. in *2024 IEEE 29th International Conference on Emerging Technologies and Factory Automation (ETFA)*. IEEE.
108. Bairapudi, A., Sastry, C.C., Krishnaiah, J., Sundeep, D., and Eswaramoorthy, K. (2024). *Experimental investigation of stereolithography and digital light processing additive manufactured pallets.* Materials Science-Poland, Vol. **42**(1), 1-31.
109. MULTIPLACAS MULTIPLACAS. [cited 2025 May]; Available from: https://multiplacas.pt/categoria-produto/contraplacado/.
110. AQUENCE (2018), *AQUENCE WL 041/1*.
111. CEN (2016). *Classification of thermoplastic wood adhesives for non-structural applications.*(EN 204:2). Brussels, Belgium: European Committee for Standardization
112. CEN (2013). *Durability of wood and wood-based products - Use classes:*

definitions, application to solid wood and wood-based products.(EN 335:2013). Brussels, Belgium: European Comittee for Standardization

113. Green, D.W., Winandy, J.E., and Kretschmann, D.E. (1999), *Chapter 4. Mechanical Properties of Wood*, in *Wood Handbook: Wood as an Engineering Material*. United States Departement of Agriculture (USDA).
114. Suota, M.J., da Silva, T.A., Zawadzki, S.F., Sassaki, G.L., Hansel, F.A., Paleologou, M., and Ramos, L.P. (2021). *Chemical and structural characterization of hardwood and softwood LignoForce™ lignins.* Industrial crops and products, Vol. **173**, 114138.
115. CivilEngineering (2025). *What is Plywood? Types of Plywood*. Civil Engineering. [cited 2025 April]; Available from: https://civiltoday.com/civil-engineering-materials/timber/203-plywood.
116. Davies, N.T., Altaner, C.M., and Apiolaza, L.A. (2016). *Elastic constants of green Pinus radiata wood.* New Zealand Journal of Forestry Science, Vol. **46**, 1-6.
117. THEWOODSOURCE (2025). *Plywood, Sheet Goods and Veneers*. The Wood Source. [cited 2025 May]; Available from: https://wood-source.com/products/plywoods-sheet-goods-and-veneers/.
118. Gerrard, C. 1987. *The equivalent orthotropic elastic properties of plywood* Wood Science and Technology, Vol. **21**, 335-348.
119. Damiati, L., Eales, M.G., Nobbs, A.H., Su, B., Tsimbouri, P.M., Salmeron-Sanchez, M., and Dalby, M.J. (2018). *Impact of surface topography and coating on osteogenesis and bacterial attachment on titanium implants.* Journal of Tissue Engineering, Vol. **9**, 2041-7314.
120. Elices, M., Guinea, G., Gomez, J., and Planas, J. (2002). *The cohesive zone model: advantages, limitations and challenges.* Engineering fracture mechanics, Vol. **69**(2), 137-163.
121. DassaultSystemes (2025). *General-Purpose Finite Element Analysis Software*. Dassault Systemes. [cited 2025 May]; Available from: https://www.3ds.com/products/simulia/abaqus.
122. Narayan, R. (2018), *Encyclopedia of biomedical engineering*. Elsevier: Amsterdam, Netherlands.
123. Yang, G., Kabel, J., Van Rietbergen, B., Odgaard, A., Huiskes, R., and Cown, S.C. (1998). *The anisotropic Hooke's law for cancellous bone and wood.* Journal of elasticity, Vol. **53**, 125-146.
124. Wang, W.H. (2012). *The elastic properties, elastic models and elastic perspectives of metallic glasses.* Progress in Materials Science, Vol. **57**(3), 487-656.
125. Madenci, E. and Oterkus, S. (2016). *Ordinary state-based peridynamics for plastic deformation according to von Mises yield criteria with isotropic hardening.* Journal of the Mechanics and Physics of Solids, Vol. **86**, 192-219.
126. ENGINEERCALCULATOR (2025). *Properties and Overview of PVAc (Polyvinyl Acetate)*. ENGINEERCALCULATOR. [cited 2025 June]; Available from: https://www.engineercalculator.com/polymer-plastic-properties-and-overview/pvac-polymer-plastic-various-properties-and-overview/.

References

Declaration of Integrity

I declare that I conducted this academic work with integrity. I did not plagiarize or apply any form of misuse of information or falsification of results throughout the process that led to its preparation. I declare that the work presented in this document is original and my own and has not previously been used for any other purpose. I further declare that I am fully aware of the Code of Ethical Conduct of P.PORTO, ISEP.

NAME: Rafael Rodrigues Rocha

Porto, October 2025

Appendix A

Table A.1 - Resulting cases of the 3-point bending test of the 80x70 mm^2 wooden beams

Specimen	Front	Back
1		
2		
3		
4		
5		

Table A.2 - Resulting cases of the 3-point bending test of the 100x80 mm^2 wooden beams

Specimen	Front	Back
1		
2		

Table A.2- Resulting cases of the 3-point bending test of the 100x80 mm^2 wooden beams (Continued)

3		
4		
5		

Table A.3 - Resulting cases of the 3-point bending test of the simple laminate joint

Specimen	Front	Back
1	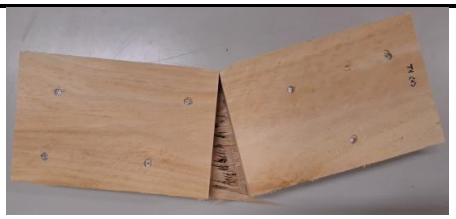	
2		
3		
4		

Table A.3 - Resulting cases of the 3-point bending test of the simple laminate joint

5		

Table A.4 - Resulting cases of the 3-point bending test of the laminate joint with junction alignment

Specimen	Front	Back
1		
2		
3		
4		
5		

Table A.5 - Resulting cases of the 3-point bending test of the double strap joint

Specimen	Front	Back
1		
2		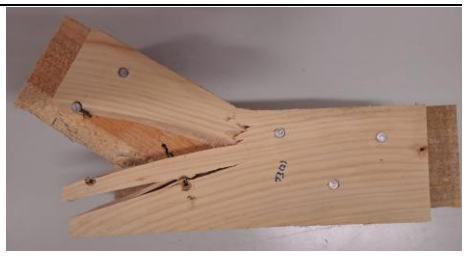
3		
4	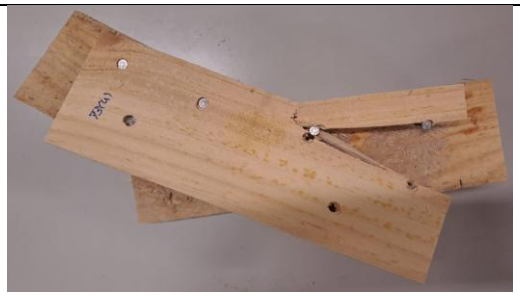	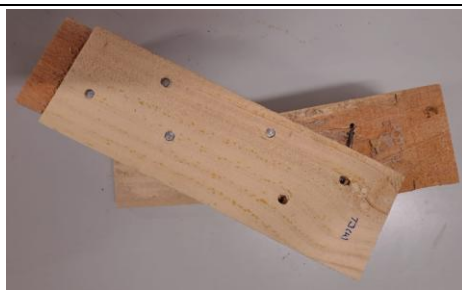
5		

Table A.6 - Resulting cases of the 3-point bending test of fastened double strap joint (M4)

Specimen	Front	Back
1		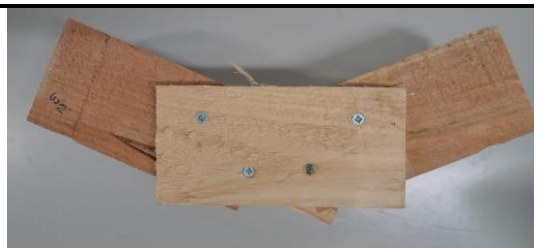
2	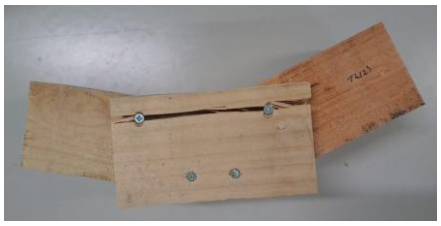	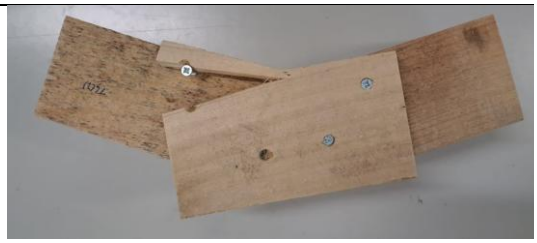
3		
4		
5		

Table A.7 - Resulting cases of the 3-point bending test of fastened double strap joint (M6)

Specimen	Front	Back
1		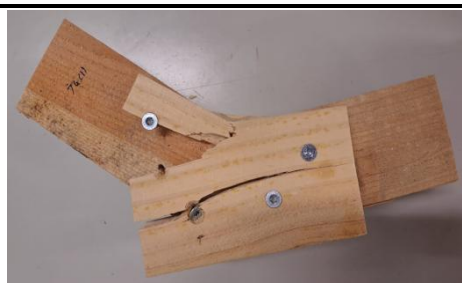

Table A.7- Resulting cases of the 3-point bending test of fastened double strap joint (M6) (Continued)

2	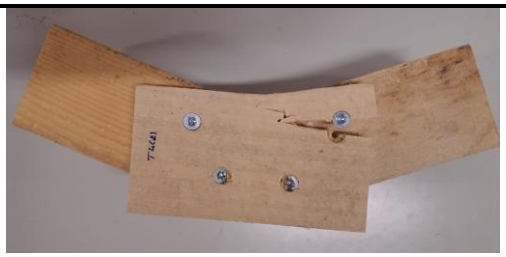	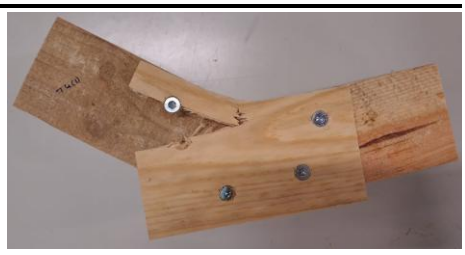
3		
4		
5		

Table A.8 - Resulting cases of the 3-point bending test of the bolted strap joint (M6)

Specimen	Front	Back
1		
2		

Table A.8- Resulting cases of the 3-point bending test of the bolted strap joint (M6) (Continued)

3		
4	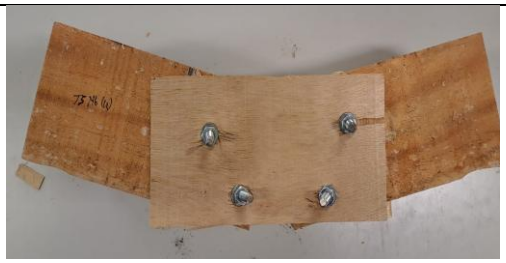	
5		

Table A.9 - Resulting cases of the 3-point bending test of the bolted strap joint (M10)

Specimen	Front	Back
1		
2		
3		
4		

Table A.9 - Resulting cases of the 3-point bending test of the bolted strap joint (M10) (Continued)

5		

Table A.10 - Resulting cases of the 3-point bending test of strap joint with chamfer (M6)

Specimen	**Front**	**Back**
1		
2		
3		
4	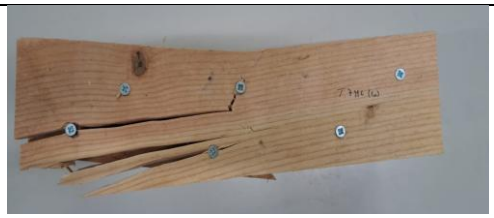	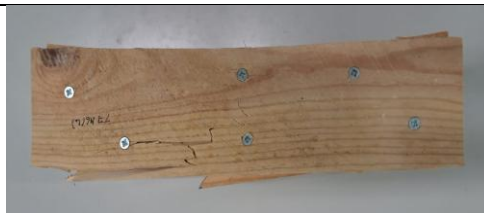
5	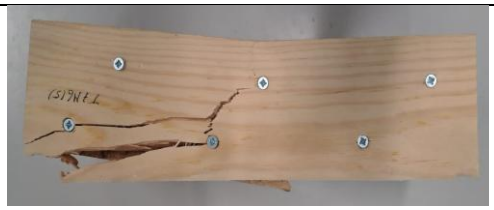	

Table A.11 - Resulting cases of the 3-point bending test of strap joint with chamfer (M10)

Specimen	**Front**	**Back**
1		

Table A.11 - Resulting cases of the 3-point bending test of strap joint with chamfer (M10) (Continued)

2		
3		
4		
5